Optimization of Damping in Self-Excited Mechanical Systems

Vom Fachbereich Maschinenbau
an der Technischen Universität Darmstadt
zur Erlangung des akademischen Grades eines
Doktor-Ingenieurs (Dr.-Ing.)
genehmigte

Dissertation

vorgelegt von

Dipl.-Ing. Dominic Jekel

aus Mutlangen

Berichterstatter:	Prof. Dr. Dr. h.c. Peter Hagedorn
Mitberichterstatter:	Prof. Dr.-Ing. Bernhard Schweizer
Tag der Einreichung:	23.07.2018
Tag der mündlichen Prüfung:	09.10.2018

Darmstadt 2018

D 17

Jekel, Dominic
Optimization of Damping in Self-Excited Mechanical Systems
Technische Universität Darmstadt
Tag der mündlichen Prüfung: 09.10.2018
Jahr der Veröffentlichung auf TUprints: 2018
URN: urn:nbn:de:tuda-tuprints-81120

Meinen Eltern gewidmet

Vorwort

Die vorliegende Arbeit befasst sich mit der Bestimmung vorteilhafter Dämpfungseigenschaften hinsichtlich des Stabilitätsverhaltens von selbsterregten mechanischen Systemen, wie beispielsweise Scheibenbremsen oder Hochspannungsleitungen. Sie entstand während meiner Tätigkeit als wissenschaftlicher Mitarbeiter in der Arbeitsgruppe Dynamik und Schwingungen an der Technischen Universität Darmstadt.

An dieser Stelle möchte ich mich bei all denen bedanken, die unmittelbar zum Gelingen dieser Arbeit beigetragen haben. Mein besonderer Dank gilt allen voran meinem Doktorvater, Herrn Prof. Peter Hagedorn, dessen wissenschaftliche Betreuung und Förderung in Verbindung mit dem nötigen Freiraum, eigene Ideen verfolgen und umsetzen zu können, wegweisend für den erfolgreichen Abschluss dieser Forschungsarbeit waren. Nicht minder bin ich auch Herrn Prof. Bernhard Schweizer für die bereitwillige Übernahme des Koreferats zum Dank verpflichtet.

Darüber hinaus bedanke ich mich bei meinen derzeitigen und ehemaligen Kollegen, insbesondere bei Dr. Eoin Clerkin, Dr.-Ing. Matthias Heymanns, Artem Karev und José Alfredo Ramírez, für die produktive Zusammenarbeit und die ausgesprochen angenehme Zeit in der Arbeitsgruppe Dynamik und Schwingungen. In gleicher Weise danke ich allen Kollegen des benachbarten Fachgebiets Numerische Berechnungsverfahren im Maschinenbau. Mein Dank gilt ferner Maria Rauck für ihre Unterstützung bei administrativen Tätigkeiten sowie den Herren Fladerer und Schmitt für die Betreuung der IT-Infrastruktur. Des Weiteren haben auch die Ideen und die Mitarbeit von Jan-Hendrik Wehner und Matthias Thomas, die ich beide im Rahmen ihrer Masterarbeit betreuen durfte, einen bedeutenden Anteil an der gelungenen Umsetzung dieses Forschungsvorhabens.

Mein persönlicher Dank gebührt in besonderem Maße meinen Eltern, die mich über meinen gesamten Werdegang hinweg nicht nur finanziell gefördert, sondern auch stets positiv in meinen Absichten bestärkt haben. Gleiches gilt überdies für meine beiden Geschwister, in deren ehrlichem Interesse an meiner Tätigkeit ein großer Teil meiner Motivation begründet liegt. Zu guter Letzt danke ich herzlich meiner Freundin, die während der gesamten Promotionsphase immer ein offenes Ohr für mich hatte und mir auf diese Weise den notwendigen privaten Rückhalt gegeben hat. Ihrem wissenschaftlichen Verständnis verdanke ich zudem viele hilfreiche Anregungen und Hinweise zur didaktischen Gestaltung dieser Arbeit.

Darmstadt, Juli 2018 Dominic Jekel

Abstract

Self-excited vibrations, such as squealing of disc brakes or galloping of overhead transmission lines, are often accompanied by undesired phenomena. The appearance of self-excitation is ascribed to an instability originating either from negative damping or from non-conservative coupling of motion coordinates. In a linearized description, the stability behavior of such circulatory systems strongly depends on the structure of the damping matrix as well as the relation of all matrices involved. Considering the distinct physical origins of energy dissipation, some of the resulting damping matrices have a stabilizing effect, while others may contribute to destabilization.

In this context, the present thesis addresses two major scientific objectives. First, a deeper understanding is promoted regarding the influence of velocity proportional forces on the stability of linear mechanical systems featuring circulatory and gyroscopic terms. Analytical investigations deliver detailed insights into the required structure of the damping matrix either for stabilization or the avoidance of destabilization. Second, stability is assessed by means of quantitative measures. On this basis, a technique for stability optimization is established. The method relies on decomposing the damping matrix into component matrices which are associated with different physical origins. Suitable variation of these submatrices yields a reduced tendency of self-excitation. Beneficial damping configurations are determined with respect to predefined constraints, as they naturally appear in engineering. The meaningfulness of the obtained results is judged in terms of dependence on parameter fluctuations and technical feasibility. Serving as representative examples, various models of disc brakes and overhead transmission lines are studied numerically at different levels of complexity.

Kurzfassung

Selbsterregte Schwingungen, wie das Quietschen von Scheibenbremsen oder das Seiltanzen von Freileitungen, werden häufig von unerwünschten Effekten begleitet. Die Entstehung der Selbsterregung wird einer Instabilität zugeschrieben, die entweder von einer negativen Dämpfung oder von einer nichtkonservativen Kopplung der Bewegungskoordinaten herrührt. In einer linearisierten Beschreibung hängt das Stabilitätsverhalten solcher zirkulatorischer Systeme stark von der Struktur der Dämpfungsmatrix sowie vom Zusammenspiel aller beteiligten Matrizen ab. Angesichts der verschiedenen physikalischen Ursprünge von Energiedissipation haben manche der resultierenden Dämpfungsmatrizen eine stabilisierende Wirkung, während andere zur Destabilisierung beitragen können.

In diesem Zusammenhang verfolgt die vorliegende Arbeit zwei Hauptziele. Zunächst wird ein tiefergehendes Verständnis gefördert hinsichtlich des Einflusses geschwindigkeitsproportionaler Kräfte auf die Stabilität linearer mechanischer Systeme mit zirkulatorischen und gyroskopischen Termen. Analytische Untersuchungen liefern detaillierte Einblicke in die erforderliche Struktur der Dämpfungsmatrix zur Stabilisierung oder zur Vermeidung von Destabilisierung. Auf Grundlage einer quantitativen Bewertung wird eine Methode zur Stabilitätsoptimierung eingeführt. Das Verfahren beruht auf der Zerlegung der Dämpfungsmatrix in einzelne Komponenten, die ihrem jeweiligen physikalischen Ursprung zugeordnet sind. Eine geeignete Variation dieser Submatrizen verringert die Tendenz zur Selbsterregung. Vorteilhafte Dämpfungskonfigurationen werden unter Berücksichtigung bestimmter Zwangsbedingungen ermittelt. Die Aussagekraft der Ergebnisse wird bezüglich ihrer Abhängigkeit von Parameterschwankungen sowie ihrer technischen Umsetzbarkeit beurteilt. Als repräsentative Beispiele werden Modelle verschiedener Komplexitätsstufen von Scheibenbremsen und Freileitungen numerisch untersucht.

Contents

Nomenclature

Notation of variables

Variables assigned to latin and greek characters are introduced in the respective chapter and not explicitly stated herein. However, their notation follows the classification scheme below.

type of variable	style of notation	examples
scalar	italic	d, T, λ
vector	bold, small	$\mathbf{q}$, $\boldsymbol{\alpha}$
matrix, dyadic	bold, capital	$\mathbf{M}$, $\boldsymbol{\Theta}$

Mathematical notations

$\dot{\square}$	time derivative
$\square'$	spatial derivative
$\mathring{\square}$	derivative with respect to dimensionless time τ
$\tilde{\square}$	dimensionless quantity
$\bar{\square}$	modal quantity
$\square^{-1}$	matrix inverse
$\square^{\mathrm{T}}$	matrix transpose
$\lvert\square\rvert$	absolute value
$\det(\square)$	determinant
$\mathrm{diag}(\square)$	diagonal matrix
$\lim(\square)$	limit
$\max(\square)$	maximum
$\mathrm{sgn}(\square)$	signum

$\mathrm{Im}(\square)$	imaginary part
$\mathrm{Re}(\square)$	real part
i	imaginary unit
δ_{ij}	KRONECKER delta
$\mathbb{C}$	space of complex numbers
$\mathbb{N}$	space of natural numbers
$\mathbb{R}$	space of real numbers

Constants

e	EULER's number
π	ARCHIMEDES' constant

Abbreviations

Eq.	equation
Fig.	figure
Tab.	table

1 Introduction

1.1 Motivation

Self-excitation is a frequently occurring phenomenon in various engineering applications. Unlike forced oscillations in which the alternating driving force exists independent of the vibratory motion, the energy supplying self-excited oscillations is generated and controlled by the motion itself. Hence, the vibratory motion does not depend on the frequency of an externally modulated power source [36, 84]. Examples of undesirable and dangerous manifestations of self-excitation are found in a broad variety of fields, such as squealing of automotive disc brakes [88], vibrations in paper calenders [188], galloping of overhead transmission lines [53], and ground resonance of helicopters [148]. Further examples of unwanted appearances are oil-whirl and oil-whip phenomena of high-speed rotors with fluid bearings [153, 154].

Negative effects of such oscillations are manifold and range from customer dissatisfaction over poor paper quality up to power outages and catastrophic failures of helicopters. Especially economic consequences resulting from customer complaints, loss of revenue, as well as maintenance and repair of defective equipment lead to high costs. In North America alone, warranty expenses corresponding to noise, vibration, and harshness including brake squeal are estimated around one billion US$ per year [3]. Costs related to galloping events have likewise been reported to exceed several million US$ [23].

The occurrence of self-excitation is generally associated with stability attributes of equilibrium states of the considered system. In most cases, the onset stems from an instability which is either related to negative damping [70] or to non-conservative coupling between coordinates [71]. The first mechanism relies on forces with a negative velocity gradient leading to an effective damping which steadily increases the system's total mechanical energy. While this

behavior can be reproduced by minimal models featuring merely one degree of freedom, the appearance of the second mechanism, which is usually referred to as flutter or mode coupling, requires at least two independent motion coordinates. Non-conservative (circulatory) forces govern the physical terms associated with self-excitation. These terms originate, for instance, from the frictional contact between the brake disc and the brake pads or from fluid-structure interactions in overhead transmission lines. Via these fundamental mechanisms, portions of the kinetic energy from a rotating brake rotor or from wind, respectively, are misrouted into an oscillating system, which may cause self-excitation.

It is well known that energy dissipation usually attenuates vibrations of structures. While this characteristic is fairly intuitive for systems exclusively described by mass, stiffness, and damping matrices, the effect of damping in general mechanical systems possessing gyroscopic and circulatory terms is far more complex [94]. Under the influence of dissipative forces, it is not a priori predictable whether or not an equilibrium state is stable. Counterintuitively, the introduction of (additional) damping does not necessarily have a stabilizing impact. Famous examples of this paradox are found in elastomechanics, such as the overhead double pendulum with follower forces [68,193], and in celestial mechanics [28]. Furthermore, circulatory systems are not only sensitive to the magnitude of the damping matrix but in particular also to its structure as well as to the relation and relative structure of all matrices involved. Both factors are decisive for stability [61, 103, 128].

In real applications, such as disc brakes or conductor cables, energy dissipation has distinct physical origins and occurs in various locations. This includes the interaction with adjacent fluids, friction between components, and damping within materials [174]. A linearized description of these inherently nonlinear processes leads to different types of damping matrices, which can have an opposing influence on stability. Some of the resulting submatrices contribute to stabilization, while others may induce the contrary. In the absence of substantial knowledge about the governing mechanisms of energy dissipation, the overall damping matrix is commonly assumed as a linear combination of the mass and the stiffness matrix. Analyses of academic minimal

models show, however, that this rather simplistic approach, which may be justified for forced vibrations, leads to diverging stability predictions in case of self-excitation. These predictions strongly depend on the specific combination of mass and stiffness proportional damping contributions [60].

In literature, numerous countermeasures to mitigate self-excited vibrations are discussed. Methods of active suppression employ sensors and actuators and thus may be expensive and elaborate to tune. This is different for typical passive techniques which can be differentiated into two groups. The first group concerns the modification of mass and stiffness properties, such as the separation of neighboring eigenfrequencies in disc brakes via a geometrical adjustment of internal ventilation channels [162, 179]. The second group focuses on the determination of favorable damping properties including damper viscosities and damper locations. In most cases, the calculation of an optimum energy dissipation is merely carried out for systems which are solely comprised of mass, stiffness, and damping matrices, e.g. [17, 25, 39, 131]. In contrast, little is known about the passive assignment of eigenvalues affected by circulatory and/or gyroscopic terms. The only approach for pole placement by means of passive damping control in self-excited systems is suggested by Ouyang [140], yet gyroscopic forces are still not explicitly taken into account. Despite the progress achieved in recent years, there is great potential for improvement. Especially a deeper understanding of the impact of the structure of the damping matrix on stability is needed. In addition, the finding of advantageous damping configurations in mechanical systems featuring circulatory and gyroscopic effects is of high interest.

1.2 Literature overview

This section provides a brief review of recent developments in the outlined research context. The literature overview presented herein is restricted to two representative examples of undesired occurrences of self-excitation in mechanical systems. Supplementary literature on stability theory, damping models, and damping optimization is elaborately given in chapter 2.

1.2.1 Brake squeal

Brake systems of vehicles are prone to various noise and vibration phenomena, an unpleasant example of which is referred to as brake squeal. Comprehensive descriptions of fundamental correlations and backgrounds thereof can be found in the review articles of Akay [3], Kinkaid et al. [88], and Ouyang et al. [141]. While there is no universal definition in literature, it is generally accepted that brake squeal is a friction-induced sound in the frequency range of 1 to 12 kHz. For most squeal events, the audible noise is dominated by one distinct frequency which is independent of the rotational speed of the disc. The majority of authors attribute the excitation mechanism to the particular structure of the linearized equations of motion which exhibit a non-symmetric coordinate proportional matrix. For certain parameter combinations, the circulatory portions lead to a pair of eigenvalues with positive real part such that the trivial solution of the equations of motion becomes unstable. The resulting flutter-type instability at the contact interface between the rotating disc and the brake pads is then interpreted as the onset of squeal. This procedure, which is referred to as complex eigenvalue analysis, has been utilized for the investigation of both, lumped minimal models [74, 157, 177] and high-dimensional finite element models [6, 49, 117].

With regard to its physical origin, energy dissipation in brake systems can be divided into material damping in respective brake components, damping at mechanical joints of the assembled structure, and damping due to the frictional contact between disc and pads. Theoretical investigations of minimal models conducted by Shin et al. [157] and Sinou & Jézéquel [158–160] reveal that distributed energy dissipation, e.g. material damping, generally reduces the squeal propensity, whereas concentrated energy dissipation, e.g. joint damping, may have the opposite effect. In their work, the magnitude and particularly the distribution of energy dissipation between the modes are identified as key factors and are thus decisive for stability. This high sensitivity of disc brakes to different modal damping levels is confirmed by Fritz et al. [41, 42] who analyzed realistic finite element models. On this basis, Cantone & Massi [19] succeeded in qualitatively comparing experiments with

finite element computations with regards to the damping distribution. The influence of mechanical joints on the dynamical behavior of brake systems is extensively studied by Kruse et al. [108] and Tiedemann [169].

While publications mentioned up to this point rather focus on the identification of inherent damping effects related to brake squeal, others concentrate on the development of remedies thereof. Beyond active or semi-active measures [72, 134, 178], which employ sensors and actuators for squeal avoidance, especially passive measures have been established in practice. Passive measures involve both the adjustment of mass and stiffness parameters, such as performed by Vomstein [176] and Wagner [179], as well as the modification of damping properties. The latter modifications concern, for example, the enhancement of the material damping capacity of disc and pads [146, 190] or the application of additional damping devices, such as shims [76, 85, 191]. These lumped insulators are usually comprised of thin, multi-layered plates of metal and elastomers. When attached to the brake assembly, shims may be able to improve the stability behavior. However, as shown by Festjens et al. [37], their global advantage is not a priori determined.

1.2.2 Conductor galloping

High-voltage overhead transmission lines are inevitably exposed to wind, the natural air flow evoking various vibration phenomena. According to Kiessling et al. [86] and Wang [184], three main types of oscillations can be differentiated based on characteristic amplitudes and frequencies. Besides aeolian vibrations (5 – 100 Hz), which are associated with a formation of vortices behind the conductors, another phenomenon is described by wake-induced subspan oscillations (1 – 5 Hz), which are due to an aerodynamic coupling of multi-conductor bundles. Vibrations referred to as galloping denote predominantly vertical motions of the span in one single or a few loops of standing waves. Frequencies typically range from 0.1 to 1 Hz with corresponding amplitudes potentially reaching the magnitude of the sag. These large displacements may lead, for instance, to contact of adjacent phases requiring an interruption of the network operation.

A comprehensive treatment of the state of the art of conductor galloping is summarized in the report edited by Cigré [23]. In the vast majority of cases, galloping relies on an aerodynamic instability when the resulting velocity proportional force comprising lift, drag, and intrinsic energy dissipation triggers a negative effective damping. This mechanism of self-excitation, which is classically ascribed to Den Hartog [31], occurs for asymmetric cable cross-sections originating from an accretion of ice or wet snow. As pointed out by Nigol & Buchan [137] and later by Wang & Lilien [185], the elastic coupling between vertical and torsional motions of bundled systems can also lead to instabilities of flutter-type.

In literature, numerous variants of both lumped minimal models with few degrees of freedom [13,53,186] as well as high-dimensional finite element models [32, 33, 53] have been developed. While these publications emphasize the nature of galloping and its correct mathematical description, little is known about its successful prevention. Galloping amplitudes are determined by the balance between the net energy supplied through aerodynamic action and the mechanical energy dissipated in the system. The dissipation mainly arises from friction and shear deformation between the individual layers of the cable strands [54] or from hysteresis at supporting points. Investigations conducted by Noiseux [138] and Stickland et al. [165] indicate, however, that the relative contribution of these mechanisms has a minor impact on the overall energy balance due to the low frequency of galloping.

Hence, external devices need to be applied for an adequate mitigation. Common methods range from aerodynamic devices over detuning pendulums up to self-damping spacers. The latter are widely used since they have proved to be effective in maintaining the distance between adjacent conductors [23]. Additionally, spacers possess adaptable viscoelastic properties for the absorption of wind-induced energy. Advantageous location schemes, which establish a high level of vibration control, have been proposed by Edwards & Ko [35] and Gross [53]. However, the damper viscosity of the installed devices has not been tailored to the respective arrangement. An optimum adjustment of design parameters has mostly been addressed for spacers which are employed to attenuate aeolian vibrations [4, 24, 63, 182].

1.3 Research objectives

On the basis of the reviewed literature, it is apparent that there is a strong demand for practical measures for the avoidance of self-excited vibrations in mechanical systems. Herein, two major aspects need to be addressed. First, it is essential to completely understand the impact of velocity proportional forces on the stability behavior of circulatory systems without limiting the magnitude of certain contributions. Theoretical investigations are necessary to gain detailed insights into the required structure of the damping matrix either for stabilization or the avoidance of destabilization. Pole placement is preferably conducted via a passive alteration of damping coefficients. Following an analytical approach for linear mechanical systems enhances the appreciation for the relative structure of all matrices involved. Aside from focusing on qualitative properties, i.e. whether or not the equilibrium state is stable, it is further required to assess stability by means of quantitative measures. The challenge is to make the trivial solution of the equations of motion as stable as possible while evaluating to what extent the computed optima depend on natural parameter fluctuations.

Second, it is indispensable to transfer and apply the theoretical knowledge to technical applications. Serving as representative examples, various models of disc brakes and overhead transmission lines are studied numerically at different levels of complexity. For both model classes, clarification is demanded on how the occurring mechanisms of energy dissipation are reflected in the overall damping matrix. The intention is to relate the submatrices to their respective physical origin. On this basis, an optimization problem can be formulated, where the ratio of these submatrices is varied to either stabilize or increase the degree of stability of the equilibrium position. Hereby, the coefficients of the respective component matrix are the optimization variables. This tailoring of damping needs to be carried out with respect to predefined constraints, as they naturally appear in engineering. In order to ensure the meaningfulness of optimized configurations, numerically obtained results have to be judged in terms of technical feasibility. For the reason of industrial relevance, the optimization technique must compulsorily apply to large matrices.

1.4 Outline

Based on the scientific setting described, this thesis is divided into six chapters, the upcoming five of which are organized as follows:

Chapter 2 frames the general theoretical context of this study, including the derivation of the equations of motion for mechanical systems. In respect of further analyses, criteria for stability determination and quantification are discussed. Moreover, an introduction to different mechanisms of energy dissipation is given, aiming to formulate an optimization approach with respect to advantageous damping properties of circulatory systems.

Chapter 3 elucidates effects of velocity proportional forces on the stability of linear mechanical systems featuring gyroscopic and circulatory terms. For the particular case of two degrees of freedom, the small number of parameters enables an analytical assessment. The explicitly derived stability boundary is investigated with regard to different structures of the damping matrix, the role of gyroscopic terms, and the spacing of the eigenfrequencies.

Chapter 4 focuses on the calculation of favorable damping configurations in disc brake systems. Numerical investigations are performed using the approach of complex eigenvalue analysis and concern both, low-dimensional minimal models as well as simplified and realistic disc brake models originating from a finite element environment. Optimization results are subsequently assessed in terms of the theoretical findings from chapter 3.

Chapter 5 addresses the influence of internal and external energy dissipation on the transverse dynamics of taut strings. Examinations incorporate model setups featuring a single or a pair of coupled strings. Design parameters of the respective damping elements, i.e. viscosities and locations, are tuned to maximize the damping ratio. The aim is to mitigate vibration modes affiliated to the lowest eigenfrequencies as they occur during galloping.

Chapter 6 concludes the major findings of this work and provides a brief outlook on possible future research in the field of damping optimization of self-excited mechanical systems.

2 Theoretical framework

This chapter places the thesis in its general context. The equations of motion for mechanical systems are derived and qualitative and quantitative criteria for stability determination are discussed. An overview of damping mechanisms and modeling is given, including the introduction of an optimization approach with respect to favorable damping properties.

2.1 Dynamics of mechanical systems

Vibratory systems consist of storage elements for kinetic energy (masses or inertias) and potential energy (springs) as well as elements which continually dissipate some of the oscillation energy into heat (dampers). The dynamical interaction of these components is described by differential equations relating the motion coordinates with their time derivatives. Aside from a formulation using NEWTON's laws, a standard approach to derive the equations of motion of (holonomic) mechanical systems having n degrees of freedom is the application of LAGRANGE's equations of the second kind

$$\frac{\mathrm{d}}{\mathrm{d}t}\frac{\partial \mathcal{L}}{\partial \dot{\mathbf{q}}} - \frac{\partial \mathcal{L}}{\partial \mathbf{q}} = \mathbf{g}. \tag{2.1}$$

This formalism incorporates the constraints directly by choice of the column vector of independent generalized coordinates $\mathbf{q} = (q_1, \ldots, q_n)^{\mathrm{T}}$. The overdot in Eq. (2.1) indicates differentiation with respect to time and the LAGRANGEian $\mathcal{L}$ is defined by

$$\mathcal{L} := \mathcal{T} - \mathcal{U}, \tag{2.2}$$

where the kinetic energy $\mathcal{T} = \mathcal{T}(q_1, \ldots, q_n, \dot{q}_1, \ldots, \dot{q}_n)$ depends on both the generalized coordinates and their time derivatives, while the potential energy $\mathcal{U} = \mathcal{U}(q_1, \ldots, q_n)$ depends on the generalized coordinates only. Forces

acting on the system and not arising from a potential, e.g. friction forces, damping forces, and excitation forces, are accounted for in the column vector of generalized non-conservative forces $\mathbf{g} = (g_1, \ldots, g_n)^{\mathrm{T}}$ [48, 143].

The LAGRANGE formalism (2.1) along with definition (2.2) yields a system of n second order ordinary differential equations of the form

$$\mathbf{f}(\ddot{\mathbf{q}}, \dot{\mathbf{q}}, \mathbf{q}, t) = \mathbf{0}, \tag{2.3}$$

which are frequently nonlinear and in general cannot be solved analytically. For many engineering applications, however, it is sufficient to approximate the dynamical behavior of system (2.3) by linearizing around a reference position, typically a static equilibrium $\mathbf{q}_s$, using a truncated TAYLOR series expansion

$$\mathbf{f}(\ddot{\mathbf{q}}, \dot{\mathbf{q}}, \mathbf{q}, t) \approx \mathbf{f}\left(\mathbf{0}, \mathbf{0}, \mathbf{q}_s, t\right) + \left.\frac{\partial \mathbf{f}}{\partial \ddot{\mathbf{q}}}\right|_{\mathbf{q}_s} \ddot{\mathbf{q}} + \left.\frac{\partial \mathbf{f}}{\partial \dot{\mathbf{q}}}\right|_{\mathbf{q}_s} \dot{\mathbf{q}} + \left.\frac{\partial \mathbf{f}}{\partial \mathbf{q}}\right|_{\mathbf{q}_s} \left(\mathbf{q} - \mathbf{q}_s\right). \tag{2.4}$$

Shifting the equilibrium to the origin via $\mathbf{x} = \mathbf{q} - \mathbf{q}_s$ and neglecting higher-order terms leads to the linearized equations of disturbed motion

$$\mathbf{M}(t)\ddot{\mathbf{x}} + \mathbf{B}(t)\dot{\mathbf{x}} + \mathbf{C}(t)\mathbf{x} = -\mathbf{f}\left(\mathbf{0}, \mathbf{0}, \mathbf{q}_s, t\right), \tag{2.5}$$

with the explicitly time-dependent matrices $\mathbf{M}(t)$, $\mathbf{B}(t)$, and $\mathbf{C}(t)$ of dimension $n \times n$ [122]. Their elements are given by

$$M_{ij}(t) = \left.\frac{\partial f_i}{\partial \ddot{q}_j}\right|_{\mathbf{q}_s}, \quad B_{ij}(t) = \left.\frac{\partial f_i}{\partial \dot{q}_j}\right|_{\mathbf{q}_s}, \quad C_{ij}(t) = \left.\frac{\partial f_i}{\partial q_j}\right|_{\mathbf{q}_s}. \tag{2.6}$$

For the study of self-excited vibrations in this thesis, the system matrices are taken to be time-invariant and the right hand side of Eq. (2.5) is set to zero. The resulting autonomous, homogeneous, linearized equations of disturbed motion near the equilibrium state $\mathbf{x} \equiv \mathbf{0}$ read

$$\mathbf{M}\ddot{\mathbf{x}} + \left(\mathbf{D} + \mathbf{G}\right)\dot{\mathbf{x}} + \left(\mathbf{K} + \mathbf{N}\right)\mathbf{x} = \mathbf{0}. \tag{2.7}$$

The generally non-symmetric matrices $\mathbf{B}$ and $\mathbf{C}$ representing velocity proportional forces and coordinate proportional forces, respectively, are decomposed into their symmetric and skew-symmetric part according to

$$\begin{aligned} \mathbf{D} &= \frac{1}{2}\left(\mathbf{B} + \mathbf{B}^{\mathrm{T}}\right), \quad \mathbf{G} = \frac{1}{2}\left(\mathbf{B} - \mathbf{B}^{\mathrm{T}}\right), \\ \mathbf{K} &= \frac{1}{2}\left(\mathbf{C} + \mathbf{C}^{\mathrm{T}}\right), \quad \mathbf{N} = \frac{1}{2}\left(\mathbf{C} - \mathbf{C}^{\mathrm{T}}\right). \end{aligned} \tag{2.8}$$

Under the assumption of an invertible mass matrix $\mathbf{M}$, another coordinate transformation $\mathbf{y} = (\mathbf{x}, \dot{\mathbf{x}})^{\mathrm{T}}$ with $\mathbf{y} \in \mathbb{R}^{2n}$ yields the first-order formulation

$$\dot{\mathbf{y}} = \mathbf{A}\mathbf{y}, \tag{2.9}$$

which is equivalent to Eq. (2.7). The square coefficient matrix $\mathbf{A}$ is generally non-symmetric and is given by

$$\mathbf{A} = \begin{pmatrix} \mathbf{0} & \mathbf{I} \\ -\mathbf{M}^{-1}(\mathbf{K}+\mathbf{N}) & -\mathbf{M}^{-1}(\mathbf{D}+\mathbf{G}) \end{pmatrix}, \tag{2.10}$$

with $\mathbf{I}$ being the $n \times n$ identity matrix. When looking for a particular solution of Eq. (2.9), the exponential *ansatz* $\mathbf{y} = \mathbf{r}\,\mathrm{e}^{\lambda t}$ is applied. The resulting eigenvalue problem reads

$$(\lambda\mathbf{I} - \mathbf{A})\,\mathbf{r} = \mathbf{0}, \tag{2.11}$$

where $\lambda \in \mathbb{C}$ and $\mathbf{r} \in \mathbb{C}^{2n}$ are the eigenvalues and the corresponding right eigenvectors, respectively. This algebraic system of equations has a non-trivial solution $\mathbf{r} \neq \mathbf{0}$ if and only if the matrix $(\lambda\mathbf{I} - \mathbf{A})$ is singular implying that λ is a root of the characteristic polynomial

$$p(\lambda) := \det(\lambda\mathbf{I} - \mathbf{A}) = \sum_{i=0}^{2n} a_i \lambda^{2n-i}, \tag{2.12}$$

where the coefficients a_i are real constants. The $2n$ roots λ_i $(i = 1, \ldots, 2n)$ of Eq. (2.12) can either be real, pairwise complex conjugate, or purely imaginary.

The different terms in Eq. (2.7) can be interpreted as generalized forces which have distinct mathematical and physical properties [130]. Premultiplying Eq. (2.7) with the vector of generalized velocities $\dot{\mathbf{x}}^{\mathrm{T}}$ and applying the quadratic relationships

$$\mathcal{T} := \frac{1}{2}\dot{\mathbf{x}}^{\mathrm{T}}\mathbf{M}\dot{\mathbf{x}}, \tag{2.13a}$$

$$\mathcal{U} := \frac{1}{2}\mathbf{x}^{\mathrm{T}}\mathbf{K}\mathbf{x} \tag{2.13b}$$

for the kinetic and potential energy gives the scalar expression

$$\frac{\mathrm{d}}{\mathrm{d}t}(\mathcal{T} + \mathcal{U}) = -\dot{\mathbf{x}}^{\mathrm{T}}\mathbf{D}\dot{\mathbf{x}} - \dot{\mathbf{x}}^{\mathrm{T}}\mathbf{N}\mathbf{x}. \tag{2.14}$$

This expression represents the time rate of change of the system's total mechanical energy. Eq. (2.7) and Eq. (2.14) are comprised of five individual contributions, where:

- $\mathbf{M}$ is the symmetric and positive definite mass matrix associated with the kinetic energy of the system.

- $\mathbf{D}$ is the symmetric damping matrix characterizing velocity proportional, non-conservative forces. For $\mathbf{D}$ positive definite, energy is dissipated in all motions and the system is completely damped. For $\mathbf{D}$ positive semi-definite, damping is called incomplete and undamped motions may be possible. However, the system may still be asymptotically stable depending on the structure of all matrices involved. This case is referred to as pervasive dissipation [121, 127, 144].

- $\mathbf{G}$ is the skew-symmetric gyroscopic matrix describing velocity proportional forces which do not contribute to the energy balance. They arise, for example, when the equations of motion are formulated in a rotating reference frame [44, 120].

- $\mathbf{K}$ is the symmetric and generally positive definite stiffness matrix associated with the potential energy of the system.

- $\mathbf{N}$ is the skew-symmetric circulatory matrix representing coordinate proportional, non-conservative forces, which may act as a source of power and thus are able to generate and maintain self-excited vibrations. They originate, for example, from follower forces in elastomechanics [66], from fluid-structure interactions [12], and from the kinematic linearization of friction forces acting on moving parts in frictional contact [62].

Depending on the relation of all matrices involved, systems with dissipative and circulatory forces are able to gain energy from the environment when part of the energy is misrouted into the oscillation, e.g. via friction or fluid-flow interactions, respectively. In systems without any dissipative and circulatory effects, i.e. $\mathbf{D} = \mathbf{0}$ and $\mathbf{N} = \mathbf{0}$, the total mechanical energy $\mathcal{T} + \mathcal{U}$ is constant.

2.2 Stability of mechanical systems

2.2.1 Qualitative measures

Stability of motion is a crucial topic in the dynamics of mechanical systems. The precise mathematical foundation of modern stability theory including the justification of linearization is based on LYAPUNOV's doctoral thesis [118]. His work addresses the asymptotic properties of solutions of nonlinear equations of motion of type

$$\dot{\mathbf{x}} = \mathbf{f}\left(\mathbf{x}(t), t\right). \tag{2.15}$$

The requirement is that small perturbations, e.g. deviations of the initial conditions, remain bounded in time for stable motions (Fig. 2.1a), converge to zero for asymptotically stable solutions (Fig. 2.1b), and diverge to infinity for unstable solutions (Fig. 2.1c). In the following, these rather intuitive formulations are mathematically expressed according to [56] and [128].

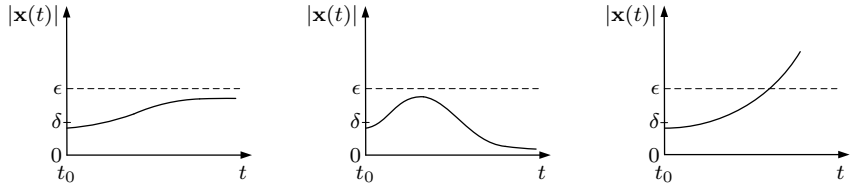

(a) LYAPUNOV stability. **(b)** Asymptotic stability. **(c)** Instability.

Figure 2.1: Distance $|\mathbf{x}(t)|$ to the equilibrium position $\mathbf{x}(t) \equiv \mathbf{0}$ over time t for a reference solution of system (2.15).

LYAPUNOV stability

The equilibrium position $\mathbf{x}(t) \equiv \mathbf{0}$ of system (2.15) with $\mathbf{f}\left(\mathbf{0}, t\right) \equiv \mathbf{0}$ is referred to as LYAPUNOV stable if for every (arbitrarily small) $\epsilon > 0$ there exists a positive number $\delta(\epsilon)$ such that the resulting disturbed motion $\mathbf{x}(t)$ satisfies

$$|\mathbf{x}(t)| < \epsilon. \tag{2.16}$$

This requirement needs to hold true for all times $t \geq t_0$ and any arbitrary initial displacement $\mathbf{x}(t_0) = \mathbf{x}_0$ with $|\mathbf{x}_0| < \delta(\epsilon)$.

Asymptotic stability

The equilibrium position $\mathbf{x}(t) \equiv \mathbf{0}$ of system (2.15) with $\mathbf{f}(\mathbf{0}, t) \equiv \mathbf{0}$ is referred to as asymptotically stable if it is LYAPUNOV stable and if the resulting disturbed motion $\mathbf{x}(t)$ additionally satisfies

$$\lim_{t \to \infty} \mathbf{x}(t) = \mathbf{0}. \tag{2.17}$$

Instability

The equilibrium position $\mathbf{x}(t) \equiv \mathbf{0}$ of system (2.15) with $\mathbf{f}(\mathbf{0}, t) \equiv \mathbf{0}$ is considered unstable if it is neither LYAPUNOV stable nor asymptotically stable.

Relation of eigenvalues and stability

One of the key ideas to judge stability is the prediction of qualitative patterns of a perturbed solution using linearization. According to the HARTMAN-GROBMAN theorem [64], eigenvalues of the coefficient matrix $\mathbf{A}$ of linearized system (2.9) sufficiently characterize the stability behavior around hyperbolic equilibria of the underlying nonlinear system (2.15). Based on this linear approximation, three cases are distinguished [156]:

1. If all eigenvalues of $\mathbf{A}$ have negative real part, i.e. $\mathrm{Re}(\lambda_i) < 0 \ \forall \ i \in \{1, \ldots, 2n\}$, the investigated reference solution is *asymptotically stable* independent of nonlinear terms.

2. If at least one eigenvalue of $\mathbf{A}$ has positive real part, i.e. $\max \mathrm{Re}(\lambda_i) > 0 \ \forall \ i \in \{1, \ldots, 2n\}$, the investigated reference solution is *unstable* independent of nonlinear terms.

3a. If at least one eigenvalue of $\mathbf{A}$ has zero real part, i.e. $\max \mathrm{Re}(\lambda_i) = 0 \ \forall \ i \in \{1, \ldots, 2n\}$, stability cannot be determined using the first approximation since the investigated equilibrium is not hyperbolic. In this

special case, a stability analysis is only feasible considering higher-order terms in TAYLOR series expansion (2.4).

For time-invariant systems of form (2.9) which are a priori linear, stability is a global system property [128].† Case 3a can thus be replaced by:

3b. If all eigenvalues of $\mathbf{A}$ have non-positive real part, one or more eigenvalues have zero real part, and the algebraic multiplicity is equal to the geometric multiplicity for all eigenvalues with zero real part, i.e. all roots of Eq. (2.12) are simple or semi-simple, the investigated system is *weakly stable* or *marginally stable*.

The application of these theorems is simplified by various criteria which give both, necessary and sufficient as well as sufficient conditions whereby all roots λ of characteristic polynomial (2.12) lie in the open left half of the complex plane. These criteria facilitate the stability determination of a solution of Eq. (2.7) respectively Eq. (2.9) without solving the system directly.

LIÉNARD-CHIPART criterion

The stability criterion of LIÉNARD & CHIPART [116] is a modified variant of the criterion of HURWITZ [77]. It combines a particular sequence of both the coefficients a_i of characteristic polynomial (2.12) and the leading principal minors H_i of the real square HURWITZ matrix

$$\mathbf{H} = \begin{pmatrix} a_1 & a_0 & 0 & \cdots & \cdots & \cdots & 0 \\ a_3 & a_2 & a_1 & a_0 & 0 & \cdots & \vdots \\ \vdots & & & & & \ddots & \vdots \\ 0 & \cdots & \cdots & \cdots & \cdots & \cdots & a_{2n} \end{pmatrix}. \tag{2.18}$$

A necessary and sufficient condition for all roots λ of characteristic polynomial (2.12) to have strictly negative real part is

$$a_{2(n-i)} > 0 \quad \wedge \quad H_{2(n-i)-1} > 0 \quad \forall \quad i \in \{0, \ldots, n-1\}. \tag{2.19}$$

†In this thesis, the stability of the trivial solution of the equations of motion linearized around an equilibrium state is referred to as 'stability of the system' or 'stability of the equations of motion'.

This criterion has the advantage that only half the number of required determinants, the order of the largest being $2n-1$, have to be computed.

For many technical problems, the critical boundary between the asymptotically stable and unstable regime plays an important role. It can be derived using ORLANDO's formula [139], which expresses the relation between the eigenvalues λ and the $(2n-1)$-th HURWITZ determinant. If parameters of linear system (2.9) are varied, starting in the asymptotically stable regime, the stability boundary is given by

$$H_{2n} = a_{2n} H_{2n-1} = 0. \tag{2.20}$$

Therein, $a_{2n} = 0$ indicates monotonic marginal stability ($\mathrm{Im}(\lambda) = 0$), while $H_{2n-1} = 0$ implies marginal stability of flutter-type ($\mathrm{Im}(\lambda) \neq 0$), which occurs immediately after exiting the asymptotically stable domain [130].

Most of the other known stability criteria are merely sufficient for asymptotic stability, rather than being necessary and sufficient. An example is the criterion introduced by FRIK [40], which takes advantage of the limitation of the RAYLEIGH quotient by the smallest and largest eigenvalue of the respective matrices in Eq. (2.7). Other examples are the criteria studied by KLIEM & POMMER [101, 102], which represent a simplified variant of LYAPUNOV's direct method. The criterion formulated by WALKER [181] yields necessary and sufficient conditions for asymptotic stability. However, these are less applicable than those by LIÉNARD and CHIPART since they are based on the existence of matrices with certain properties satisfying LYAPUNOV's matrix equation and thus are not straightforward to verify. In contrast, the LIÉNARD-CHIPART criterion gives explicit conditions for asymptotic stability based on the coefficients of the characteristic polynomial. They naturally become less feasible for systems with a large number of degrees of freedom.

Relation of matrix properties and stability

Stability criteria based on the distribution of roots of the characteristic polynomial neglect the special structure of the matrices $\mathbf{M}$, $\mathbf{D}$, $\mathbf{G}$, $\mathbf{K}$, and $\mathbf{N}$ in the equations of motion (2.7). The solution of the stability problem using an energy-based method, however, allows a physical interpretation of the stability

conditions which depend on the properties and the interaction of all matrices involved [119, 128, 192, 193]. For example, a conservative **MK**-system with positive definite mass and stiffness matrix always has simple or semi-simple, purely imaginary eigenvalues. The equilibrium position is marginally stable given that the underlying system is linear. This can be verified by referring to the vanishing right-hand side of Eq. (2.14) which implies that the total mechanical energy is constant. Adding pervasive dissipation[†] results in complex conjugate pairs of eigenvalues with negative real part. In this case, the right-hand side of Eq. (2.14) is non-positive and only vanishes in the equilibrium position. The total mechanical energy decreases continuously and the system is asymptotically stable. This does not necessarily require a positive definite damping matrix $\mathbf{D}$.

While these instances are fairly intuitive, the effect of damping terms in general systems with $\mathbf{G} \neq \mathbf{0}$ and $\mathbf{N} \neq \mathbf{0}$ is more complex. One of the few generic results is that undamped systems of type **MGKN** are mostly unstable unless all coefficients of odd powers of λ in Eq. (2.12) vanish. This occurrence is referred to as an academic special case [62]. The introduction of (infinitesimally small) damping may not only stabilize but also destabilize such systems. The extended theorem of Thomson & Tait [168] states that marginally stable **MK**-systems cannot be destabilized by adding velocity proportional terms of the form $(\mathbf{D} + \mathbf{G})\,\dot{\mathbf{x}}$ if the corresponding dissipation function is at least positive semi-definite. The characteristics of its eigenvalues, i.e. the sign of the real parts, then only depend on the definiteness of the damping matrix and are independent of gyroscopic terms [128]. In contrast, pervasive damping in gyroscopically stabilized systems with an indefinite stiffness matrix always leads to instability, as it happens, for instance, in satellite mechanics [28].

The structure of the damping matrix is also crucial for the stability behavior of circulatory systems [16, 91, 92, 96–98]. Most authors focus on rather academic problems with a low number of degrees of freedom, an example of which is the famous overhead double pendulum with follower forces [66–68]. The theorems published by Hagedorn et al. [61] hold for arbitrarily large

[†]Pervasive damping means that no eigenvector and thus no component of the motion lies in the null space of the damping matrix.

values of n, as they naturally appear in finite element environments. None of the matrices are assumed to be small in contrast to standard perturbation approaches [163]. Moreover, they are independent of an underlying **MK**-system with double eigenfrequencies, which can be particularly prone to self-excitation [161]. The theorems prove that on the one hand, any **MKN**-system with purely imaginary eigenvalues can either have an asymptotically stable or an unstable trivial solution under the influence of dissipative forces. Both cases can be achieved by adding a suitable damping matrix of arbitrarily small norm since only the structure of the matrix is relevant. On the other hand, any system of type **MDGKN** can always be stabilized asymptotically by adding an at least positive semi-definite damping matrix. As a result, any engineering system which may be unstable due to intrinsic damping, e.g. friction within materials, can always be stabilized asymptotically by adding more (non-negative) damping of a certain structure.

It is trivial that this stabilization cannot be achieved by a damping matrix of arbitrarily small norm, and there is no information about the required structure. For non-gyroscopic systems, however, Done [34] and Walker [180] simultaneously developed sufficient damping configurations which (i) assuredly do not have a destabilizing impact and (ii) show a stabilizing effect in all scenarios considered. The special case when the damping matrix is proportional to the mass matrix is such an example, whereas the more general formulation of **D** being a linear combination of **M** and **K** is not always stabilizing, cf. section 2.3.1. More recently, Kirillov & Seyranian [95] established a class of matrix structures which is necessary and sufficient to stabilize circulatory systems with velocity-dependent forces.

2.2.2 Quantitative measures

For many technical applications, asymptotic stability alone is not sufficient. A further requirement is that the trivial solution is as stable as possible given that parameters governing the dynamical behavior, e.g. stiffness and damping coefficients, may be varied within a specific range. Among the most common criteria to quantitatively assess the stability of these systems are the degree of

stability ζ_{abs} (absolute stability reserve) and the damping ratio ζ_{rel} (relative stability reserve). An advantage of both measures is the independence of the initial conditions $\mathbf{y}(t_0)$ of linear system (2.9). The degree of stability geometrically represents the distance

$$\zeta_{\text{abs}} := -\max_i \left[\text{Re}(\lambda_i)\right], \qquad i = 1, \ldots, 2n, \tag{2.21}$$

of the imaginary axis to the eigenvalue with largest real part, cf. Fig. 2.2a, and is a measure of describing how rapidly oscillations decay after disturbance. The larger the degree of stability, the faster the motion generally decays.

For systems with complex conjugate pairs of eigenvalues, the damping ratio is defined as

$$\zeta_{\text{rel}} := -\max_i \left[\frac{\text{Re}(\lambda_i)}{|\lambda_i|}\right], \qquad i = 1, \ldots, 2n, \tag{2.22}$$

and can be geometrically interpreted as the sine of the angle spanned by the position vector of the eigenvalue with largest real part and the imaginary axis, cf. Fig. 2.2b. The damping ratio indicates after how many periods of oscillation an initial deflection has decayed to a certain fraction, i.e. a high damping ratio leads to a decay within a few periods [128, 130].

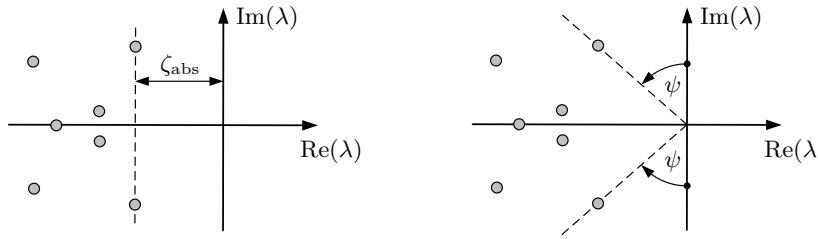

(a) Degree of stability ζ_{abs}. **(b)** Damping ratio $\zeta_{\text{rel}} = \sin\psi$.

Figure 2.2: Geometric interpretation of quantitative stability measures.

2.3 Damping mechanisms and modeling

Damping of a vibrating structure is the irreversible transition of mechanical energy into other forms of energy. This includes the interaction of structures with adjacent fluids, friction between components, and energy dissipation within materials [174]. While mass and stiffness matrices can be precisely determined from geometry and material parameters, damping often is not well defined and has to be identified experimentally. As Scanlan [149] pointed out, the specific mechanisms of energy dissipation are not completely understood and thus any mathematical representation of damping in the equations of motion is only an approximation of the underlying true physical process. In many cases, however, there are models yielding acceptable results. Among these are the phenomenological models of viscous damping, material damping, and friction damping [122].

2.3.1 Viscous damping

The most common approach to model damping mathematically is to assume viscous damping, which may be used for linear and nonlinear damping mechanisms. In the vast majority of engineering applications, energy dissipation can sufficiently be described by an equivalent viscous damping. In analogy to the functionals of the kinetic energy and the potential energy in Eq. (2.13), Rayleigh [166] introduced the dissipation function

$$\mathcal{D} := \frac{1}{2}\dot{\mathbf{q}}^{\mathrm{T}}\mathbf{D}\dot{\mathbf{q}}, \tag{2.23}$$

which is a quadratic form in the generalized velocities $\dot{\mathbf{q}}$. This scalar function represents half the time rate of change of the energy dissipation due to viscous damping. The corresponding vector of generalized non-conservative forces in Lagrange's equations (2.1) is given by

$$\mathbf{g} = -\frac{\partial \mathcal{D}}{\partial \dot{\mathbf{q}}}. \tag{2.24}$$

The resulting damping force arising, for example in liquid lubrication between moving parts, is directly proportional to the relative velocity of the two ends of the damping device.

A special case of the viscous damping model is frequently referred to as classical damping [2]. The equations of motion of classically damped **MDK**-systems can be decoupled in the real domain. For this purpose, the modal transformation matrix $\mathbf{R} = (\mathbf{r}_1\ \mathbf{r}_2\ \ldots\ \mathbf{r}_n)$ is used, which is defined by the eigenvectors of the corresponding undamped system. The resulting coefficient matrices $\mathbf{R}^{\mathrm{T}}\mathbf{M}\mathbf{R}$, $\mathbf{R}^{\mathrm{T}}\mathbf{D}\mathbf{R}$, and $\mathbf{R}^{\mathrm{T}}\mathbf{K}\mathbf{R}$ are inherently diagonalized. Thus, the system can be treated as a collection of single degree of freedom oscillators [43]. Caughey & O'Kelly [20,21] established that the power series representation

$$\mathbf{D} = \sum_{i=1}^{n} \alpha_i \mathbf{M} \left(\mathbf{M}^{-1}\mathbf{K}\right)^{i-1}, \qquad \alpha_i \in \mathbb{R}, \tag{2.25}$$

defining the damping matrix in terms of the mass and the stiffness matrix, is a necessary and sufficient condition fulfilling this requirement. An alternative variant of this formulation is given by Adhikari [1]. Experimental modal testing suggests, however, that the assumption of classical damping is invalid for many engineering applications [155].

In the absence of precise knowledge of the distribution of energy dissipation, the damping matrix is commonly expressed as a linear combination of mass and stiffness matrix

$$\mathbf{D} = \alpha_1\mathbf{M} + \alpha_2\mathbf{K}, \tag{2.26}$$

corresponding to the first two terms of Caughey series (2.25). This approach is usually referred to as Rayleigh damping since it is ascribed to his assertion of damped systems possessing classical normal modes [166]. In literature, the mass matrix proportional part $\alpha_1\mathbf{M}$ is sometimes associated with external damping, whereas the stiffness matrix proportional part $\alpha_2\mathbf{K}$ is often referred to as inner or material damping.

On the one hand, in systems of type **MDK**, the specific structure of the damping matrix plays a minor role for the study of free and forced vibrations. Approach (2.26) may lead to satisfying results, particularly for weakly damped systems. On the other hand, systems containing circulatory and gyroscopic terms can be very sensitive to the structure of **D**, which may have a significant influence on their stability boundary, cf. section 2.2.1. This be-

havior is demonstrated by a simple numerical example with two degrees of freedom featuring the matrices

$$\mathbf{M} = \begin{pmatrix} 1 & 0 \\ 0 & 1 \end{pmatrix}, \quad \mathbf{G} = \begin{pmatrix} 0 & \gamma \\ -\gamma & 0 \end{pmatrix}, \quad \mathbf{K} + \mathbf{N} = \begin{pmatrix} \omega_1^2 & \nu \\ -\nu & \omega_2^2 \end{pmatrix}. \tag{2.27}$$

The damping matrix is of form (2.26), where α_1 and α_2 are real positive scalars. In this example, the dimensionless parameters are set to $\omega_1^2 = 2$, $\omega_2^2 = 1$, $\nu = 0.499$, and $\gamma = 0.005$. The resulting stability map in the α_1-α_2-plane is shown in Fig. 2.3a. For $\alpha_1 > 0.04$, the trivial solution is asymptotically stable for any value of α_2, while its stability strongly depends on the inner damping $\alpha_2\mathbf{K}$ for $\alpha_1 < 0.02$. In this region, asymmetrical damping introduced by the unequal circular eigenfrequencies ω_1 and ω_2 cannot be compensated by the symmetric, mass proportional terms such that adding damping by increasing α_2 contributes to destabilization.

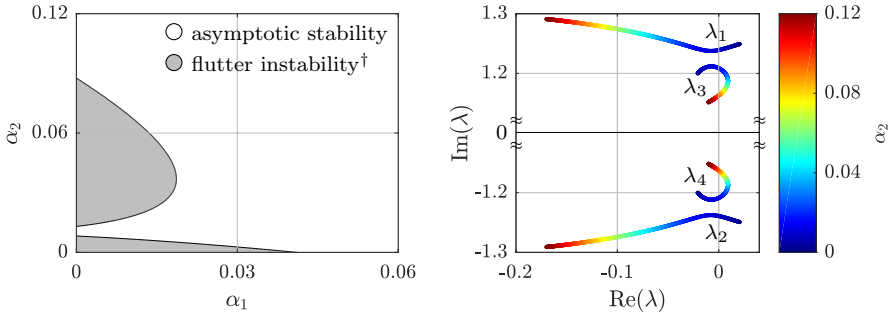

(a) Stability map in the α_1-α_2-plane. **(b)** Root loci of eigenvalues for $\alpha_1 = 0$.

Figure 2.3: Stability of a **MDGKN**-system with $n = 2$ and RAYLEIGH damping.

Fig. 2.3b features the root loci of the complex eigenvalues for $\alpha_1 = 0$ and variation of α_2. In the undamped case ($\alpha_1 = \alpha_2 = 0$), the eigenvalue pair $\lambda_{3,4}$ lies in the open left half of the complex plane, while $\lambda_{1,2}$ lies in the open right half. The trivial solution is thus unstable. With growing inner damping $\alpha_2\mathbf{K}$

†This type of instability occurs when a pair of complex conjugate eigenvalues with $\mathrm{Im}(\lambda) \neq 0$ crosses the imaginary axis.

the real part of $\lambda_{1,2}$ moves in negative direction, whereas the real part of $\lambda_{3,4}$ initially increases but remains negative. For $0.008 < \alpha_2 < 0.013$, the trivial solution is asymptotically stable followed by an unstable behavior when $\lambda_{3,4}$ crosses the imaginary axis. The real part of eigenvalue pair $\lambda_{3,4}$ continues to increase with α_2 until a maximum value is reached. Subsequently, this motion is reversed leading to an asymptotically stable solution for $\alpha_2 > 0.087$. A conclusion drawn from this example is the strong dependence of the damping effect in gyroscopic and circulatory systems ($\mathbf{G} \neq \mathbf{0}$, $\mathbf{N} \neq \mathbf{0}$) on the structure of the damping matrix.

2.3.2 Material damping

In solid materials subject to cyclic loads, a portion of the deformation energy is irreversibly converted into heat through a variety of physical mechanisms, e.g. dislocations, grain boundaries, and atomic motion [112]. The inherent energy loss per unit volume during one hysteresis cycle of period T is given by

$$W_D = \oint \sigma \, \mathrm{d}\varepsilon = \int_0^T \sigma(t)\dot{\varepsilon}(t) \, \mathrm{d}t, \tag{2.28}$$

where σ is the stress and ε is the strain. In the ε-σ-plane plotted in Fig. 2.4a, W_D geometrically depicts the area enclosed by the hysteresis loop, which is elliptical for linear viscoelastic solids [14, 150].

Despite Lazan [112] elaborating on its deficiencies, a suitable approximation of this behavior is the Kelvin-Voigt model, which consists of a massless viscous damper (damping coefficient d) connected in parallel with a massless elastic spring (stiffness coefficient k). The total force acting in the direction of motion is comprised of the sum of spring and damper force. Assuming harmonic excitation of the form

$$q = \hat{q} \cos(\Omega t + \varphi), \tag{2.29}$$

yields the energy loss over one period $T = 2\pi/\Omega$ which is given by

$$W_D^v = \pi d \Omega \hat{q}^2. \tag{2.30}$$

This energy loss is proportional to the excitation frequency Ω and to the square of the amplitude $\hat{q}$. Experiments reveal that many materials undergoing cyclic loading exhibit energy losses which are proportional to the amplitude squared but do not vary with frequency. The independence of frequency variation is an approximation, yet it applies for a wide frequency range [9, 87]. This implies

$$W_D^m = \pi \chi k \hat{q}^2, \tag{2.31}$$

with the dimensionless loss factor χ being an aggregate of energy dissipation due to numerous microscopic sources and mechanisms characteristic for the given material and structure. From a continuum mechanical perspective, the loss factor corresponds to the complex YOUNG's modulus

$$E = E_s \left(1 + \mathrm{i}\, \chi\right), \tag{2.32}$$

where E_s is the storage modulus and χ is the tangent of the phase angle describing the time displacement by which the stress leads the strain [105]. Comparison of Eq. (2.30) and Eq. (2.31) leads to the definition of the equivalent viscous damping coefficient

$$d_{\mathrm{eq}}^m = \frac{\chi k}{\Omega} \tag{2.33}$$

satisfactorily replacing a system with material damping by its viscous equivalent, which is defined by the same energy loss per cycle [27]. This is indicated in Fig. 2.4b, where the frequency dependence of the energy dissipation of a system with material damping is compared to a viscously damped system. While the requirement $W_D^v = W_D^m$ is fulfilled exactly at the circular reference frequency Ω_{ref}, the effective damping is overestimated for $\Omega > \Omega_{\mathrm{ref}}$ and underestimated for $\Omega < \Omega_{\mathrm{ref}}$.

In general, the law of material damping is restricted to harmonically excited systems with one degree of freedom. It is unknown for systems with multiple modes and no external excitation (oscillations are self-excited) [135]. Nevertheless, the procedure of assigning an equivalent damping applied to homogeneous systems with $n > 1$ may yield acceptable results if $\chi \ll 1$, i.e. the damping forces do not change the modes of vibration [22, 27, 46]. In fact,

the values for loss factors encountered in practice range from $\chi = 2 \times 10^{-5}$ for aluminum [8] to $\chi = 10^{-1}$ for cast iron [112], which justifies the assumption of weakly damped solutions. In analogy to Eq. (2.33), the equivalent viscous damping matrix is given by

$$\mathbf{D}_m = \frac{1}{\Omega} \sum_{i=1}^{l} \chi_i \mathbf{K}_i, \tag{2.34}$$

with l appropriate values of χ_i and $\mathbf{K}_i$ in each elastic component of the system. Since Ω is unknown until the homogeneous equations of motion are solved, it is often replaced by a conservatively chosen circular reference frequency Ω_{ref} larger than the actual Ω. This assures that the effective damping is not overestimated in the frequency range of interest.

The representation of equivalent viscous damping in Eq. (2.33) and Eq. (2.34) has physical limitations. As noted by CRANDALL [27] and SCANLAN [149], the assumption of a frequency-independent loss factor χ is non-causal, i.e. the response anticipates the excitation, leading to physically unfeasible results in the time domain. However, since many problems in vibration theory are analyzed within a limited frequency range, the approach remains applicable.

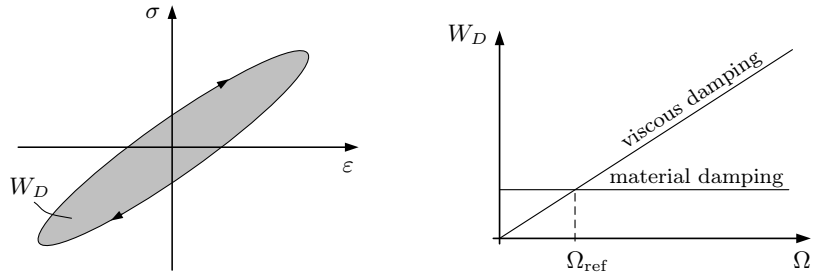

(a) Closed elliptical hysteresis loop in simple harmonic motion.

(b) Energy dissipation per cycle as a function of the circular frequency.

Figure 2.4: Features of the material damping model.

2.3.3 Friction damping

Another source of energy dissipation in vibrating structures is non-viscous damping due to dry friction generated by the relative motion of two solid surfaces in contact. This concerns, for example, the interface between the brake pad and the brake disc as well as riveted, bolted, glued, and keyed joints in assembled structures [7,15,45,145]. Especially in metal structures, damping resulting from joints is typically much higher than material damping [152]. A simplified phenomenological description of sliding friction is governed by COULOMB's law

$$F_R = -\mu F_N \operatorname{sgn}(\dot{q}) \tag{2.35}$$

relating the friction force F_R with the normal force F_N and the constant kinetic friction coefficient μ [30]. A change in sign of the relative velocity $\dot{q}$ causes a discontinuous change of the direction of the friction forces acting on the system, i.e. the transition between stick and slip is unsteady. As illustrated in [72] and later in [69, 71], the kinematic linearization of Eq. (2.35) causes both velocity proportional and coordinate proportional terms in the equations of motion (2.7). These terms are not necessarily symmetric for systems with at least two degrees of freedom. COULOMB friction therefore not only has a stabilizing influence, its circulatory parts may furthermore lead to flutter instability depending on the relation of all matrices involved.

Under the assumption of a relative displacement of form (2.29), the area enclosed by the rectangular shaped hysteresis loop is proportional to the absolute value of the friction force and to the first power of the amplitude. This area is thus expressed as

$$W_D^c = 4\mu F_N \hat{q}. \tag{2.36}$$

The energy balance of Eq. (2.30) and Eq. (2.36) leads to the equivalent viscous damping coefficient

$$d_{\mathrm{eq}}^c = \frac{4\mu F_N}{\pi \Omega \hat{q}}, \tag{2.37}$$

which in contrast to Eq. (2.33) depends on the amplitude $\hat{q}$ and thus leads to the conclusion that COULOMB friction represents a nonlinear form of damping.

The description of friction according to Eq. (2.35) does not allow elastic deformations prior to interfacial slip; it merely accounts for sliding of the entire surface. A solution to this fundamental drawback is the JENKIN-element, which is ascribed to MASING [124]. He used a parallel distribution of these elements to model the dynamical behavior of mechanical joints. The JENKIN-element is a combination of a linear elastic spring connected in series with an ideal COULOMB friction damper. It is characterized by the tangential contact stiffness k, the preload F_N, as well as the static and kinetic friction coefficient μ_0 and μ, respectively. Based on the assumption of harmonic motion of form (2.29), the dissipated energy per cycle of oscillation is

$$W_D^j = 4\mu F_N \hat{q} \left(1 - \frac{\mu F_N}{k\hat{q}}\beta\right), \tag{2.38}$$

where the relation $\mu_0 > \mu$ is considered by the correction factor

$$\beta = 1 - \frac{1}{4}\left(\frac{\mu_0}{\mu} - 1\right)^2. \tag{2.39}$$

As demonstrated in [99], equating the potential energies of the KELVIN-VOIGT-element with the JENKIN-element yields the equivalent nonlinear stiffness

$$k_{\mathrm{eq}}^j = \begin{cases} k & \text{if } |\hat{q}| < q_{\mathrm{tr}} \\ \frac{\mu^2 F_N^2}{k\hat{q}^2} & \text{if } |\hat{q}| \geq q_{\mathrm{tr}} \end{cases}. \tag{2.40}$$

In a similar manner, the balance of dissipated energies of the respective model results in the equivalent nonlinear damping coefficient

$$d_{\mathrm{eq}}^j = \begin{cases} 0 & \text{if } |\hat{q}| < q_{\mathrm{tr}} \\ \frac{4\mu F_N}{\pi\Omega|\hat{q}|}\left(1 - \frac{\mu F_N \beta}{k|\hat{q}|}\right) & \text{if } |\hat{q}| \geq q_{\mathrm{tr}} \end{cases}. \tag{2.41}$$

From Eq. (2.40) and Eq. (2.41) it becomes apparent that the JENKIN-element can adopt two different states. First, if the slider is stuck, there is no energy dissipation and the model behaves like a linear elastic spring with constant stiffness. Second, once the amplitude exceeds the static threshold

$$q_{\mathrm{tr}} := \frac{\mu_0 F_N}{k}, \tag{2.42}$$

the sliding motion triggers COULOMB damping which acts in parallel with the spring. As evident from Fig. 2.5, the equivalent stiffness declines with $1/\hat{q}^2$ after reaching amplitude threshold (2.42), while the equivalent damping exhibits a sharp initial increase. When d_{eq}^{j} reaches its maximum at $|\hat{q}| = \frac{2\beta\mu}{\mu_0} q_{\mathrm{tr}}$, the equivalent stiffness has dropped to $\frac{k}{4\beta^2}$, i.e. approximately one quarter of its original value. The maximum possible energy dissipation is proportional to the ratio between contact stiffness and the product of oscillation frequency and correction factor (2.39). It does not explicitly depend on the friction coefficient. For amplitudes $\hat{q}$ approaching infinity, the equivalent stiffness and damping coefficients decay to zero. The points specifying the analytical damping maximum in Fig. 2.5b apply for the range $1 \leq \frac{\mu_0}{\mu} \leq \sqrt{3}$. This requirement on the ratio between static and kinetic friction coefficient is fulfilled for most technically relevant material pairings [109].

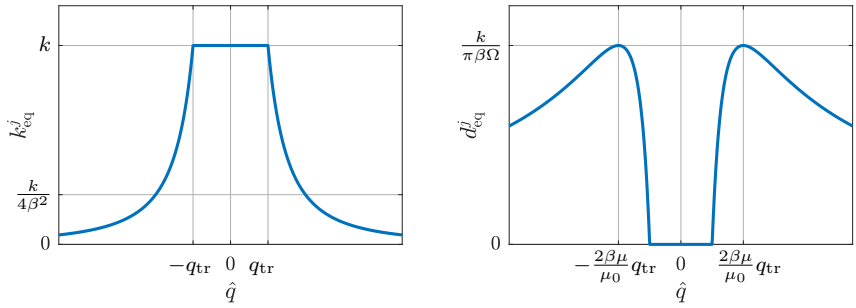

(a) Equivalent stiffness. **(b)** Equivalent damping.

Figure 2.5: Amplitude-dependent properties of the JENKIN-element.

2.4 Damping optimization

The dynamical behavior of system (2.9) is considered to depend smoothly on a vector of real parameters $\boldsymbol{\alpha} \in \mathbb{R}^s$ whereby the eigenvalues λ of the governing coefficient matrix $\mathbf{A}$ are continuous functions of $\boldsymbol{\alpha}$. In engineering, the s independent parameters can be varied within a limited range, the objective

typically being that random perturbations from the trivial solution decay to zero in the fastest possible way. This involves the eigenvalue with largest real part to be as negative as possible. Despite a weak sensitivity of the real part of $\lambda(\boldsymbol{\alpha})$ to a variation of mass and stiffness properties, the focus often lies on structural optimization [52, 162]. Wagner [179], for example, successfully separated neighboring eigenfrequencies of brake rotors through geometrical modifications in order to suppress self-excited oscillations in a certain frequency band.

In this thesis, the emphasis is on the determination of favorable damping configurations including the tailoring of damper viscosities as well as the location of the most desirable damper positions. In connection with the quantitative stability criteria defined in section 2.2.2, the parameter optimization requires either the degree of stability ζ_{abs} or the damping ratio ζ_{rel} to be as large as possible. This is mathematically stated as

$$\zeta_{\text{abs}} \rightarrow \max_{\boldsymbol{\alpha}} \quad \text{or} \tag{2.43a}$$

$$\zeta_{\text{rel}} \rightarrow \max_{\boldsymbol{\alpha}}, \tag{2.43b}$$

where, depending on the problem, additional restrictions can be imposed on $\boldsymbol{\alpha}$ and λ. For instance, equality constraints $\mathbf{c}_{\text{eq}}(\boldsymbol{\alpha}) = \mathbf{0}$ and inequality constraints $\mathbf{c}(\boldsymbol{\alpha}) \leq \mathbf{0}$ limit the admissible parameter space, while conditions $f_{\text{lb}} \leq |\max_i \operatorname{Im}(\lambda_i)| \leq f_{\text{ub}}$ keep the frequency within a desired range of interest [173]. Optimization problem (2.43) is nonlinear since the stability measures ζ_{abs} and ζ_{rel} exhibit points of infinite slope when varying the parameters $\boldsymbol{\alpha}$ [25]. A further complication is due to the required solution of an eigenvalue problem in each evaluation of the objective function. As a consequence, numerical treatment becomes expensive when dealing with systems with many degrees of freedom.

From a mathematical programming perspective, the lack of a bounded gradient of the objective functions ζ_{abs} and ζ_{rel} in Eq. (2.43) requires the adoption of a direct search approach. Unlike more traditional optimization techniques, which use information about the derivatives of the cost function, direct search algorithms compare a set of trial points neighboring the current solution. The algorithm searches for points at which the value of the objective function is

lower than the value at the current solution. There are numerous direct search techniques available, such as the methods described by Hooke & Jeeves [75] as well as Nelder & Mead [133]. More examples are given in the review articles [115] and [147].

One of the most common approaches is the generalized pattern search algorithm possessing proven global convergence properties [113,114,171]. Starting from an initial point, the algorithm computes a set of trial points (mesh) which is formed by adding the starting point to a scalar multiple (step length) of a set of vectors (pattern). The search directions are specified by the number of independent variables, i.e. the patterns are usually positive bases with a cardinality between $s+1$ and $2s$ spanning the parameter space $\mathbb{R}^s$. An iteration is successful if there exists a point in the mesh which improves the objective function. While in the opportunistic poll strategy this point becomes the new starting point in the next iteration step, the complete poll strategy evaluates all points of the mesh and chooses the point with smallest objective function value. At the end of each successful iteration, the step length is potentially increased. If the iteration fails to identify a better point, the step length is reduced by a half and the poll continues from the current point. Iteration steps are repeated until a stopping criterion is satisfied, e.g. the step length is sufficiently small or the number of iterations exceeds a predefined value.

The provided optimum is not guaranteed to be global. However, the pattern search solver implemented in Matlab's global optimization toolbox is designed to search through more than one basin of attraction if neighboring points belong to different basins [125]. Therefore, this toolbox in conjunction with the generalized pattern search algorithm described above is used for the computation of all optimization problems formulated in this work.

Reviewing the literature on damping optimization, little is known about the passive assignment of eigenvalues affected by circulatory and gyroscopic terms. The only approach for pole placement by means of passive damping control in self-excited systems is suggested by Ouyang [140]. In contrast, a large number of publications has been devoted to optimum damping in systems of type **MDK** when the respective matrix structure is restricted to particular subclasses. Cox [25], for instance, addressed optimization problem (2.43a)

by numerical means using a derivative-free direct search method. Moreover, he obtained exact analytical solutions within the class of systems possessing classical normal modes and established mass proportional damping to be a maximizer of the degree of stability [26]. His findings have been generalized by Freitas & Lancaster [39] who provided the best possible decay rate for the mechanical energy and showed its attainability for more than one damping matrix. Under certain conditions, this matrix does not necessarily have to be positive definite. More recently, Kuzmanović et al. [110] presented explicit formulas for optimal parameters when $\mathbf{D}$ is either proportional to the mass matrix or to the stiffness matrix. In the case of Rayleigh damping, i.e. the damping matrix is a linear combination of both the mass and the stiffness matrix, they showed the optimum configuration to be a unique solution of a system of two nonlinear equations.

Aside from optimization criteria (2.43), which are based on the spectrum of $\mathbf{A}$, another category concerns the minimization of the total mechanical energy of the system. This is equivalent to minimizing either the trace or a norm of a solution of the corresponding Lyapunov matrix equation [131,175]. Optimization problems of this form have been intensively studied, for example, in [10, 17, 132, 172] and the references therein.

3 Stability of a two degree of freedom MDGKN-system

This chapter covers effects of velocity proportional terms on the stability of linear circulatory systems for the particular case $n = 2$. The study includes analyses of the explicit stability boundary with regard to different structures of the damping matrix, the role of gyroscopic terms, and the spacing of the eigenfrequencies. The results presented resume and extend prior investigations originally published in [83].

3.1 Derivation of the stability boundary

Although many problems in mechanical engineering are inherently nonlinear, a standard stability analysis approach involves linearizing the equations of motion around an equilibrium. For the study of self-excited vibrations, the resulting system of second order differential equations is of type (2.7) when time-variance is neglected. The 2×2 system matrices

$$\begin{aligned} \mathbf{M} &= \begin{pmatrix} 1 & 0 \\ 0 & 1 \end{pmatrix}, \quad \mathbf{D} = \delta \begin{pmatrix} 1 & d_{12} \\ d_{12} & d_{22} \end{pmatrix}, \quad \mathbf{G} = \delta \begin{pmatrix} 0 & \gamma \\ -\gamma & 0 \end{pmatrix}, \\ \mathbf{K} &= \begin{pmatrix} \omega_1^2 & 0 \\ 0 & \omega_2^2 \end{pmatrix}, \quad \mathbf{N} = \begin{pmatrix} 0 & \nu \\ -\nu & 0 \end{pmatrix} \end{aligned} \tag{3.1}$$

characterize inertial, damping, gyroscopic, stiffness, and circulatory forces, respectively. Without loss of generality, they are taken to be normalized with respect to the mass matrix. The corresponding orthogonal transformation leads to a diagonal stiffness matrix with the diagonal elements being the squares of the undamped circular eigenfrequencies ω_1 and ω_2. Unless the system is classically damped, the normalization does not necessarily yield a

diagonal damping matrix. This is accounted for by d_{12} and d_{22} which describe the structure of $\mathbf{D}$, while its magnitude is defined by the scaling factor δ. The formulation according to Eq. (3.1) has seven free parameters and is the most general form a linear, autonomous two degree of freedom system can adopt. The small number of variables enables an analytical evaluation of the influence of different terms on stability.

First, the stability behavior of the underlying **MKN**-system is discussed with the velocity proportional matrices set to zero. In this case, the $2n$ roots of characteristic polynomial (2.12) are

$$\lambda^2 = -\frac{1}{2}\left(\omega_1^2 + \omega_2^2 \pm \nu\sqrt{\vartheta^2 - 4}\right). \tag{3.2}$$

Therein, the dimensionless ratio

$$\vartheta := \frac{\omega_1^2 - \omega_2^2}{\nu} \tag{3.3}$$

is a quantitative measure of the spacing of two neighboring circular eigenfrequencies. The difference is induced, for example, by asymmetric stiffness properties, where asymmetry in the sense used here refers to a non-uniform distribution over the modes considered. Depending on the absolute value of ϑ, two cases of stability behavior can be distinguished. For $|\vartheta| \geq 2$, all eigenvalues λ_i $(i = 1, \ldots, 4)$ are purely imaginary and the **MKN**-system is marginally stable. In contrast, it is exponentially unstable for $|\vartheta| < 2$ since λ^2 is no longer an element of the set of real negative numbers and the square root of an expression of the form $x + \mathrm{i}\, y$ $(x,\, y \in \mathbb{R}_{\neq 0})^{\dagger}$ always has a solution with positive real part [18]. The split between neighboring eigenfrequencies causes ϑ to increase which contributes to stabilization, whereas circulatory terms have a destabilizing effect. In the absence of damping, double eigenfrequencies ($\vartheta = 0$) therefore generically lead to instability independent of the magnitude of the circulatory terms. This does not only hold for the special case of two degrees of freedom but also for arbitrarily large n [163].

Second, the stability boundary of the complete **MDGKN**-system defined by matrices (3.1) is derived analytically by applying the necessary and suffi-

[†] $\mathbb{R}_{\neq 0} = \{x \in \mathbb{R} \,|\, x \neq 0\}$

cient criterion of Liénard and Chipart, cf. section 2.2.1. For two-dimensional systems, conditions (2.19) simplify to

$$a_4 > 0, \quad H_3 = \begin{vmatrix} a_1 & a_0 & 0 \\ a_3 & a_2 & a_1 \\ 0 & a_4 & a_3 \end{vmatrix} > 0, \quad a_2 > 0, \quad H_1 = a_1 > 0, \tag{3.4}$$

where the boundary between the asymptotically stable and unstable regime is given by Eq. (2.20) leading to

$$a_4 H_3 = 0. \tag{3.5}$$

The coefficient $a_4 = \nu^2 + \omega_1^2 \omega_2^2$ is always positive given that the governing parameters ω_1, ω_2, and ν are non-zero. The boundary of flutter-type instability is thus determined by $H_3 = 0$ which yields the critical damping factor

$$\delta^2_{\text{crit}} := \frac{\nu^2 \left[(d_{22}+1)^2 + 2\gamma\vartheta\,(d_{22}-1) - d_{22}\vartheta^2 + 4\gamma^2 \right]}{(d_{22}+1)\,(d_{22} - d_{12}^2 + \gamma^2)\,(d_{22}\omega_1^2 + \omega_2^2 + 2\gamma\nu)}. \tag{3.6}$$

As a consequence, system (2.7) along with matrices (3.1) is asymptotically stable if and only if

$$\delta^2 > \delta^2_{\text{crit}} \quad \text{if} \;\; d_{22} \geq d_{12}^2 - \gamma^2, \tag{3.7a}$$

$$\delta^2 < \delta^2_{\text{crit}} \quad \text{if} \;\; d_{22} < d_{12}^2 - \gamma^2. \tag{3.7b}$$

Criterion (3.7a) corresponds to the standard case occurring in most technically relevant applications with an at least positive semi-definite damping matrix, i.e. $d_{22} \geq d_{12}^2$. Criterion (3.7b) covers the case of indefinite damping. These necessary and sufficient stability conditions are a generalization of those published by Hagedorn et al. [60] in which neither gyroscopic effects nor off-diagonal damping terms are accounted for. The critical damping factor presented therein is naturally included in Eq. (3.6) as a special case for $d_{12} = \gamma = 0$. A similar criterion is obtained by Spelsberg-Korspeter [163] following a perturbational approach. His approximation applies for arbitrary n but is restricted to small velocity proportional and circulatory terms and can only be evaluated numerically.

3.2 Influence of velocity proportional terms

3.2.1 General observations

Since this study focuses on the influence of damping on stability, the major qualitative properties of Eq. (3.6) are analyzed in the d_{22}-δ-plane shown in Fig. 3.1. Without damping, the underlying **MKN**-system is assumed to be marginally stable ($|\vartheta| > 2$) and the stability domains are identified using criteria (3.7). The graph is split into two sections via the pole at $d_{22} = d_{12}^2 - \gamma^2$. To achieve asymptotic stability, the scaling factor δ has to be smaller than δ_{crit} on the left side, while it has to exceed the critical value on the right side. For large values of d_{22}, the limit of the stability boundary approaches zero, i.e. $\lim_{d_{22}\to\infty} \delta_{\text{crit}} = 0$.

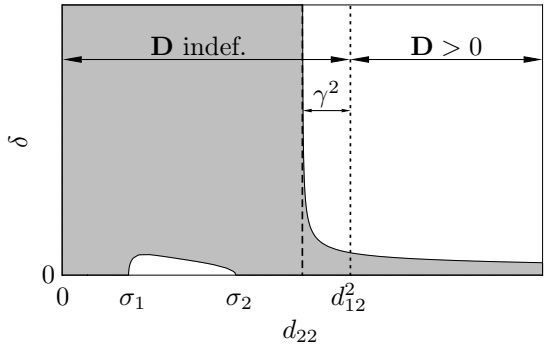

Figure 3.1: Qualitative attributes of stability boundary (3.6). ○ asymptotic stability, ◍ flutter instability.

From Fig. 3.1 it is apparent that an indefinite damping matrix originating from large off-diagonal damping terms ($d_{12}^2 > d_{22}$) is not sufficient for instability. In the area above δ_{crit} bounded by the dashed and the dotted line, all eigenvalues lie in the open left half of the complex plane although the damping matrix is indefinite. The same applies to the area bounded by the roots

$$\sigma_{1,2} = \underbrace{\frac{1}{2}\vartheta^2 - \gamma\vartheta - 1}_{=:\sigma_0} \mp \underbrace{\frac{1}{2}\sqrt{(\vartheta^2-4)\,(\vartheta-2\gamma)^2}}_{=:\Delta\sigma}, \tag{3.8}$$

which determine the stability boundary for infinitesimally small damping implying that stabilization can be achieved by a damping matrix of arbitrarily small norm. In this case, however, δ needs to be smaller than the critical value for all eigenvalues to have strictly negative real part. Other factors influencing the qualitative behavior of Eq. (3.6) are the velocity proportional terms γ and d_{12}, the latter of which move the pole of δ_{crit} in positive d_{22}-direction. To a certain degree, off-diagonal damping terms compensate the positive effect of diagonal damping and thus contribute to destabilization. Gyroscopic terms have two contrary aspects. They move both the pole of δ_{crit} and the roots $\sigma_{1,2}$ in negative d_{22}-direction. While the pole movement generally diminishes the instability regime, large values of γ may prevent the stability boundary to possess positive real roots, i.e. $\sigma_{1,2} \in \mathbb{R}_{\geq 0}$[†], which cancels the phenomenon of asymptotic stability due to infinitesimally small damping.

The approach of Liénard & Chipart [116] used to derive stability boundary (3.6) is necessary and sufficient. Alternative methods are merely sufficient for stability, such as the criteria introduced by Frik [40] as well as Kliem & Pommer [101,102]. In Fig. 3.2, these methods are compared qualitatively to the exact solution for two different parameter configurations. Configuration 3.2a features a system of type **MDKN** with diagonal damping matrix and configuration 3.2b covers a numerical example with only non-zero parameters. The colored areas below the respective critical damping factor depict flutter instability, where the stability boundary for symmetric stiffness properties ($\vartheta = 0$) is given by the dashed line.

In both configurations, the instability domains predicted by the sufficient criteria are larger and thus more conservative than those determined by Eq. (3.6) and Eq. (3.7). Since the latter are necessary and sufficient, they naturally imply the result obtained by complex eigenvalue analysis of coefficient matrix (2.10). In comparison to the criteria of Frik [40] and Kliem & Pommer [101], which both delineate the same stability boundary, the criterion of Kliem & Pommer [102] coinciding with $\vartheta = 0$ in configuration 3.2a performs more accurately. The former criteria are neither able to reproduce the pole of δ_{crit} nor its limit for large values of d_{22} (there always remains an offset). In

[†] $\mathbb{R}_{\geq 0} = \{x \in \mathbb{R} \,|\, x \geq 0\}$

contrast, the latter criterion approaches the exact solution for these extreme points. As a consequence, the method of Kliem & Pommer [102] is capable of predicting asymptotic stability when the damping matrix is indefinite in configuration 3.2b. This does not hold for the other two sufficient criteria which do not account for the stabilizing effects of the spacing of the eigenfrequencies and the gyroscopic terms. In both configurations, the stability boundary is more conservative than the dashed line representing the case of double eigenfrequencies. Besides, none of the sufficient criteria is able to capture the correct roots. For configuration 3.2b, the approach of Kliem & Pommer [102] predicts a particular d_{22} at which the system can be stabilized asymptotically by adding arbitrarily small damping even if this point does not match the correct $\sigma_{1,2}$. In this configuration, the theorem holds to model the destabilization paradox which states that adding diagonal damping for a given δ may lead to instability. In contrast, in configuration 3.2a, this is only accounted for by the Liénard-Chipart criterion. From a numerical perspective, the procedure of finding suitable matrices satisfying Lyapunov's matrix equation is cumbersome. For this reason, the computational cost when applying the criteria of Kliem & Pommer [101, 102], which both are based on Lyapunov's direct method, is higher compared to all other approaches mentioned.

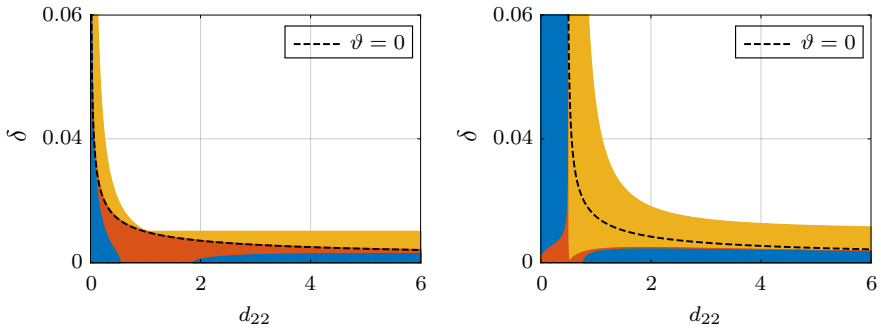

(a) $\gamma = 0$, $d_{12} = 0$. **(b)** $\gamma = 0.4$, $d_{12} = -0.8$.

Figure 3.2: Comparison of instability domains obtained by different criteria. ● Liénard & Chipart [116]; ● Kliem & Pommer [102]; ● Frik [40], Kliem & Pommer [101].

3.2.2 Infinitesimally small damping

A peculiar characteristic of circulatory systems is their potential to be asymptotically stable with a damping matrix of arbitrarily small norm. The stability boundary is described by the critical values σ_1 and σ_2 of Eq. (3.8). Depending on the absolute ratio between the spacing of the eigenfrequencies and the circulatory terms, three different cases can be distinguished, cf. Table 3.1. A necessary condition for all eigenvalues to have strictly negative real part with infinitesimally small damping is a marginally stable **MKN**-system. This behavior ensures the critical values $\sigma_{1,2}$ to be an element of the set of real numbers. For the limit case of $|\vartheta| = 2$, the condition $d_{22} = \sigma_0 > d_{12}^2$ has to be satisfied requiring a positive definite damping matrix. In contrast, for the case where $|\vartheta| > 2$, the diagonal damping coefficient d_{22} can be chosen within the finite interval (σ_1, σ_2) and the damping matrix does not necessarily have to be positive definite for asymptotic stabilization.

underlying **MKN**-system	$\lvert\vartheta\rvert$	asymptotic stability with infinitesimally small δ if
marginally stable	> 2	$\sigma_1 < d_{22} < \sigma_2$
	$= 2$	$d_{22} = \sigma_0 > d_{12}^2$
unstable	< 2	–

Table 3.1: Necessary conditions for asymptotic stability with a damping matrix of arbitrarily small norm.

According to Eq. (3.8), the distance between the two roots of the stability boundary as well as their position in space is subject to gyroscopic terms γ and the dimensionless ratio ϑ, which describes the spacing of the eigenfrequencies. The former move both roots in negative d_{22}-direction, while ϑ causes a shift of σ_1 in negative and σ_2 in positive direction. In technically relevant applications, damping coefficients are generally positive, i.e. $d_{22} > 0$. This requires at least one positive value of $\sigma_{1,2}$ for the eigenvalues to be in the open left half of the complex plane under the assumption of infinitesimally small damping. The phenomenon occurs when σ_0 is greater than zero and geometrically

corresponds to the area below the dashed line in Fig. 3.3a. In addition, all parameter combinations lying in the gray domain, the boundary of which is given explicitly by

$$\gamma_{1,2} = \frac{1}{4}\left(\vartheta \mp \sqrt{\vartheta^2 - 4}\right), \tag{3.9}$$

satisfy the requirement of one positive solution of Eq. (3.8). These configurations are characterized by asymptotic stabilization which can be achieved not only by an arbitrarily small δ but also by an arbitrarily small d_{22} since σ_1 is negative. In the blue region, where both roots of the stability boundary are elements of positive reals, this does not hold. For stabilization, d_{22} has to exceed the threshold $\sigma_1 > 0$. Therefore, marginally stable, non-gyroscopic systems of type (3.1) can always be stabilized asymptotically with a damping matrix of arbitrarily small norm since $\sigma_{1,2} > 0$ is guaranteed for $\gamma = 0$.

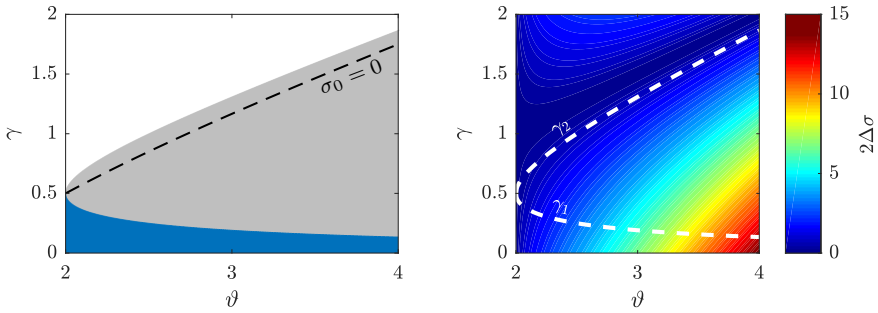

(a) Position of σ_1 and σ_2. ● $\sigma_{1,2} > 0$, ○ $\sigma_1 < 0 \wedge \sigma_2 > 0$, ○ $\sigma_{1,2} < 0$.

(b) Spacing between σ_1 and σ_2.

Figure 3.3: Properties of Eq. (3.8) in the ϑ-γ-plane.

As shown in Fig. 3.3b, the distance between σ_1 and σ_2 denoted by $2\Delta\sigma$ enlarges with increasing ϑ, yet it diminishes with growing γ. Therefore, asymmetric stiffness properties, which cause the separation of neighboring eigenfrequencies, contribute to stabilization. The asymmetry extends the region of possible configurations to achieve asymptotic stability with infinitesimally small damping. In order to ensure at least one positive solution of Eq. (3.8),

the respective gyroscopic terms need to be smaller than the critical value γ_2. For $\gamma > \gamma_2$, which corresponds to the white domain in Fig. 3.3a, both roots of the stability boundary are negative. The stabilization phenomenon with a damping matrix of arbitrarily small norm vanishes for this case due to an inherent positive value of $d_{22} > 0$ in most technical systems.

3.2.3 Incomplete damping

In systems with positive definite damping matrix, energy dissipation is distributed over all motions. Many technically relevant applications, however, possess a damping matrix which is only positive semi-definite. In this limiting case, damping is incomplete and the amplitudes of some motions may not continuously decay with time. Yet, the system can be asymptotically stable if the modes are coupled appropriately leading to pervasive dissipation. As examples, positive semi-definite damping matrices of the form

$$\mathbf{D}_1 = \delta \begin{pmatrix} 1 & 0 \\ 0 & 0 \end{pmatrix}, \tag{3.10a}$$

$$\mathbf{D}_2 = \delta \begin{pmatrix} 1 & -1 \\ -1 & 1 \end{pmatrix} \tag{3.10b}$$

are considered. In damping matrix (3.10a), the first degree of freedom is directly damped, while the second one remains undamped due to $d_{22} = 0$. In systems with damping according to Eq. (3.10b), both degrees of freedom are equally damped, where the off-diagonal damping terms have the same absolute value. Using these exemplary damping matrices stability boundary (3.6) simplifies to

$$\delta^2_{\mathrm{crit}_1} = \frac{\nu^2 \left(4\gamma^2 - 2\gamma\vartheta + 1\right)}{\gamma^2 \left(2\gamma\nu + \omega_2^2\right)}, \tag{3.11a}$$

$$\delta^2_{\mathrm{crit}_2} = \frac{\nu^2 \left(4\gamma^2 - \vartheta^2 + 4\right)}{2\gamma^2 \left(2\gamma\nu + \omega_1^2 + \omega_2^2\right)}, \tag{3.11b}$$

respectively. In a numerical example, the dimensionless parameters are set to $\omega_2 = 10$ and $\nu = 0.1$. The resulting stability boundaries are shown in Fig. 3.4,

where the regions of flutter instability are indicated by condition (3.7a). In the following, the two cases are discussed separately.

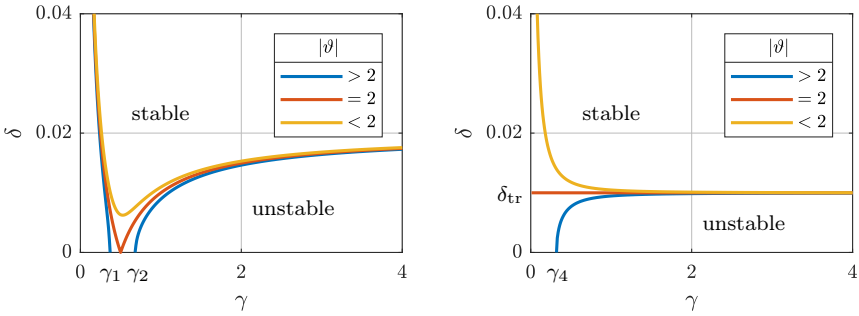

(a) Damping matrix (3.10a). **(b)** Damping matrix (3.10b).

Figure 3.4: Stability boundaries as a function of $|\vartheta|$ in the γ-δ-plane.

Damping matrix $\mathbf{D}_1$

It follows from Eq. (3.11a) that the critical damping coefficient becomes infinitely large as γ approaches zero, i.e. $\lim_{\gamma\to 0} \delta_{\mathrm{crit}_1} = \infty$. In the absence of gyroscopic effects, there is no finite value $\delta > 0$ satisfying stability criterion (3.7a). The second degree of freedom remains undamped since the modes are not coupled pervasively. Despite a possibly marginally stable undamped system, the resulting $\mathbf{MD}_1\mathbf{KN}$-system is exponentially unstable with arbitrary damping [61,129]. To achieve asymptotic stability, the gyroscopic terms need to be greater than zero, cf. Fig. 3.4a. Depending on the behavior of the underlying **MKN**-system, the stabilization can be obtained by adding infinitesimally small damping. Similar to section 3.2.2, three cases are distinguished. For $|\vartheta| > 2$, the gyroscopic terms are required to lie within the finite interval (γ_1, γ_2), where the roots $\gamma_{1,2}$ are determined explicitly by Eq. (3.9). In the limit case $|\vartheta| = 2$, stabilization is possible if γ equals exactly one half. Unstable **MKN**-systems cannot be stabilized with an arbitrarily small, positive semi-definite damping matrix of form (3.10a).

Damping matrix $\mathbf{D}_2$

In opposition to the first example, the limit of δ_{crit_2} for γ approaching zero depends on the stability behavior of the underlying **MKN**-system. Again, three cases are differentiated, cf. Tab. 3.2. For $|\vartheta| > 2$, the resulting $\mathbf{MD}_2\mathbf{KN}$-system is asymptotically stable with a damping matrix of arbitrarily small norm [129]. This stabilization is also possible for systems with $\gamma \neq 0$ if the gyroscopic terms lie within the finite interval $(0, \gamma_4)$. The right interval boundary is given explicitly by

$$\gamma_4 = \sqrt{\frac{1}{4}\vartheta^2 - 1}, \tag{3.12}$$

which is the positive root of Eq. (3.11b). In all other cases ($|\vartheta| \leq 2$), asymptotic stability cannot be achieved with infinitesimally small damping since the roots of the stability boundary are no longer an element of the set of real numbers. When $|\vartheta| = 2$, stability can be obtained if the damping factor δ exceeds a specific threshold value δ_{tr}. Unstable **MKN**-systems, where $|\vartheta| < 2$, cannot be stabilized by a positive semi-definite damping matrix of the form (3.10b) since there is no finite value $\delta > 0$ satisfying stability criterion (3.7a). The resulting $\mathbf{MD}_2\mathbf{KN}$-system is exponentially unstable for arbitrary damping, cf. Fig. 3.4b.

underlying **MKN**-system	$\lvert\vartheta\rvert$	$\lim_{\gamma\to 0} \delta_{\mathrm{crit}_2}$
marginally stable	> 2	$-\infty$
	$= 2$	$\delta_{\mathrm{tr}} := \sqrt{\frac{2\nu^2}{\omega_1^2+\omega_2^2}}$
unstable	< 2	∞

Table 3.2: Limit of stability boundary (3.11b) for γ approaching zero.

3.2.4 Indefinite damping

Aside from infinitesimally small or incomplete damping matrices, mechanical systems may also exhibit indefinite damping matrices. While the first two are

at least positive semi-definite and generally lead to energy dissipation, indefinite damping matrices act as a source of power and thus are able to generate and maintain self-excited vibrations. They frequently originate, for example, from kinematic linearization of friction forces arising at contact interfaces with COULOMB friction. As shown by KLIEM et al. [100,103] following a perturbational approach, circulatory systems may, in certain cases, be stabilized asymptotically despite this negative damping effect. Their approximation applies for arbitrary n but is restricted to small damping terms.

A non-gyroscopic system of type **MDKN** is therefore considered illustrating an example where this restriction does not hold. Setting $\gamma = 0$ in Eq. (3.6) yields the critical damping factor

$$\delta^2_{\mathrm{crit}_3} = \frac{\nu^2 \left[(d_{22}+1)^2 - d_{22}\vartheta^2 \right]}{(d_{22}+1)\,(d_{22}-d_{12}^2)\,(d_{22}\omega_1^2+\omega_2^2)} =: \frac{f_1}{f_2}, \tag{3.13}$$

where numerator and denominator are denoted by f_1 and f_2, respectively. The sign of these two functions is crucial for stability. First, the sign of f_2 merely depends on the structure of the damping matrix, i.e. the denominator function is positive for $\mathbf{D}$ being positive definite and is negative for an indefinite damping matrix[†], cf. Fig. 3.5b. The boundary $f_2 = 0$ between the respective domains is explicitly defined as

$$d_{12} = \sqrt{d_{22}}. \tag{3.14}$$

Second, the sign of f_1 depends on the dimensionless ratio ϑ and the diagonal damping coefficient d_{22}. In general, the larger the spacing of the eigenfrequencies, the more negative the numerator function and the more stable the undamped system becomes, cf. Fig. 3.5a. The boundary between the positive and negative domain is determined by the roots of Eq. (3.13) given by

$$|\vartheta| = \frac{d_{22}+1}{\sqrt{d_{22}}}, \tag{3.15}$$

which has a global minimum at $P(1,2)$. For $|\vartheta| < 2$, where the underlying **MKN**-system is exponentially unstable, the numerator function f_1 is positive independent of diagonal damping d_{22}. To place all eigenvalues in the

[†]Indefiniteness in the sense used here refers to the case where $d_{12}^2 > d_{22}$.

open left half of the complex plane, this behavior requires a positive denominator function f_2 which implies the damping matrix to be positive definite in the absence of gyroscopic terms. According to stability condition (3.7a), damping needs to be sufficiently large. In contrast, the critical damping factor $\delta^2_{\mathrm{crit}_3}$ is negative with indefinite damping. There exists no finite scaling coefficient $\delta > 0$ which fulfills stability condition (3.7b). As a consequence, it is impossible to stabilize an exponentially unstable **MKN**-system defined by matrices (3.1) using an indefinite damping matrix unless $\gamma > 0$.

For $|\vartheta| > 2$, i.e. the underlying **MKN**-system is marginally stable, there is a region where the numerator function f_1 is negative. This area shown in Fig. 3.5a is bounded on the bottom by Eq. (3.15) and on the left and the right by σ_1 and σ_2, respectively. Parameters $\sigma_{1,2}$ describe the stability boundary for infinitesimally small damping. In the depicted region, indefinite damping may lead to asymptotic stability since critical damping factor (3.13) is positive. Stabilization is possible if the scaling coefficient δ is chosen such that $0 < \delta^2 < \delta^2_{\mathrm{crit}_3}$ is satisfied. The eigenvalue placement in the open left half of the complex plane can be achieved by an indefinite damping matrix of arbitrarily small norm. However, a sufficiently large scaling coefficient contributes to destabilization. Upon addition of gyroscopic terms, the regime of asymptotic stability with indefinite damping is extended. Their presence ensures stabilization using a large indefinite damping matrix, cf. Fig. 3.1.

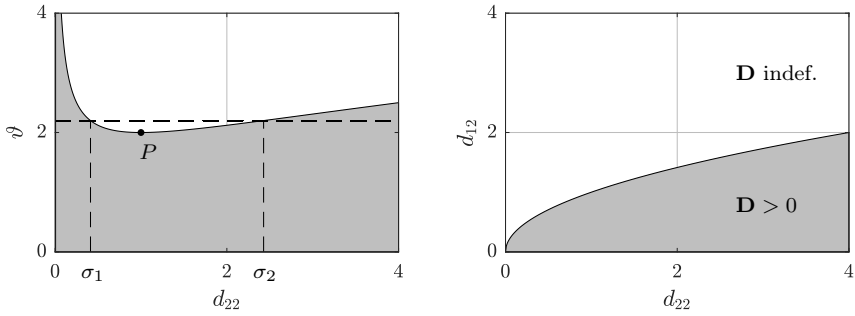

(a) Numerator function f_1. **(b)** Denominator function f_2.

Figure 3.5: Sign of numerator and denominator of Eq. (3.13). ● $f_i > 0$, ○ $f_i < 0$.

3.3 Optimum damping

Up to this point, the behavior of a linear system defined by matrices (3.1) is judged qualitatively under the influence of velocity proportional terms. All investigations focus on whether the trivial solution is either unstable or asymptotically stable. For technically relevant applications, however, the latter property may not be sufficient. It is further required that the equilibrium position is as stable as possible for a given parameter set. With reference to section 2.4, the emphasis is often on the determination of favorable damping configurations. This includes tailoring both the magnitude and the structure of the damping matrix yielding the parameter vector $\boldsymbol{\alpha} = (\delta, d_{22})^{\mathrm{T}}$.

A suitable optimization scheme involves maximizing the degree of stability (2.21) which implies the eigenvalue with largest real part to be as negative as possible. Even for the considered system with only two degrees of freedom, an analytical approach is not feasible. Due to the non-differentiability of the objective function at certain points in its domain, optimization needs to be performed numerically. In an example, the dimensionless values $\omega_2 = 10$, $\nu = 0.1$, and $\vartheta = 2.1$ correspond to a marginally stable **MKN**-system. The example illustrates the influence of velocity proportional terms on the optimum damping distribution, where no additional constraints are imposed on the parameter vector $\boldsymbol{\alpha}$. Resulting contour plots are shown in Fig. 3.6.

First, it is apparent for all three subfigures that the d_{12}-γ-plane is generally split into two sections via the straight line given by $\gamma = d_{12}$. For all parameter configurations satisfying this condition, the pole of the stability boundary is at $d_{22} = 0$, cf. Fig. 3.1. Above this characteristic line, the pole is located in the negative range leading to the highest possible $\zeta_{\mathrm{abs}}^{\mathrm{opt}}$. In the triangular area indicated in red in Fig. 3.6a, the optimized degree of stability equals approximately the eigenfrequencies of the undamped system. This corresponds to an optimum damping ratio near identity ($\zeta_{\mathrm{rel}}^{\mathrm{opt}} \approx 1$) since the imaginary part of the respective eigenvalue vanishes. The perturbed system does not exhibit a single oscillation and returns to equilibrium in the fastest possible manner. In the region where the off-diagonal elements of the damping matrix exceed the gyroscopic terms ($d_{12} > \gamma$), the pole of the stability boundary is located at

$d_{22} > 0$. The optimized degree of stability $\zeta_{\text{abs}}^{\text{opt}}$ declines significantly as d_{12} increases. The theoretically ideal damping ratio of $\zeta_{\text{rel}}^{\text{opt}} = 1$ is not attained since neither diagonal damping nor gyroscopic terms are capable of compensating the negative effects of the off-diagonal damping elements.

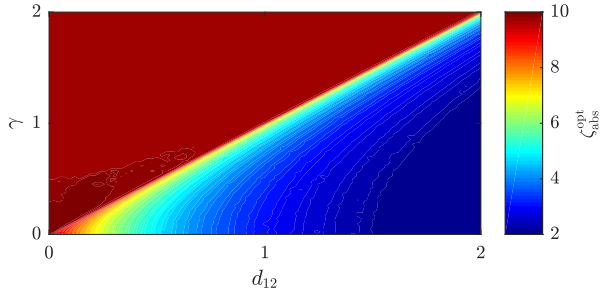

(a) Degree of stability.

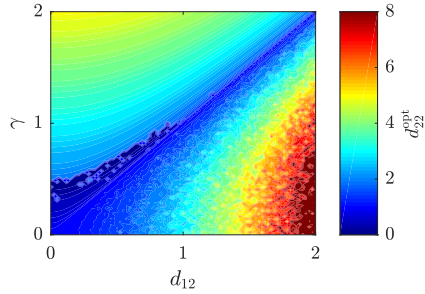

(b) Structure of the damping matrix.

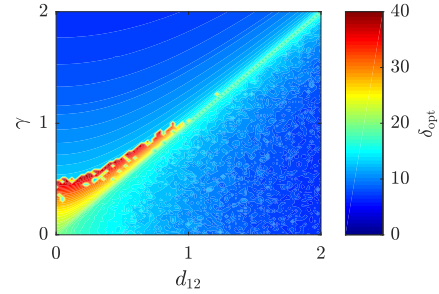

(c) Magnitude of the damping matrix.

Figure 3.6: Optimum damping distribution in the d_{12}-γ-plane supposing marginal stability of the underlying **MKN**-system.

Second, in order to achieve the optimum stability behavior, the damping matrix needs to possess a specific structure and magnitude. For all points lying on the characteristic line $\gamma = d_{12}$, symmetric damping properties ($d_{22} = 1$) are most satisfactory, cf. Fig. 3.6b. A uniform distribution over both modes corresponds to mass proportional damping. Beyond this particular configuration, the effects of velocity proportional perturbations do not cancel com-

pletely. The pole movement of the stability boundary is then compensated by diagonal damping terms which are not equal to one. Especially off-diagonal damping terms, not only shifting the pole in positive d_{22}-direction but also affecting the definiteness of the damping matrix, cause an asymmetric damping distribution. In the parameter range plotted, the optimum diagonal damping d_{22}^{opt} is up to eight times the optimum value at $\gamma = d_{12}$.

The majority of d_{12}-γ-combinations features one basin of attraction in the two-dimensional parameter space spanned by $\boldsymbol{\alpha}$. On the contrary, in the area where $d_{22}^{\mathrm{opt}} < 1$, there occur two attractive domains. The basin of attraction which contains the global optimum of the degree of stability is characterized by a comparably large value of δ_{opt}, cf. Fig. 3.6c. However, the phenomenon of two different basins of attraction only exists when $\gamma > d_{12}$ and immediately vanishes as γ or d_{12} exceed specific threshold values. Furthermore, the optimum magnitude of the damping matrix is approximately constant on the characteristic line and generally decreases with growing velocity proportional influences. In the domain where the gyroscopic terms are larger than the off-diagonal damping elements, the opposing behavior of d_{22}^{opt} and δ_{opt} leads to an almost constant trace of the damping matrix.

A conclusion drawn from these numerical evaluations is the general profile of the optimum damping distribution in the d_{22}-δ-plane under velocity proportional perturbations. With the exception of the special case where $d_{12} = \gamma$, the optimum parameter combination is shifted towards large diagonal damping values and low magnitudes of the damping matrix as gyroscopic and off-diagonal damping terms increase.

3.4 Discussion

The present chapter highlights effects of velocity proportional terms on the stability of linear circulatory systems. With exception of damping optimization, which is performed numerically, the small number of variables elsewise enables an analytical assessment. The application of the necessary and sufficient criterion of Liénard & Chipart [116] yields the explicit stability boundary of a general two-dimensional system of type **MDGKN**. Alternative meth-

ods which are merely sufficient for stability, such as the criteria introduced by Frik [40] as well as Kliem & Pommer [101, 102], are not invariably capable of reproducing essential characteristics. In all approaches mentioned, the asymptotically stable regime is predicted too conservative. Moreover, none of the sufficient criteria is able to capture the correct roots $\sigma_{1,2}$ which describe the stability boundary for infinitesimally small damping. This property of stabilization with a damping matrix of arbitrarily small norm is influenced primarily by two factors. The distance between the two roots as well as their position in the parameter space is subject to gyroscopic terms γ and the ratio ϑ between the spacing of the eigenfrequencies and the circulatory terms. On the one hand, γ moves both roots in negative direction and ϑ causes a shift of σ_1 in negative and σ_2 in positive direction. On the other hand, the distance between the roots enlarges with increasing ϑ, yet it diminishes with growing γ. Therefore, asymmetric stiffness properties inducing the separation of neighboring eigenfrequencies contribute to stabilization.

While gyroscopic terms are rather disadvantageous for the occurrence of this phenomenon, they are of crucial importance when the damping matrix is merely positive semi-definite. As pointed out, for example, by Kirillov [93], gyroscopic terms may, in certain cases, ensure appropriate mode coupling for damping to be pervasive. Their magnitude and the stability behavior of the undamped system then determine whether or not asymptotic stabilization can be achieved by infinitesimally small damping. In a similar manner, the presence of gyroscopic terms extends the stable regime when the damping matrix is indefinite. This is confirmed by the results obtained following perturbational approaches [29, 100, 102]. In contrast, off-diagonal damping terms generally have a detrimental impact on the stability behavior. To a certain degree, they compensate the positive effect of diagonal damping. This is documented by a significant decline of the highest possible degree of stability. Off-diagonal damping furthermore leads to a non-uniform damping distribution in both considered modes if its influence is not canceled by sufficiently large gyroscopic terms. As a result, the optimum structure of the damping matrix depends on a specific parameter combination consisting of gyroscopic and off-diagonal damping terms.

4 Optimum damping in disc brake systems

In this chapter, the objective is to determine favorable damping configurations in different disc brake systems with respect to an equilibrium position which is as stable as possible. Performed numerical analyses concern low-dimensional minimal models as well as simplified and realistic brake models originating from finite element environments. The results presented resume and extend prior investigations originally published in [81, 82, 167, 187].

4.1 Two degree of freedom minimal model

4.1.1 Modeling

A straightforward model which is able to capture the basic behavior of disc brake squeal was developed by VON WAGNER et al. [177]. The model depicted in Fig. 4.1 consists of a rigid disc in prestressed point contact with two massless pins whose movement is restricted to the $\mathbf{n}_3$-direction. Under the assumption of a small thickness to radius ratio $\kappa = h/r$, the inertial properties of the symmetric disc are fully covered by the dyadic

$$ {}^{\mathfrak{D}}\boldsymbol{\Theta} = \begin{pmatrix} \Theta & 0 & 0 \\ 0 & \Theta & 0 \\ 0 & 0 & 2\Theta \end{pmatrix}, \tag{4.1} $$

where Θ is the mass moment of inertia relative to the axes $\mathbf{d}_1$ and $\mathbf{d}_2$ of the body fixed frame $\mathfrak{D}$. The pins represent idealized brake pads with stiffness and damping properties k_p and d_p, respectively. The restoring force of the spring-damper elements in conjunction with the prestress N_0 is considered large enough to invariably maintain contact. Based on experiments conducted

in [72], the contact between disc and pads is assumed to be of COULOMB type with a constant and isotropic friction coefficient μ. Stick-slip phenomena do not occur as long as the disc rotates sufficiently fast. As a consequence, friction forces are continuous and linearization of the equations of motion is admissible. The disc is mounted in its center of mass and bedded viscoelastically by rotational springs (stiffness k_t) and dampers (damping coefficient d_t). While rotating with a prescribed angular velocity Ω around the $\mathbf{n}_3$-axis, the disc is free to tilt with the angles q_1 and q_2 being minimal coordinates. This is mathematically accounted for by the non-holonomic constraint

$$ {}^{\mathfrak{N}}\boldsymbol{\omega} \cdot \mathbf{n}_3 = \Omega = \text{const.}, \tag{4.2} $$

where ${}^{\mathfrak{N}}\boldsymbol{\omega}$ is the angular velocity which describes the spatial wobbling motion of the disc with respect to the NEWTONian reference frame $\mathfrak{N}$.

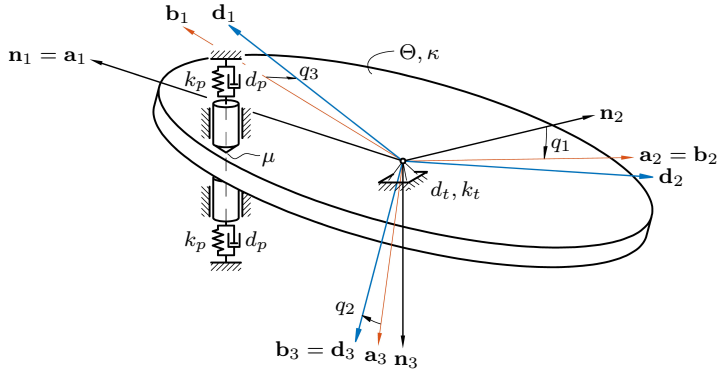

Figure 4.1: Minimal model of wobbling disc brake adapted from [177].

4.1.2 Equations of motion

The intermediate coordinate frames $\mathfrak{A}$ and $\mathfrak{B}$ along with CARDAN angles q_i $(i = 1, 2, 3)$ uniquely determine the orientation of the disc in space. Executing three consecutive elemental rotations about the $\mathbf{n}_1$-, $\mathbf{a}_2$-, and $\mathbf{b}_3$-axis yields the angular velocity of the disc in the inertial frame

$$ {}^{\mathfrak{N}}\boldsymbol{\omega} = \dot{q}_1 \mathbf{n}_1 + \dot{q}_2 \mathbf{a}_2 + \dot{q}_3 \mathbf{b}_3. \tag{4.3} $$

The balance of angular momentum leads to

$$\frac{\mathrm{d}}{\mathrm{d}t}({}^{\mathfrak{N}}\boldsymbol{\Theta} \cdot {}^{\mathfrak{N}}\boldsymbol{\omega}) = \mathbf{M}_{\mathrm{res}}, \tag{4.4}$$

which is a system of inherently nonlinear equations. A transformation of the inertia dyadic to the NEWTONian frame can be obtained via ${}^{\mathfrak{N}}\boldsymbol{\Theta} = \mathbf{T}\,{}^{\mathfrak{D}}\boldsymbol{\Theta}\,\mathbf{T}^{-1}$ with $\mathbf{T}$ originating from CARDAN rotation [189]. Following the kinematic relations in [177], the resulting torque $\mathbf{M}_{\mathrm{res}}$ acting on the disc arises from viscoelastic suspension, contact forces including friction, and constraint (4.2) which induces the constant driving torque

$$M_t = 2\mu N_0 r. \tag{4.5}$$

After elimination of $\dot{q}_3$ and subsequent linearization around the equilibrium position $\mathbf{q} = (q_1, q_2)^{\mathrm{T}} \equiv \mathbf{0}$, the equations of motion are of form (2.7). Geometrical linearization is applicable since the occurring vibration amplitudes during squeal are in the range of micrometers [47]. In order to reduce the number of independent variables and to ensure quantitative comparability of parameters, nondimensionalization is conducted on these equations. To this end, the vector of generalized coordinates $\mathbf{q}$ and time t are scaled introducing the substitutions

$$\mathbf{q} = q_c \mathbf{p}, \tag{4.6a}$$

$$t = t_c \tau, \tag{4.6b}$$

with the new vector of generalized coordinates $\mathbf{p}$ and the new time scale τ. Inserting transformations (4.6) into the equations of motion (2.7) and applying the chain rule yields

$$\frac{q_c}{t_c^2}\mathbf{M}\mathring{\mathring{\mathbf{p}}} + \frac{q_c}{t_c}\left(\mathbf{D} + \mathbf{G}\right)\mathring{\mathbf{p}} + q_c\left(\mathbf{K} + \mathbf{N}\right)\mathbf{p} = \mathbf{0}, \tag{4.7}$$

where the overcircle denotes differentiation with respect to τ. The respective system matrices can be rewritten in terms of dimensionless quantities if the characteristic constants are chosen according to

$$q_c = \frac{1}{N_0 r}, \tag{4.8a}$$

$$t_c = \frac{1}{\Omega_{\mathrm{ref}}}. \tag{4.8b}$$

The resulting nondimensionalized system matrices read

$$
\begin{aligned}
\tilde{\mathbf{M}} &= \begin{pmatrix} \tilde{\Theta} & 0 \\ 0 & \tilde{\Theta} \end{pmatrix}, \\
\tilde{\mathbf{D}} &= \begin{pmatrix} 2\tilde{d}_p + \tilde{d}_t + \frac{\mu\kappa^2}{2\tilde{\Omega}} & -\frac{1}{2}\mu\kappa\tilde{d}_p \\ -\frac{1}{2}\mu\kappa\tilde{d}_p & \tilde{d}_t \end{pmatrix}, \\
\tilde{\mathbf{G}} &= \begin{pmatrix} 0 & 2\tilde{\Theta}\tilde{\Omega} + \frac{1}{2}\mu\kappa\tilde{d}_p \\ -(2\tilde{\Theta}\tilde{\Omega} + \frac{1}{2}\mu\kappa\tilde{d}_p) & 0 \end{pmatrix}, \\
\tilde{\mathbf{K}} &= \begin{pmatrix} 2\tilde{k}_p + \tilde{k}_t + \kappa & -\frac{1}{4}\mu[(2\tilde{k}_p - \kappa)\kappa + 4] \\ -\frac{1}{4}\mu[(2\tilde{k}_p - \kappa)\kappa + 4] & \tilde{k}_t + (1+\mu^2)\kappa \end{pmatrix}, \\
\tilde{\mathbf{N}} &= \begin{pmatrix} 0 & \frac{1}{4}\mu[(2\tilde{k}_p + \kappa)\kappa + 4] \\ -\frac{1}{4}\mu[(2\tilde{k}_p + \kappa)\kappa + 4] & 0 \end{pmatrix},
\end{aligned}
\tag{4.9}
$$

with the tilde indicating dimensionless parameters. Except for the mass matrix $\tilde{\mathbf{M}}$ all matrices are affected by COULOMB friction arising at the interface between disc and pads. The circulatory matrix $\tilde{\mathbf{N}}$ originates exclusively from the kinematic linearization of friction forces. For $\mu = 0$, its skew-symmetric coupling terms, which make the system susceptible to self-excitation, vanish. Aside from viscous damping due to the viscoelastic mounting of the disc and the energy dissipation in the pads, the damping matrix $\tilde{\mathbf{D}}$ contains portions which are due to frictional contact. They act on both the first entry on the diagonal and the off-diagonal entries. In combination with the pad damping, which is active only in the first degree of freedom, this yields a non-uniform damping distribution over both modes.[†] The stiffness matrix $\tilde{\mathbf{K}}$ has a similar structure. In this case, the asymmetry introduced via the pad stiffness contributes to stabilization as it separates the eigenfrequencies of the disc. This positive effect is partially canceled by a simultaneous increase of circulatory terms. The gyroscopic matrix $\tilde{\mathbf{G}}$, which in contrast to $\tilde{\mathbf{D}}$ is not associated with energy dissipation, occurs due to the disc rotation, yet it also contains terms due to friction.

[†]Non-uniformly distributed dissipation in the sense used here corresponds to unequal diagonal elements of the damping matrix. In contrast, a uniform distribution denotes a matrix with equal diagonal entries.

For the purpose of stability analysis and optimization, numerical values are chosen in accordance with [177], where Tab. 4.1 shows their relation to the respective dimensional quantity. The parameter set published therein has been identified experimentally. The inertial and stiffness properties of the rigid wobbling disc correspond to two measured eigenmodes of a real, elastic disc which are characterized by three nodal diameters [72, 80]. Application of KIRCHHOFF's plate theory to the brake disc and subsequent discretization by two appropriate shape functions representing the observed eigenmodes leads approximately to the same equations of motion [73]. Thus, the simplified assumption of a rigid disc is justified.

symbol	numerical value	relation to dimensional quantity	parameter description
$\tilde{\Theta}$	0.101	$\frac{\Theta\Omega_{\mathrm{ref}}^2}{N_0 r}$	mass moment of inertia
$\tilde{k}_p$	260	$\frac{k_p r}{N_0}$	pad stiffness
$\tilde{k}_t$	48205	$\frac{k_t}{N_0 r}$	rotational stiffness
$\tilde{d}_p$	3.40×10^{-3}	$\frac{d_p r \Omega_{\mathrm{ref}}}{N_0}$	pad damping
$\tilde{d}_t$	4.03×10^{-3}	$\frac{d_t \Omega_{\mathrm{ref}}}{N_0 r}$	disc damping
μ	0.6	μ	friction coefficient
κ	0.154	$\frac{h}{r}$	thickness to radius ratio

Table 4.1: Dimensionless parameter set based on [177].

4.1.3 Stability behavior

Besides the geometry, load, and stiffness parameters investigated in [177], the stability of a system defined via matrices (4.9) is influenced by damping due to the disc and the pads. The $\tilde{d}_t$-$\tilde{d}_p$-plane depicted in Fig. 4.2 is used to illustrate dissipative effects on the qualitative behavior of the trivial solution. Both dimensionless damping coefficients are normalized with respect to their reference values $\tilde{d}_t^{\mathrm{ref}}$ and $\tilde{d}_p^{\mathrm{ref}}$ calculated with $\Omega_{\mathrm{ref}} = \Omega/\tilde{\Omega} = 5\pi\,\mathrm{s}^{-1}$. All other parameters are held constant according to Tab. 4.1.

Fig. 4.2a shows the stability boundary for various rotational speeds of the brake disc. Below the respective boundary the trivial solution is unstable since there exist eigenvalues with positive real part. This is associated with self-excitation which can be interpreted as squeal. In the linearized case, flutter instability is characterized by oscillations which theoretically grow infinitely large in the absence of damping. In contrast, the amplitudes of the corresponding real, nonlinear system remain bounded, for example, due to a stiffening material characteristic of the brake pad, and ultimately reach a limit cycle. From Fig. 4.2a it is apparent that the lines of constant angular speed are similar. When $\tilde{\Omega}$ increases, the stability boundary is shifted parallelly towards the upper right corner of the $\tilde{d}_t$-$\tilde{d}_p$-plane. For stabilization, this movement needs to be compensated either by damping in the disc or in the pads. Despite the latter evoking a positive semi-definite damping matrix, dissipation is pervasive since sufficiently large pad damping invariably leads to asymptotic stability. If the only damping contribution is of COULOMB friction type, i.e. $\tilde{d}_p = \tilde{d}_t = 0$, the trivial solution is unstable.

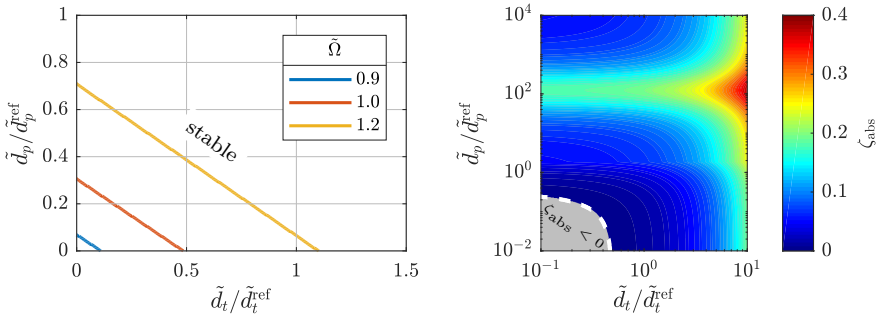

(a) Stability boundary for varying $\tilde{\Omega}$. **(b)** Degree of stability for $\tilde{\Omega} = 1$.

Figure 4.2: Effects of disc and pad damping on stability.

The quantitative stability behavior is discussed using the degree of stability in Fig. 4.2b, where the angular velocity is exemplarily set to $\tilde{\Omega} = 1$. The white dashed line corresponds to the red line in Fig. 4.2a defining the boundary between the asymptotically stable and unstable regime. In general, disc damping

has a stabilizing influence for all parameter configurations plotted. On the contrary, every contour line $\zeta_{\mathrm{abs}} = \text{const.}$ has a turning point at $\tilde{d}_p \approx 120\,\tilde{d}_p^{\mathrm{ref}}$ implying that energy dissipation in the pads does not necessarily contribute to stabilization. Pad damping is pervasive but causes a non-uniform distribution over both modes which may negatively affect stability, cf. section 3.2. Numerical simulations suggest, however, that the trivial solution cannot become unstable via $\tilde{d}_p > 120\,\tilde{d}_p^{\mathrm{ref}}$. The eigenvalue with maximum real part converges to zero as $\tilde{d}_p$ approaches infinity. To reach the global optimum, damping in the brake pads needs to be around two orders of magnitude larger than its reference value given in Tab. 4.1. For this reason, the technical relevance and feasibility of this optimum remains questionable.

4.1.4 Optimization approach

During the development process of disc brakes, manufacturers want to meet certain geometry, performance, and comfort goals. A common remedy to improve noise issues in structures is the modification of damping properties. Within the scope of the present model, this concerns damping in the disc as well as damping in the pads. For the formulation of an optimization problem and to account for distinct physical origins of energy dissipation, the damping matrix $\tilde{\mathbf{D}}$ of Eq. (4.9) is written as a linear combination

$$\begin{aligned}\tilde{\mathbf{D}} &= \tilde{\mathbf{D}}_0 + \sum_{i=1}^{s} \alpha_i \tilde{\mathbf{D}}_i \\ &= \underbrace{\begin{pmatrix} \frac{\mu\kappa^2}{2\tilde{\Omega}} & -\frac{1}{2}\mu\kappa\tilde{d}_p \\ -\frac{1}{2}\mu\kappa\tilde{d}_p & 0 \end{pmatrix}}_{\tilde{\mathbf{D}}_c} + \alpha_1 \underbrace{\begin{pmatrix} \tilde{d}_t & 0 \\ 0 & \tilde{d}_t \end{pmatrix}}_{\tilde{\mathbf{D}}_t} + \alpha_2 \underbrace{\begin{pmatrix} 2\tilde{d}_p & 0 \\ 0 & 0 \end{pmatrix}}_{\tilde{\mathbf{D}}_p},\end{aligned} \tag{4.10}$$

where $\tilde{\mathbf{D}}_0$ is a matrix containing fixed damping terms and $\tilde{\mathbf{D}}_i$ are α_i-weighted damping matrices whose relative contribution to the overall damping is to be varied. As a consequence, the different physical origins of energy dissipation are treated independently which reflects in the parameter vector $\boldsymbol{\alpha} = (\alpha_1, \alpha_2)^{\mathrm{T}}$ of dimension $1 \times s$. Decomposition (4.10) reveals characteristic matrix properties. The Coulomb damping matrix $\tilde{\mathbf{D}}_c$ resulting from the kinematic lin-

earization of friction forces is indefinite, whereas the portions $\tilde{\mathbf{D}}_t$ and $\tilde{\mathbf{D}}_p$ are positive definite and positive semi-definite, respectively.

Using complex eigenvalue analysis and a damping matrix of form (4.10), stability can be enhanced by variation of the weighting factors α_i. For this purpose, a system is considered to be more stable if its eigenvalue with largest real part is as negative as possible which implies the degree of stability to become as large as possible. With reference to section 2.4, the objective of finding a favorable damping configuration is mathematically expressed as

$$\max_{\boldsymbol{\alpha}} \zeta_{\text{abs}} \quad \text{subject to} \quad \mathbf{c}(\boldsymbol{\alpha}) \leq \mathbf{0}, \tag{4.11}$$

with $\mathbf{c}(\boldsymbol{\alpha})$ imposing additional restrictions on the parameter vector. In the specified model, the parameter optimization involves varying the ratio of damping in the disc and damping in the pads in order to determine the most beneficial distribution. Hence, it is convenient to define $\alpha_1 + \alpha_2 \leq 2$ which is equivalent to the linear inequality constraints

$$\sum_{i=1}^{s} \alpha_i \leq s, \quad \alpha_i \geq 0, \tag{4.12}$$

where the weighting factors are taken to be non-negative. Numerical treatment of Eq. (4.11), which is linearly constrained by Eq. (4.12), is sought using a generalized pattern search algorithm implemented in MATLAB's global optimization toolbox, cf. section 2.4.

4.1.5 Optimization results

The main function of friction brakes is the reduction of vehicle speed by a conversion of kinetic to thermal energy. A suitable performance measure thereof is the braking torque (4.5), which is proportional to the radius of the disc and the conditions at the contact interface between disc and pads. The governing parameters are subject to natural fluctuations. Especially the friction coefficient depends on the operating conditions of the brake, e.g. temperature, lubrication, and wear [111]. In order to generate the braking torque, these uncertainties need to be compensated by an appropriately large normal

force given that the geometry of the brake system is fixed. Aside from the capability of reducing vehicle speed, comfort issues like squeal progressively play a role in brake design. As pointed out, for example, by VON WAGNER et al. [177], low friction coefficients in conjunction with high normal forces are advantageous to stability. In addition, energy dissipation in the disc and the pads contributes to stabilization, cf. section 4.1.3. This raises the question how to design the corresponding damping distribution without conflicting the performance of the brake system.

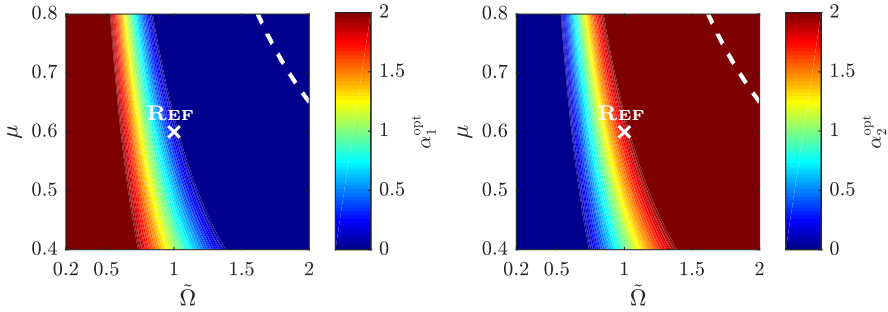

(a) Disc damping. **(b)** Pad damping.

Figure 4.3: Optimum damping distribution between disc and pads for constant braking torque over various angular velocities and friction coefficients.

Fig. 4.3 features the optimum ratio between damping in the disc and damping in the pads for various angular velocities and friction coefficients. The braking torque is held constant, i.e. high friction coefficients correspond to low normal forces and vice versa. As indicated by the graphs, the admissible damping range is fully exploited. In the entire $\tilde{\Omega}$-μ-plane, the optimum lies on the triangular boundary defined by $\alpha_1 + \alpha_2 = 2$ and non-negative weighting factors. For small angular velocities and friction coefficients, energy dissipation is beneficial in the disc, while for large $\tilde{\Omega}$ and μ, damping in the pads becomes more favorable even though this portion leads to an asymmetric distribution over both modes. The behavior described above is due to gyroscopic effects which grow with $\tilde{\Omega}$. At high angular velocities, a uniform damping dis-

tribution generated by the energy dissipation in the disc is not satisfactory. As pointed out in section 3.3, large gyroscopic perturbations require a compensation via non-uniformly distributed dissipation which corresponds to pad damping in this case. However, even an optimal distribution is not invariably sufficient for stability within the linearly constrained parameter region. For parameter combinations which are located on the right of the white dashed line, the system's total damping content needs to be increased to ensure a stable trivial solution. In this domain, an improvement of noise behavior exclusively via the structure of $\tilde{\mathbf{D}}$ and complementary damping coefficients is not possible. In contrast, for medium rotational speeds, i.e. $0.8 < \tilde{\Omega} < 1.2$, there exists an optimum configuration for every operating point. For example, at the reference point marked 'REF', which is extensively studied in [81] and [187], the optimized weighting factors are $\alpha_{1,\mathrm{ref}}^{\mathrm{opt}} = 0.16$ and $\alpha_{2,\mathrm{ref}}^{\mathrm{opt}} = 1.84$. Comparison to their non-optimized equivalents $\alpha_{1,\mathrm{ref}} = 1$ and $\alpha_{2,\mathrm{ref}} = 1$ shows the advantage of shifting damping from the disc to the pads with regard to an improved stability at this point.

The previously described stability enhancement is based on an optimum distribution of energy dissipation in the disc and in the pads and merely applies to one specific operating point. In technically relevant systems, however, damping coefficients cannot be reselected arbitrarily for each parameter combination. The system is rather tailored to a certain operating regime and thus subject to perturbations. In Fig. 4.4, contour plots of two configurations are compared, the first of which concerns the non-optimized case and the second of which is tuned to a specific operating point. The degree of stability is normalized with respect to its optimized counterpart resulting from the determination of individual weighting factors at each point in the $\tilde{\Omega}$-μ-plane. If the ratio $\zeta_{\mathrm{abs}}/\zeta_{\mathrm{abs}}^{\mathrm{opt}}$ equals identity, damping is optimally distributed and the trivial solution of the minimal model is as stable as possible within linear constraints (4.12). The non-optimized state is covered in Fig. 4.4a, where $\alpha_1 = 1$ and $\alpha_2 = 1$. Although the weighting factors remain unchanged, there is a narrow band with maximum degree of stability, i.e. the ratio $\zeta_{\mathrm{abs}}/\zeta_{\mathrm{abs}}^{\mathrm{opt}}$ is equal to one. At the reference point, the absolute stability reserve is approximately 80 % of its optimum value and decreases rapidly with growing $\tilde{\Omega}$ since

damping in the pads becomes more advantageous. The stability boundary is therefore shifted towards smaller friction coefficients and angular velocities. In comparison to the optimized configuration whose stability boundary is indicated by the white dashed line, the unstable domain enlarges when the damping matrix is not adapted to certain operating conditions.

Fig. 4.4b depicts a configuration tailored to the previously introduced reference point 'REF'. The corresponding damping distribution yields the largest possible degree of stability for $\tilde{\Omega} = 1$ and $\mu = 0.6$. While the optimum regime, where $\zeta_{\mathrm{abs}}/\zeta_{\mathrm{abs}}^{\mathrm{opt}} = 1$, is more narrow than in Fig. 4.4a, the area where the ratio is close to identity is yet more dominant especially for medium to large angular velocities. Compared to the non-optimized case, this reflects in an improved stability boundary which approaches the limit calculated individually for each operating point. The stability boundary is closely attainable with a constant damping distribution if the ratio of energy dissipation between the disc and the pads at the design point corresponds qualitatively to the ratio at the stability boundary. However, if the design point lies in the domain of small angular velocities where damping in the disc is beneficial, the degree of stability as well as the stability boundary can be affected negatively. As a result, robust tuning of damping properties within the scope of technical feasibility can only satisfyingly be achieved in a specific velocity range.

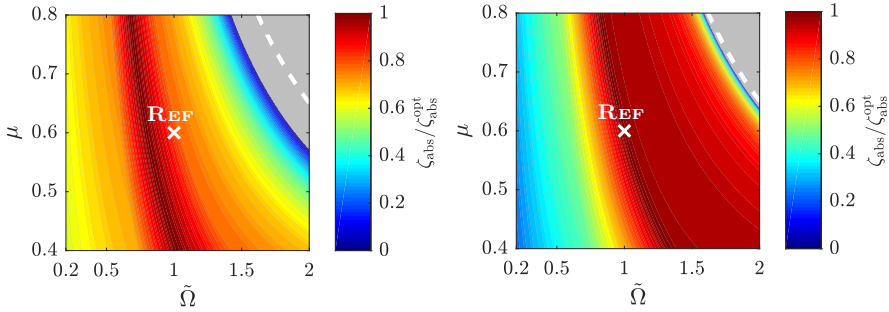

(a) $\zeta_{\mathrm{abs}}(\alpha_1 = 1, \alpha_2 = 1)$. **(b)** $\zeta_{\mathrm{abs}}(\alpha_1 = \alpha_{1,\mathrm{ref}}^{\mathrm{opt}}, \alpha_2 = \alpha_{2,\mathrm{ref}}^{\mathrm{opt}})$.

Figure 4.4: Normalized degree of stability for constant braking torque over various angular velocities and friction coefficients. ● $\zeta_{\mathrm{abs}} < 0$, i.e. flutter instability.

4.2 Eight degree of freedom minimal model

4.2.1 Modeling

The linearized minimal model presented previously is able to reproduce the principal concept of squeal onset originating from a flutter-type instability at the contact zone between a rotating disc and pads. More realistic applications, however, incorporate brake components, such as a caliper and back plates, which have not yet been considered. Experimental observations reveal that these features are essential to the brake system's dynamics. The lowest eigenfrequencies of the caliper, for instance, may be close to the squealing frequency of the disc [72, 80]. Moreover, modal analyses of assembled brake systems conducted in [170] identify mechanical joints, e.g. the caliper/back plate interface, as a major source of energy dissipation.

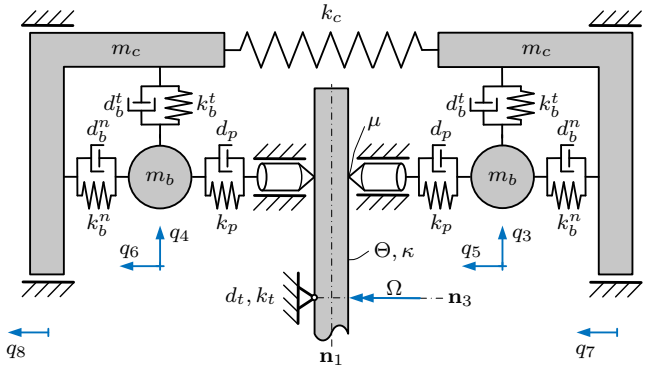

Figure 4.5: Extended minimal model of wobbling disc brake with additional degrees of freedom for caliper and back plates.

In view of the above, an extended model depicted in Fig. 4.5 includes additional degrees of freedom introduced by a caliper and back plates. With reference to section 4.1.1, the model consists of a viscoelastically mounted, rigid disc in prestressed frictional point contact with two guided pins representing idealized brake pads. The geometry of the disc (thickness to radius ratio κ), its mass moment of inertia Θ, and the stiffness and damping at-

tributes of the rotational bearing, i.e. k_t and d_t, are adopted from the two degree of freedom model. All assumptions and limitations apply accordingly. In particular, this concerns the contact definition using a constant friction coefficient μ as well as the disc revolution with angular velocity Ω which is impressed by means of non-holonomic constraint (4.2). The spatial wobbling motion of the disc is described by the tilt angles q_1 and q_2.

In contrast to the two degree of freedom model, where the massless pads are supported against ground, here each pad is connected to a discrete mass particle m_b representing the back plate. The viscoelastic material characteristic of the pads is approximated by a linear spring with stiffness k_p and a damper of viscosity d_p. Both back plates are embedded in a bending-resistant caliper and are free to move in the $\mathbf{n}_1$-$\mathbf{n}_3$-plane. Their transversal motion is described by the minimal coordinates q_3 to q_6. In the floating caliper variety shown in Fig. 4.5, the caliper surrounds the disc and is allowed to slide along a guidance, where its motion is determined by the coordinates q_7 and q_8. The caliper's inertia is lumped into two particles of mass m_c which are elastically attached to a translational spring with stiffness k_c. The suspension of the back plates to the caliper is implemented via standard KELVIN-VOIGT-elements whose stiffness and damping coefficients are given by k_b^n and d_b^n, respectively. This suspension acts in normal direction to the disc. In tangential direction, the spring-damper modules are denoted by the coefficients k_b^t and d_b^t. In total, the minimal model is comprised of eight degrees of freedom including an idealized representation of disc, pads, caliper, and back plates.

4.2.2 Equations of motion

The extended minimal model encompasses both rotational (q_1, q_2) and translational (q_3 to q_8) degrees of freedom. While the spatial wobbling motion of the disc is captured by balancing the angular momentum (4.4), the mathematical formulation of the back plates' and caliper motion requires the application of NEWTON's second law

$$\frac{\mathrm{d}^2}{\mathrm{d}t^2}(m\,{}^{\mathfrak{N}}\mathbf{u}) = {}^{\mathfrak{N}}\mathbf{F}_{\mathrm{res}}. \tag{4.13}$$

This fundamental principle establishes a connection between the net force $\mathbf{F}_{\mathrm{res}}$ acting on a body of mass m and the second time derivative of its position vector $\mathbf{u}$ with respect to the inertial frame $\mathfrak{N}$. A vectorial representation of all relevant forces and kinematic relations of the extended model is derived in [167]. Therein, the formal derivation of the equations of motion is sought using the commercial software package MotionGenesis [126]. Geometrical linearization around the equilibrium state $\mathbf{q} = (q_1, q_2, \ldots, q_8)^{\mathrm{T}} \equiv \mathbf{0}$ yields a second order system of the form

$$\mathbf{M}\ddot{\mathbf{q}} + \mathbf{B}\dot{\mathbf{q}} + \mathbf{C}\mathbf{q} = \mathbf{0}. \tag{4.14}$$

Coherent to section 4.1.2, nondimensionalization is conducted on these equations. However, a scalar coordinate transformation as shown in Eq. (4.6a) is not expedient since the rows of system (4.14) are incompatible with respect to their dimensions. Rotational degrees of freedom are defined by angles, while translational displacements are of unit length. Hence, the vector of generalized coordinates is scaled introducing the substitution

$$\mathbf{q} = \mathbf{Q}_c^{\frac{1}{2}}\mathbf{p}, \tag{4.15}$$

where $\mathbf{Q}_c = \mathrm{diag}(q_{c_1}, q_{c_2}, \ldots, q_{c_8})$ is a diagonal matrix with constants q_{c_i} on its principal diagonal and $\mathbf{p}$ is the new vector of generalized coordinates. Inserting transformations (4.6b) and (4.15) into the equations of motion (4.14), applying the chain rule, and premultiplying with $\mathbf{Q}_c^{\frac{1}{2}}$ to preserve the symmetry properties of the system matrices yields

$$\underbrace{\frac{1}{t_c^2}\mathbf{Q}_c^{\frac{1}{2}}\mathbf{M}\mathbf{Q}_c^{\frac{1}{2}}}_{\tilde{\mathbf{M}}}\overset{\circ\circ}{\mathbf{p}} + \underbrace{\frac{1}{t_c}\mathbf{Q}_c^{\frac{1}{2}}\mathbf{B}\mathbf{Q}_c^{\frac{1}{2}}}_{\tilde{\mathbf{B}}}\overset{\circ}{\mathbf{p}} + \underbrace{\mathbf{Q}_c^{\frac{1}{2}}\mathbf{C}\mathbf{Q}_c^{\frac{1}{2}}}_{\tilde{\mathbf{C}}}\mathbf{p} = \mathbf{0}. \tag{4.16}$$

Introducing the time constant $t_c = 1/\Omega_{\mathrm{ref}}$ and choosing the diagonal elements of $\mathbf{Q}_c$ according to

$$q_{c_i} = \begin{cases} \frac{1}{N_0 r} & \text{for } i = 1, 2 \\ \frac{r}{N_0} & \text{for } i = 3, 4, \ldots, 8 \end{cases}, \tag{4.17}$$

the three summands $\tilde{\mathbf{M}}$, $\tilde{\mathbf{B}}$, and $\tilde{\mathbf{C}}$ are rewritten to state dimensionless quantities. This transformation approach results in the dimensionless system matrices depicted below, where $\tilde{\mathbf{B}}$ and $\tilde{\mathbf{C}}$ are decomposed into their symmetric and skew-symmetric parts as specified by Eq. (2.8). Entries depending on the angles q_1 and q_2 correspond to matrices (4.9) of the two degree of freedom model. For the extended system, the mass matrix

$$\tilde{\mathbf{M}} = \begin{pmatrix} \tilde{\Theta} & & & & & & & \\ & \tilde{\Theta} & & & & & & \\ & & \tilde{m}_b & & & & & \\ & & & \tilde{m}_b & & & & \\ & & & & \tilde{m}_b & & & \\ & & & & & \tilde{m}_b & & \\ & & & & & & \tilde{m}_c & \\ & & & & & & & \tilde{m}_c \end{pmatrix} \tag{4.18}$$

is diagonal with the diagonal elements characterizing the inertias of disc, back plates, and caliper. In opposition to all other matrices, $\tilde{\mathbf{M}}$ is not affected by Coulomb friction at the contact interface between disc and pads.

The symmetric parts of the velocity and coordinate proportional forces, respectively, i.e. the damping matrix

$$\tilde{\mathbf{D}} = \begin{pmatrix} 2\tilde{d}_p+\tilde{d}_t+\frac{\kappa^2\mu}{2\tilde{\Omega}} & -\frac{\kappa\mu\tilde{d}_p}{2} & -\frac{\mu\tilde{d}_p}{2} & \frac{\mu\tilde{d}_p}{2} & -\tilde{d}_p & -\tilde{d}_p & 0 & 0 \\ & \tilde{d}_t & 0 & 0 & \frac{\kappa\mu\tilde{d}_p}{4} & \frac{\kappa\mu\tilde{d}_p}{4} & 0 & 0 \\ & & \tilde{d}_b^t & 0 & \frac{\mu\tilde{d}_p}{2} & 0 & 0 & 0 \\ & & & \tilde{d}_b^t & 0 & -\frac{\mu\tilde{d}_p}{2} & 0 & 0 \\ & \text{sym.} & & & \tilde{d}_b^n+\tilde{d}_p & 0 & -\tilde{d}_b^n & 0 \\ & & & & & \tilde{d}_b^n+\tilde{d}_p & 0 & -\tilde{d}_b^n \\ & & & & & & \tilde{d}_b^n & 0 \\ & & & & & & & \tilde{d}_b^n \end{pmatrix} \tag{4.19}$$

and the stiffness matrix

$$\tilde{\mathbf{K}} = \begin{pmatrix} 2\tilde{k}_p+\tilde{k}_t+\kappa & \frac{\mu}{4}(\kappa^2-2\kappa\tilde{k}_p-4) & \frac{\mu}{4}(\kappa-2\tilde{k}_p) & \frac{\mu}{4}(2\tilde{k}_p-\kappa) & -\tilde{k}_p & -\tilde{k}_p & 0 & 0 \\ & \tilde{k}_t+(1+\mu^2)\kappa & 1+\frac{\mu^2}{2} & -1-\frac{\mu^2}{2} & \frac{\kappa\mu\tilde{k}_p}{4} & \frac{\kappa\mu\tilde{k}_p}{4} & 0 & 0 \\ & & \tilde{k}_b^t & 0 & \frac{\mu\tilde{k}_p}{2} & 0 & 0 & 0 \\ & & & \tilde{k}_b^t & 0 & -\frac{\mu\tilde{k}_p}{2} & 0 & 0 \\ & \text{sym.} & & & \tilde{k}_b^n+\tilde{k}_p & 0 & -\tilde{k}_b^n & 0 \\ & & & & & \tilde{k}_b^n+\tilde{k}_p & 0 & -\tilde{k}_b^n \\ & & & & & & \tilde{k}_b^n+\tilde{k}_c & -\tilde{k}_c \\ & & & & & & & \tilde{k}_b^n+\tilde{k}_c \end{pmatrix}, \tag{4.20}$$

possess a similar structure. This similarity arises from the viscoelastic nature of most joints within the extended brake model, cf. Fig. 4.5. Merely

the connection between the lumped mass particles m_c is designed purely elastically. Without the incorporation of energy dissipation in the caliper, the corresponding entry $D_{78} = D_{87}$ equals zero.

The skew-symmetric contributions in the equations of motion, i.e. the gyroscopic matrix

$$\tilde{\mathbf{G}} = \begin{pmatrix} 0 & 2\tilde{\Theta}\tilde{\Omega}+\frac{\kappa\mu\tilde{d}_p}{2} & \frac{\mu\tilde{d}_p}{2} & -\frac{\mu\tilde{d}_p}{2} & 0 & 0 & 0 & 0 \\ & 0 & 0 & 0 & \frac{\kappa\mu\tilde{d}_p}{4} & \frac{\kappa\mu\tilde{d}_p}{4} & 0 & 0 \\ & & 0 & 0 & \frac{\mu\tilde{d}_p}{2} & 0 & 0 & 0 \\ & & & 0 & 0 & -\frac{\mu\tilde{d}_p}{2} & 0 & 0 \\ & \text{skew-sym.} & & & 0 & 0 & 0 & 0 \\ & & & & & 0 & 0 & 0 \\ & & & & & & 0 & 0 \\ & & & & & & & 0 \end{pmatrix} \tag{4.21}$$

and the circulatory matrix

$$\tilde{\mathbf{N}} = \begin{pmatrix} 0 & \frac{\mu}{4}(\kappa^2+2\kappa\tilde{k}_p+4) & \frac{\mu}{4}(\kappa+2\tilde{k}_p) & -\frac{\mu}{4}(\kappa+2\tilde{k}_p) & 0 & 0 & 0 & 0 \\ & 0 & -\frac{\mu^2}{2} & \frac{\mu^2}{2} & \frac{\kappa\mu\tilde{k}_p}{4} & \frac{\kappa\mu\tilde{k}_p}{4} & 0 & 0 \\ & & 0 & 0 & \frac{\mu\tilde{k}_p}{2} & 0 & 0 & 0 \\ & & & 0 & 0 & -\frac{\mu\tilde{k}_p}{2} & 0 & 0 \\ & \text{skew-sym.} & & & 0 & 0 & 0 & 0 \\ & & & & & 0 & 0 & 0 \\ & & & & & & 0 & 0 \\ & & & & & & & 0 \end{pmatrix}, \tag{4.22}$$

exhibit a similar composition since most zero entries have identical indices. Exceptions are the elements G_{23} and G_{24} which unlike their counterparts N_{23} and N_{24} are independent of μ. While $\tilde{\mathbf{G}}$ occurs due to both COULOMB friction and disc rotation, the circulatory matrix $\tilde{\mathbf{N}}$ is determined exclusively by the conditions at the frictional contact interface. This is especially relevant to the viscoelastic attributes of the pads, where its damping $\tilde{d}_p$ is considered in $\tilde{\mathbf{G}}$ and its stiffness $\tilde{k}_p$ is accounted for in $\tilde{\mathbf{N}}$. The circulatory matrix vanishes if the friction coefficient μ equals zero.

For the purpose of stability analysis and optimization, the parameter set is chosen to agree with the configuration listed in Tab. 4.1, which has been extracted from measurements for the two degree of freedom model [177]. The reference angular velocity is set to $\Omega_{\text{ref}} = 5\pi\,\text{s}^{-1}$. The extended minimal model requires the identification of seven additional mass, stiffness, and damping parameters for which no experimental data are available. In particular,

this concerns the additional damping coefficients. Numerical stiffness values of caliper and back plates are chosen to compare with [50], where Tab. 4.2 shows their relation to the respective dimensional quantity.

symbol	numerical value	relation to dimensional quantity	parameter description
$\tilde{m}_b$	1.60×10^{-3}	$\frac{m_b r \Omega_{\text{ref}}^2}{N_0}$	back plate mass
$\tilde{m}_c$	1.36×10^{-4}	$\frac{m_c r \Omega_{\text{ref}}^2}{N_0}$	caliper mass
$\tilde{k}_b^n$	130	$\frac{k_b^n r}{N_0}$	back plate stiffness in normal direction
$\tilde{k}_b^t$	260	$\frac{k_b^t r}{N_0}$	back plate stiffness in tangential direction
$\tilde{k}_c$	$43.\bar{3}$	$\frac{k_c r}{N_0}$	caliper stiffness

Table 4.2: Dimensionless mass and stiffness parameters of the extended model.

Tuning these components with respect to their eigenfrequencies yields an estimation of their inertial properties. The caliper mass, for example, corresponds to a measured eigenfrequency which lies within a frequency band of audible squeal noise [72]. The back plates' mass is approximated accordingly. A representation of a mass distribution observed in real brake systems is thus not guaranteed. Counterintuitively, the caliper is found to be lighter than the back plates and both masses are small in relation to the disc. However, since subsequent analyses require conformity of simulated and measured eigenfrequencies, the outlined approach is suitable and herein justified.

4.2.3 Stability behavior

The influence of the rotational speed as well as specific mass and stiffness properties on the stability of the equilibrium position is systematically investigated in [167]. Moreover, stability of the extended model defined via matrices (4.18)–(4.22) depends on the energy dissipation within its viscoelastic joints. This concerns damping due to disc, pads, and back plates which is

characterized by the dimensionless coefficients $\tilde{d}_t$, $\tilde{d}_p$, $\tilde{d}_b^t$, and $\tilde{d}_b^n$, respectively. Since exact numerical values are not available, basic features are discussed; pairs of these damping coefficients are contrasted. The remaining coefficients are set to zero in order to assess their individual contributions, where nondimensionalization ensures quantitative comparability. Inertial and stiffness parameters are held constant according to Tab. 4.1 and Tab. 4.2.

Fig. 4.6 depicts the stability boundary for various rotational speeds of the brake disc. Below the respective boundary, the trivial solution is unstable as there exists at least one eigenvalue with positive real part. Since eigenvalues occur in complex conjugate pairs, this is associated with a flutter-type instability which is interpreted as squeal.

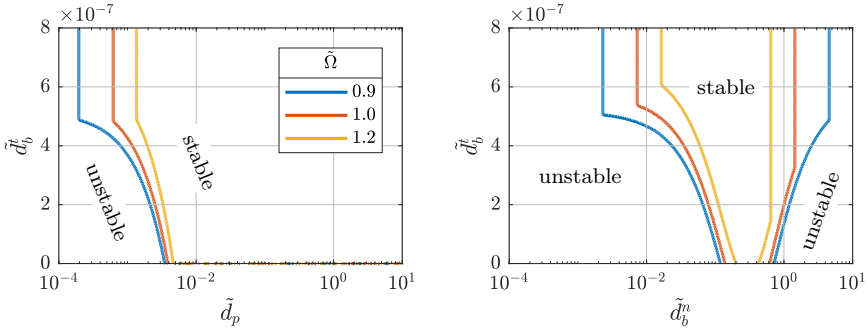

(a) $\tilde{d}_t = \tilde{d}_b^n = 0$. **(b)** $\tilde{d}_t = \tilde{d}_p = 0$.

Figure 4.6: Effects of pad and back plate damping on the stability boundary for various angular velocities.

As shown in Fig. 4.6a, the lines of constant angular speed are similar. Increasing $\tilde{\Omega}$ leads to a parallel shift of the stability boundary towards the upper right corner of the $\tilde{d}_p$-$\tilde{d}_b^t$-plane. Stabilization requires a compensation of this movement by damping in both normal and tangential direction to the disc. Hence, pad and tangential back plate dissipation need to be non-zero. The corresponding disc motion is damped by friction-induced forces and thus $\tilde{d}_t \neq 0$ is not necessary for asymptotic stability. It is furthermore apparent that an arbitrarily small $\tilde{d}_p$ in conjunction with an accordingly large $\tilde{d}_b^t$ is

not sufficient for a stable equilibrium position. In fact, energy dissipation in normal direction to the disc has to exceed a velocity-specific threshold. A comparison between Fig. 4.6a and Fig. 4.6b reveals that this value is approximately one order of magnitude smaller if pad damping is used instead of perpendicular back plate damping. If the only damping contribution is of COULOMB friction type, i.e. $\tilde{d}_t = \tilde{d}_p = \tilde{d}_b^n = \tilde{d}_b^t = 0$, the trivial solution is unstable in the entire velocity range. These features apply similarly to Fig. 4.6b, where energy dissipation in normal direction to the disc is implemented via the back plates instead of the pads. In this case, however, damping does not invariably contribute to stabilization as the trivial solution becomes unstable for sufficiently large values of $\tilde{d}_b^n$ independent of $\tilde{d}_b^t$.

As a conclusion, an asymptotically stable equilibrium position is not attainable as long as $\tilde{d}_b^t = 0$ since the tangential motion of the back plates is undamped in this case. Unlike in the two degree of freedom model, a single viscous damper is not capable of stabilizing the extended system. Neither energy dissipation in the disc nor in the pads nor in the back plates is pervasive, i.e. the trivial solution is unstable on the abscissa and the ordinate of the respective plane shown in Fig. 4.6.

4.2.4 Optimization approach

Optimization of the minimal model with two degrees of freedom encompasses a modification of the damping properties of both disc and pads. The extended model discussed here contains two additional points of energy dissipation, namely damping due to the back plates in normal and tangential direction, respectively. To account for the different physical origins, the damping matrix $\tilde{\mathbf{D}}$ of Eq. (4.19) is written as a linear combination

$$\begin{aligned} \tilde{\mathbf{D}} &= \tilde{\mathbf{D}}_0 + \sum_{i=1}^{s} \alpha_i \tilde{\mathbf{D}}_i \\ &= \tilde{\mathbf{D}}_c + \alpha_1 \tilde{\mathbf{D}}_t + \alpha_2 \tilde{\mathbf{D}}_p + \alpha_3 \tilde{\mathbf{D}}_b^n + \alpha_4 \tilde{\mathbf{D}}_b^t. \end{aligned} \tag{4.23}$$

The summands are itemized in appendix A.1, where $\tilde{\mathbf{D}}_0 = \tilde{\mathbf{D}}_c$ covers energy dissipation originating from COULOMB friction. The independent treatment

of damper viscosities is reflected in the parameter vector $\boldsymbol{\alpha} = (\alpha_1, \ldots, \alpha_4)^{\mathrm{T}}$ governing the relative contribution of the respective matrix to the overall damping. Comparison of decompositions (4.10) and (4.23) reveals that characteristic matrix properties are not preserved consistently. Due to the additional six degrees of freedom, the disc damping matrix is no longer positive definite. With exception of $\tilde{\mathbf{D}}_c$, which remains indefinite, all damping matrices are positive semi-definite and none of these contributions is pervasive.

In analogy to section 4.1.4, using standard complex eigenvalue analysis and a damping matrix of form (4.23), stability can be enhanced by variation of the weighting factors α_i. The extended system is considered to be more stable if its degree of stability is as large as possible. The objective of finding a favorable damping configuration is mathematically expressed following Eq. (4.11). In the specified model, the parameter optimization involves varying the ratio of damping in the disc, damping in the pads, and damping in the back plates. In order to determine the most beneficial distribution, inequality constraints (4.12) are imposed on the parameter vector $\boldsymbol{\alpha} \in \mathbb{R}^s$, where the number of optimization parameters is $s = 4$.

symbol	numerical value	relation to dimensional quantity	parameter description
$\tilde{d}_b^n$	0.001	$\frac{d_b^n r \Omega_{\mathrm{ref}}}{N_0}$	normal back plate damping
$\tilde{d}_b^t$	0.001	$\frac{d_b^t r \Omega_{\mathrm{ref}}}{N_0}$	tangential back plate damping
$\tilde{d}_p$	0.001	$\frac{d_p r \Omega_{\mathrm{ref}}}{N_0}$	pad damping
$\tilde{d}_t$	0.001	$\frac{d_t \Omega_{\mathrm{ref}}}{N_0 r}$	disc damping

Table 4.3: Dimensionless damping coefficients of the extended model.

While damper viscosities of the two degree of freedom model are based on experimental data, numerical values are unknown for the present system. For a conceptual study, the dimensionless damping coefficients $\tilde{d}_t$, $\tilde{d}_p$, $\tilde{d}_b^n$, and $\tilde{d}_b^t$ are assumed to be equal and small compared to Tab. 4.1. The corresponding reference values are listed in Tab. 4.3. Pad and disc damping relate approx-

imately to one third respectively one quarter of their measured equivalent given in Tab. 4.1. Numerical treatment of the outlined optimization problem is sought using a generalized pattern search algorithm implemented in MATLAB's global optimization toolbox, cf. section 2.4.

4.2.5 Optimization results

In agreement with section 4.1.5, presentation of optimization results is motivated by the governing parameters' natural dependence on the operating conditions. Irrespective of these uncertainties, an adequate braking torque needs to be ensured. Aside from the capability of reducing vehicle speed, preventing self-excited vibrations is part of the development process of disc brakes. The onset of squeal is related to the energy dissipation in the respective component as well as its relative contribution to the overall damping.

Fig. 4.7 highlights the optimum ratio between all damper viscosities involved for various angular velocities and friction coefficients. This particularly concerns damping in the disc, damping in the pads, and perpendicular and tangential damping in the back plates. In each contour plot, the braking torque is held constant according to Eq. (4.5), i.e. high friction coefficients correspond to low normal forces and vice versa. The graphs indicate that the admissible damping range is fully exploited. The global optimum in the $\tilde{\Omega}$-μ-plane lies on the boundary defined by $\alpha_1 + \alpha_2 + \alpha_3 + \alpha_4 = 4$ and non-negative weighting factors.

Most of the damping is divided among disc and pads. For small angular velocities and friction coefficients, energy dissipation is found to be more beneficial in the disc, while for large $\tilde{\Omega}$ and μ, damping in the pads becomes more favorable. From a qualitative perspective, this distribution corresponds to the two degree of freedom model. The additional translational degrees of freedom thus do not affect the principal behavior according to which gyroscopic perturbations require a compensation via non-uniformly distributed dissipation in the form of pad damping, cf. section 3.3.

Energy dissipation in the back plates plays a minor, yet non-negligible role. As pointed out in section 4.2.3, stabilization requires sufficiently large damp-

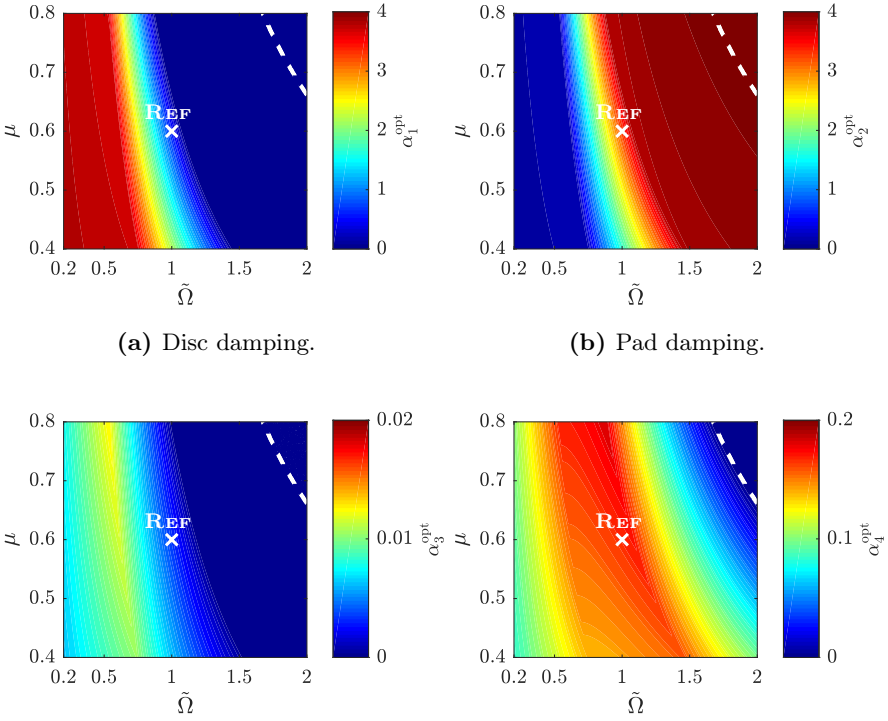

(a) Disc damping.

(b) Pad damping.

(c) Back plate damping (normal).

(d) Back plate damping (tangential).

Figure 4.7: Optimum damping distribution between disc, pads, and back plates for constant braking torque over various angular velocities and friction coefficients.

ing in both normal and tangential direction to the disc. This implies non-zero values for either α_2 or α_3 in addition to α_4, which is reflected in the optimization. Corresponding factors weighting the back plate damping are one to two orders of magnitude smaller than their equivalents scaling disc and pad damping. In tangential direction, back plate damping is advantageous especially for medium rotational speeds, yet its impact decays when approaching the stability boundary. In normal direction, the optimum is coupled to the ratio between disc and pad damping. On the lower end of the speed range where the disc dominates energy dissipation, pads and back plates act coop-

eratively. With growing rotational speed, the latter contribution declines and approaches zero. Thereafter, pad damping alone provides a more suitable way to compensate motions perpendicular to the disc.

Similar to the two degree of freedom model, an optimal distribution is not invariably sufficient for stability within the linearly constrained parameter region. For parameter combinations which are located on the right of the white dashed line, the system's total damping needs to be increased to ensure a stable trivial solution, e.g. via raising the initial damping coefficients from Tab. 4.1. In this domain, an improvement of the noise behavior exclusively via the structure of $\tilde{\mathbf{D}}$ and complementary damping coefficients is not possible.

Up to this point, stability enhancement is based on the optimum distribution of energy dissipation in disc, pads, and back plates and is tailored to merely one specific reference point. As stated in section 4.1.5, damping coefficients in real systems cannot be chosen individually for each parameter combination. Instead, the system is optimized to an operating regime and thus exposed to perturbations. In Fig. 4.8, the contour plot of a non-optimized configuration is compared to a case which is tuned to the operating point 'Ref'. Normalization of the degree of stability is performed with respect to its optimized equivalent. The latter is obtained from determining individual weighting factors at each point in the $\tilde{\Omega}$-μ-plane. Damping is optimally distributed and the trivial solution is as stable as possible within linear constraints (4.12) when the ratio $\zeta_{\mathrm{abs}}/\zeta_{\mathrm{abs}}^{\mathrm{opt}}$ equals identity.

The non-optimized state is captured in Fig. 4.8a in which all weighting factors remain equal to one. Unlike the two degree of freedom model, there exists no band with maximum degree of stability, i.e. the ratio $\zeta_{\mathrm{abs}}/\zeta_{\mathrm{abs}}^{\mathrm{opt}}$ is smaller than one in the entire parameter range. In the best case, the absolute stability reserve is approximately 84 % of its theoretically possible optimum value and decreases rapidly with growing $\tilde{\Omega}$. The stability boundary is therefore shifted towards smaller friction coefficients and angular velocities. In comparison to the optimized configuration whose stability boundary is indicated by the white dashed line, the unstable domain enlarges when the damping matrix is not adapted to certain operating conditions. With regard to Fig. 4.4a, the non-optimized state in the extended model leads to a significantly larger

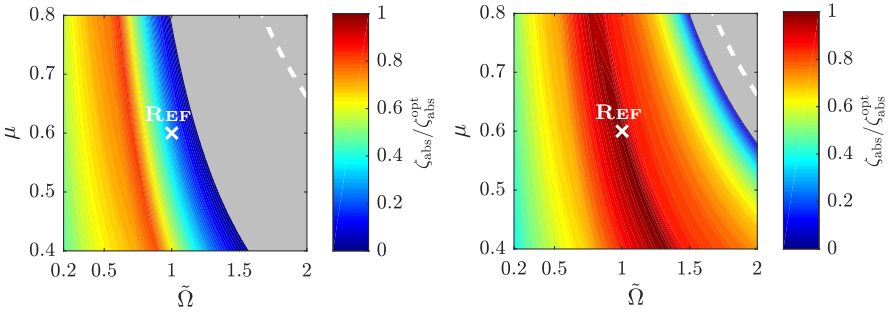

(a) $\zeta_{\mathrm{abs}}(\alpha_1 = 1, \ldots, \alpha_4 = 1)$. **(b)** $\zeta_{\mathrm{abs}}(\alpha_1 = \alpha_{1,\mathrm{ref}}^{\mathrm{opt}}, \ldots, \alpha_4 = \alpha_{4,\mathrm{ref}}^{\mathrm{opt}})$.

Figure 4.8: Normalized degree of stability for constant braking torque over various angular velocities and friction coefficients. ◉ $\zeta_{\mathrm{abs}} < 0$, i.e. flutter instability.

instability region. A uniform damping distribution according to Tab. 4.3 thus is less favorable in the minimal model with eight degrees of freedom.

Fig. 4.8b depicts a configuration tailored to the reference point. The corresponding damping distribution yields the largest possible degree of stability for $\tilde{\Omega} = 1$ and $\mu = 0.6$. The optimum regime, where the ratio $\zeta_{\mathrm{abs}}/\zeta_{\mathrm{abs}}^{\mathrm{opt}}$ is close to identity, is more dominant than in Fig. 4.8a especially for medium to large angular velocities. This also reflects in an improved stability boundary, which approaches the limit calculated individually for each operating point. Compared to the two degree of freedom model, however, the attained stability boundary is more conservative. The extended system becomes unstable for smaller friction coefficients and angular velocities if the energy dissipation due to disc, pads, and back plates is tuned to the design point 'REF', cf. Fig. 4.4b.

The results presented above are summarized by an example illustrating the evolution of the weighting factors and the degree of stability for a constant friction coefficient and varying angular velocity. As denoted by the dashed lines in Fig. 4.9, the plot range is classified into three sections via $\tilde{\Omega}_1$ and $\tilde{\Omega}_2$. At these angular velocities, the optimized degree of stability is not differentiable since a different eigenvalue becomes objective. The optimized weighting factors of disc, pads, and back plates exhibit a kink at these values

of $\tilde{\Omega}$, cf. Fig. 4.9a. In sector ①, optimum energy dissipation is dominated by damping in the disc; other contributions are one to two orders of magnitude smaller. Damping of motions perpendicular to the disc is distributed among the back plates and the pads, the latter of which take up a larger part. In sector ②, where $\tilde{\Omega}_1 < \tilde{\Omega} < \tilde{\Omega}_2$, the proportions of disc and back plates (normal) are transferred progressively to the pads, whose contribution increases with growing angular velocity by the equivalent amount. This behavior is qualitatively similar to the two degree of freedom model and occurs in the same rotational velocity band. In sector ③, energy dissipation is favorable in the pads. The only non-zero contribution besides the pads is the tangential component of the back plates. This component does not change significantly over the entire velocity range. Optimization results thus depict the utilization of a small portion of the overall damping for tangential back plate damping indicating its necessity for asymptotic stability.

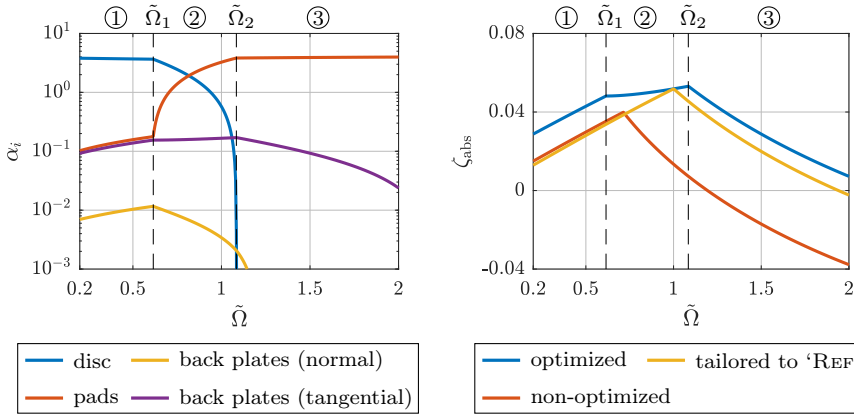

(a) Weighting factors. **(b)** Degree of stability.

Figure 4.9: Evolution of objective function and solution of optimization problem (4.11) at $\mu = 0.6$ for varying angular velocity.

The corresponding optimized degree of stability is depicted in Fig. 4.9b. In comparison to the non-optimized case, the absolute stability reserve is increased by tuning the damping distribution among all brake components

involved. An optimum adjustment of energy dissipation additionally prevents its early decay in sector ② due to which the non-optimized system becomes unstable for $\tilde{\Omega} > 1.2$. If damping is tailored to an operating regime, the maximum possible ζ_{abs} is merely attained at the reference point, where $\tilde{\Omega} = 1$. However, this specific configuration increases the average degree of stability over the entire plot range and enlarges the stable domain since the stability boundary is shifted towards higher angular velocities.

4.3 High-dimensional finite element models

4.3.1 Modeling

Subsequent to the extension of the minimal model to eight degrees of freedom, a further refinement step is the approximation of the brake geometry by a finite number of discrete elements. The analyses include two high-dimensional systems of different levels of detail. Fig. 4.10a shows a model with simplified geometry having a coarse mesh with 4600 degrees of freedom. Fig. 4.10b represents the current state of the art of an internally ventilated disc brake used in automotive industry with 104 000 degrees of freedom. Both models consist of a disc which rotates with a prescribed angular speed Ω and is in prestressed frictional contact with two rigidly guided pads. Unlike the simplified variant, where the pads are elastically attached to the caliper, in the more realistic model, the pads are fixed to back plates and further embedded in the caliper. In both cases, the latter is axially supported against ground.

Assumptions and limitations in the finite element environment are similar to those in the minimal models with two and eight degrees of freedom, respectively. The contact between disc and pads is assumed to be of COULOMB-type with a velocity-independent and isotropic friction coefficient μ. The pads are loaded with a constant pressure p which is considered large enough to invariably maintain contact. Stick-slip phenomena are ruled out as long as the disc rotates sufficiently fast which implies a non-vanishing relative velocity at the contact interface. As a consequence, friction forces are continuous and linearization of the equations of motion is admissible. Damping within the

respective brake components is modeled by a material specific loss factor χ. This dimensionless parameter is an aggregate of energy dissipation due to numerous microscopic sources and mechanisms which are characteristic for the given material and structure, cf. section 2.3.2.

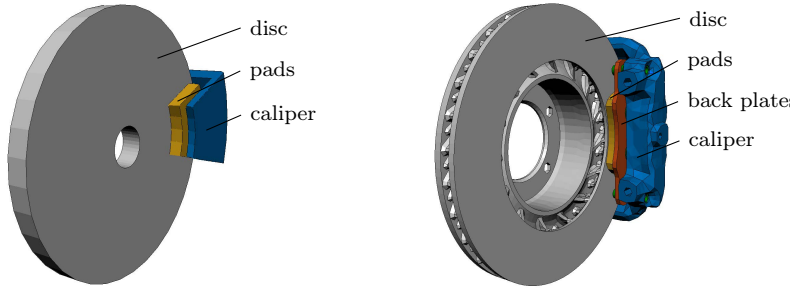

(a) Simplified model adopted from [78]. **(b)** Realistic model used in industry.

Figure 4.10: High-dimensional finite element models of disc brakes.[†]

4.3.2 Equations of motion

In a finite element environment, the linearized equations of disturbed motion near a static equilibrium can be written in the general form

$$\mathbf{M}\ddot{\mathbf{q}} + \mathbf{B}\dot{\mathbf{q}} + \mathbf{C}\mathbf{q} = \mathbf{0}, \tag{4.24}$$

where time-variance of mass and stiffness properties as well as external forces are neglected. With respect to an inertial coordinate frame, the corresponding velocity and coordinate proportional matrices read

$$\mathbf{B} = \mathbf{D}_* + \frac{\Omega_{\text{ref}}}{\Omega}\mathbf{D}_c + \frac{\Omega}{\Omega_{\text{ref}}}\mathbf{G}, \tag{4.25a}$$

$$\mathbf{C} = \mathbf{K} + \mathbf{K}_c + \left(\frac{\Omega}{\Omega_{\text{ref}}}\right)^2 \mathbf{K}_g + \mathbf{N}, \tag{4.25b}$$

resulting from a mathematical formulation of the dynamics of a rotating, elastic system including frictional contacts [89]. Since the friction coefficient

[†]In the following, the simplified variant adopted from [78] is referred to as 'model 4.10a', while the realistic variant used in industry is referred to as 'model 4.10b'.

is assumed to be constant and the influence of centrifugal loads on the contact state is negligible, contact forces do not depend on the magnitude of the rotational speed. As a consequence, variation of Ω is admissible a posteriori, i.e. after the equations of motion (4.24) have been derived. An advantage of this procedure is a reduction of computational cost since the system matrices need to be generated for merely one single reference angular velocity Ω_{ref}.

In commercial finite element software packages, such as PERMAS, the formal derivation of matrices (4.25) is generally comprised of two steps [78]. The initial equations of motion are of type **MK** describing a non-rotating, unloaded, and undamped brake. In the first step, a nonlinear static analysis is performed in order to establish the contact state under given static loads, such as braking pressure and rotational speed of the disc. The resulting contact forces are decomposed vectorially by means of COULOMB's law (2.35). Subsequent kinematic linearization and differentiation between symmetric and skew-symmetric contributions yields three additional matrices. Coordinate proportional terms specify the contact stiffness matrix $\mathbf{K}_c$ as well as the circulatory matrix $\mathbf{N}$, while velocity proportional terms define the COULOMB damping matrix $\mathbf{D}_c$. Coherent to the minimal models, the latter is inversely proportional to the angular velocity of the disc, i.e. friction-induced energy dissipation decays with Ω. The second step encompasses a linear static analysis in order to consider effects arising from the brake disc rotation. Determination of the internal stress state under centrifugal loads results in coordinate proportional terms depending on the square of the rotational speed. These terms lead to a stiffening of the brake disc with growing Ω and are concatenated in $\mathbf{K}_g$, which is commonly referred to as geometric stiffness matrix. It further contains convective portions originating from an EULERian formulation of the equations of motion [90]. Another outcome is the gyroscopic matrix $\mathbf{G}$, which depends linearly on the rational speed.

The existence and structure of $\mathbf{D}_*$ relies on the modeling of energy dissipation. In order to treat its physical origins independently, the damping matrix $\mathbf{D}_* = \mathbf{D}_v + \mathbf{D}_m$ is decomposed into a matrix $\mathbf{D}_v$ covering miscellaneous viscous damping contributions and a matrix $\mathbf{D}_m$ accounting for energy dissipation in each brake component. In finite element software packages, the

latter is usually modeled via a complex stiffness approach [104]. However, following the discussion in section 2.3.2, material damping is satisfactorily expressed in terms of its viscous equivalent, which is defined by the same energy loss per cycle of oscillation. In analogy to Eq. (2.34), the equivalent viscous damping matrix for $\chi \ll 1$ is given by

$$\mathbf{D}_m = \frac{1}{\Omega_{\mathrm{cev}}} \sum_{i=1}^{l} \chi_i \mathbf{K}_i, \tag{4.26}$$

with an individual loss factor and elastic stiffness matrix for each of the l components of the brake assembly. In Eq. (4.26), the frequency dependence is neglected by setting a circular reference frequency Ω_{cev} [79]. A conservative choice, i.e. picking Ω_{cev} greater or equal than the actual Ω, assures that the effective damping is not overestimated in the frequency range of interest.

Due to the large number of degrees of freedom and generally asymmetric system matrices, numerical eigenvalue determination of system (4.24) is elaborate. On this account, the standard reduction technique of modal truncation is applied leading to a system of smaller scale while maintaining its essential dynamical behavior [11, 43]. Since brake squeal occurs within a bounded frequency band, i.e. $f \in [f_{\mathrm{lb}}, f_{\mathrm{ub}}] \subset \mathbb{R}$, a transformation to a subspace containing only modes up to a certain frequency limit $f_{\mathrm{lim}} > f_{\mathrm{ub}}$ is beneficial. Eigenvalue analysis of the undamped, conservative system

$$\mathbf{M}\ddot{\mathbf{q}} + \mathbf{K}\mathbf{q} = \mathbf{0}, \tag{4.27}$$

with positive definite mass and stiffness matrix of dimension $n \times n$, yields purely imaginary eigenvalues $\lambda_1, \lambda_2, \ldots, \lambda_{2n}$ and guarantees real eigenvectors $\mathbf{r}_1, \mathbf{r}_2, \ldots, \mathbf{r}_{2n}$ [62]. This simplification is obtained from the original system (4.24) by neglecting disc rotation as well as effects of friction and velocity proportional forces. Assuming a minor influence of the omitted terms on the mode shapes, the span of m eigenvectors associated with the first m eigenfrequencies forms the basis of the subspace transformation. This span of eigenvectors of the **MK**-system defines the columns of the rectangular modal matrix

$$\mathbf{R} = (\mathbf{r}_1 \ \mathbf{r}_2 \ \ldots \ \mathbf{r}_m), \tag{4.28}$$

where $|\operatorname{Im}(\lambda_1)| < |\operatorname{Im}(\lambda_2)| < \cdots < |\operatorname{Im}(\lambda_m)|$ and $\mathbf{R} \in \mathbb{R}^{n\times m}$. Introducing the approximate coordinate substitution

$$\mathbf{q} = \mathbf{R}\mathbf{p} \tag{4.29}$$

into the equations of motion (4.24) and subsequent premultiplication with the transpose $\mathbf{R}^{\mathrm{T}}$ to preserve the symmetry properties of the respective matrices leads to the truncated second-order system

$$\bar{\mathbf{M}}\ddot{\mathbf{p}} + \bar{\mathbf{B}}\dot{\mathbf{p}} + \bar{\mathbf{C}}\mathbf{p} = \mathbf{0}. \tag{4.30}$$

Herein, the bar denotes the modal matrices $\bar{\mathbf{M}} = \mathbf{R}^{\mathrm{T}}\mathbf{M}\mathbf{R}$, $\bar{\mathbf{B}} = \mathbf{R}^{\mathrm{T}}\mathbf{B}\mathbf{R}$, and $\bar{\mathbf{C}} = \mathbf{R}^{\mathrm{T}}\mathbf{C}\mathbf{R}$ of dimension $m \times m$. The upper frequency limit f_{lim} determines the number of modes to be computed and thus specifies the m-dimensional subspace. For $m \ll n$, the projected system (4.30) is of smaller scale in comparison to its high-dimensional original. The outlined technique leads to a decrease of computational cost as it limits the eigenvalue calculation to a predefined frequency interval. An alternative variant of model reduction by means of eigenvectors of the non-simplified **MBC**-system is derived in [51].

4.3.3 Convergence study

The solution of truncated system (4.30) with respect to its $2m$ eigenvalues and eigenvectors is based on a transformation projecting the physical coordinates onto a domain of lower dimension. The quality of this approximation depends on the number of eigenvectors spanning the corresponding subspace. Commonly, the highest occurring frequency in the subspace is taken to be a factor of two to three times larger than the upper frequency bound of interest, i.e. $f_{\mathrm{lim}} \geq 2 - 3 f_{\mathrm{ub}}$. However, there is no general law on how to choose f_{lim} for a given frequency interval.

To study the size of the subspace and its qualitative influence on the solutions of system (4.30), the model with simplified geometry depicted in Fig. 4.10a is used. The angular velocity of the disc is exemplarily set to $\Omega = \pi\,\mathrm{s}^{-1}$. Fig. 4.11 shows the evolution of eigenvalues with positive real part over the frequency ratio $f_{\mathrm{lim}}/f_{\mathrm{ub}}$ and over m/n, which is a normalized

measure of the subspace dimension and grows approximately linearly with the frequency ratio. In the plotted range between $f_{\mathrm{lb}} = 0.5\,\mathrm{kHz}$ and $f_{\mathrm{ub}} = 6\,\mathrm{kHz}$, three modes are unstable. Since damping is small and thus has little impact on the natural eigenfrequencies, the imaginary part can be reproduced with sufficient accuracy using few eigenvectors of the **MK**-system, cf. Fig. 4.11a. The course of all three imaginary parts is virtually constant over the size of the subspace. This does not apply to the real part presented in Fig. 4.11b. The higher the frequency, i.e. the imaginary part, the more eigenvectors are required for convergence. The real part of λ_1 and λ_2 is converged for a frequency ratio greater than two, while $\mathrm{Re}(\lambda_3)$ approaches its effective value for $f_{\mathrm{lim}}/f_{\mathrm{ub}} > 4$. As Gräbner [49] pointed out for a more realistic brake model, the number of unstable eigenvalues is not necessarily constant over the subspace dimension. With growing frequency limit f_{lim}, further eigenvalues with positive real part may be detected. Hence, truncation of physical coordinates may lead to unsatisfactory stability information if m is not chosen sufficiently large. Although this case does not occur in the simplified variant considered here, the common recommendation of $f_{\mathrm{lim}} \geq 2 - 3f_{\mathrm{ub}}$ results in an estimate of $\mathrm{Re}(\lambda_3)$ which is too conservative. For this reason, all subsequent analyses are performed using a frequency ratio greater than or equal to four.

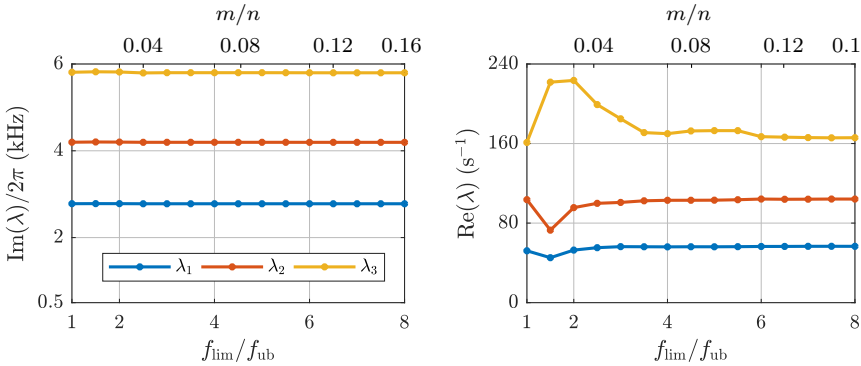

(a) Imaginary part. **(b)** Real part.

Figure 4.11: Evolution of eigenvalues with positive real part for varying frequency ratio and subspace dimension.

4.3.4 Optimization approach

Determination of favorable damping configurations for the minimal models with two and eight degrees of freedom, respectively, incorporates the tailoring of damper viscosities at discrete locations. In the finite element models discussed here, energy dissipation is distributed over each component of the brake assembly. This is modeled by a material-specific loss factor which by means of Eq. (4.26) expresses an equivalent viscous damping. To account separately for material damping in disc, pads, back plates, and caliper, the symmetric part of velocity proportional matrix (4.25a) is written as

$$\begin{aligned}\mathbf{D} &= \frac{\Omega_{\mathrm{ref}}}{\Omega}\mathbf{D}_c + \mathbf{D}_* \\ &= \underbrace{\frac{\Omega_{\mathrm{ref}}}{\Omega}\mathbf{D}_c + \mathbf{D}_v}_{\mathbf{D}_0} + \sum_{i=1}^{s} \alpha_i \mathbf{D}_{m,i}.\end{aligned} \tag{4.31}$$

The first two summands, i.e. the matrices covering COULOMB damping as well as miscellaneous viscous damping portions, constitute the matrix $\mathbf{D}_0$ which remains unaffected during optimization. The third summand is a linear combination of α_i-weighted material damping matrices whose relative contribution to the overall damping is to be varied. Since each $\mathbf{D}_{m,i}$ is proportional to χ_i, the approach directly involves the variation of the corresponding loss factors. Their independent treatment reflects in the parameter vector $\boldsymbol{\alpha} = (\alpha_1, \ldots, \alpha_4)^{\mathrm{T}}$, where Tab. 4.4 assigns the indices to the respective component of the brake assembly.

Decomposition (4.31) along with complex eigenvalue analysis enables stability enhancement of system (4.24) by tuning the weighting factors α_i. For this purpose, a system is considered to be more stable if its eigenvalue with largest real part is as small as possible. In compliance with section 2.4, this is mathematically stated as

$$\begin{aligned}&\max_{\boldsymbol{\alpha}} \zeta_{\mathrm{abs}} \\ &\text{subject to} \\ &f_{\mathrm{lb}} \leq \frac{|\operatorname{Im}(\lambda)|}{2\pi} \leq f_{\mathrm{ub}} \quad \text{and} \quad \mathbf{c}(\boldsymbol{\alpha}) \leq \mathbf{0}.\end{aligned} \tag{4.32}$$

The lower and upper bounds f_{lb} and f_{ub} limit the objective function to a desired frequency range of interest in which brake squeal mainly occurs. Depending on the considered brake system, further restrictions are imposed on the admissible parameter space via $\mathbf{c}(\boldsymbol{\alpha})$. Determination of the most beneficial damping distribution in simplified model 4.10a, for example, requires linear inequality constraints according to Eq. (4.12). In the more realistic model 4.10b, optimization for a given range of loss factors demands the limitation of the parameter vector to an interval defined by

$$\boldsymbol{\alpha}_{\mathrm{lb}} \leq \boldsymbol{\alpha} \leq \boldsymbol{\alpha}_{\mathrm{ub}}. \tag{4.33}$$

In both variants, parameter optimization involves varying the ratio of damping in disc, pads, caliper, and back plates (model 4.10b only). In real brake systems, these components are made of different materials. The disc material, for example, is usually cast iron, while the caliper is commonly made of aluminum. The corresponding loss factors are listed in Tab. 4.4, where their magnitude complies with numerical values encountered in literature [8]. As stated by references reviewed in [136], however, these values may vary over several orders of magnitude. This variation handicaps the rating of the technical relevance and feasibility of the computed optima. For a conceptual study, the assumption of equal χ_i serves as a benchmark. The resulting damping distribution obtained from optimization is hence further assessed in terms of suitable materials for the individual brake components.

i	part	material	loss factor χ_i	
			model 4.10a	model 4.10b
1	disc	cast iron	5×10^{-3}	
2	pads	complex composite	5×10^{-3}	
3	back plates	steel	n/a	5×10^{-3}
4	caliper	aluminum	5×10^{-3}	

Table 4.4: Components and corresponding loss factors of the finite element models.

Although damping is tailored with respect to a modal subspace defined by rectangular matrix (4.28), back transformation of optimization results into the physical domain is admissible. This is facilitated by decomposition (4.31), which combines the respective damping matrices linearly. The invariance of these scalar multiplications allows for a back transformation into the physical space via coordinate substitution (4.29). Coherent to previous evaluations, the outlined problem is sought using a generalized pattern search algorithm implemented in MATLAB's global optimization toolbox, cf. section 2.4.

4.3.5 Optimization results

A comparison between analytical and numerical calculations obtained in [49] shows that stability-relevant effects, such as friction and rotation, are considered correctly in the finite element environment. The investigated low-dimensional brake model is able to reproduce the impacts of, among others, gyroscopic and circulatory terms including COULOMB damping. Thus, the implementation of matrices (4.25) proposed in [5] is validated.

In agreement with previously presented results, the product $\mu \cdot p$, which is an analogous measure of braking torque (4.5), is held constant, i.e. high friction coefficients correspond to low braking pressures and vice versa. Optimization results of models depicted in Fig. 4.10a and Fig. 4.10b are discussed individually. In both cases, the reference angular velocity is set to $\Omega_{\mathrm{ref}} = 5\pi\,\mathrm{s}^{-1}$ which along with $\mu = 0.6$ defines a virtual operating point 'REF'. The frequency range of interest is limited by $f_{\mathrm{lb}} = 0.5\,\mathrm{kHz}$ and $f_{\mathrm{ub}} = 5\,\mathrm{kHz}$.

Model 4.10a

Fig. 4.12 shows the influence of material damping in disc, pads, and caliper on the degree of stability at the reference point. Coherent to the minimal models with two and eight degrees of freedom, respectively, both magnitude and location of energy dissipation are decisive for stability. The unstable regime ($\zeta_{\mathrm{abs}} < 0$) is split into two sections via the dashed line indicating the number of unstable modes within the considered frequency range. Regime ① is comprised of one unstable mode, while in regime ② there are two eigenvalue pairs

with positive real part. The same applies to the origin, where all loss factors vanish and the only damping contribution is of COULOMB friction type. In Fig. 4.12a, stabilization requires a sufficiently large value of χ_1, χ_2, or a combination of both. Beyond velocity-specific thresholds, the trivial solution is asymptotically stable on the abscissa and the ordinate which implies pervasive dissipation in disc and pads. This is similar to the minimal model with two degrees of freedom, cf. Fig. 4.2a. In contrast to disc and pad damping, energy dissipation in the caliper is not pervasive since even an arbitrarily large χ_4 is not exclusively able of stabilizing the trivial solution, cf. Fig. 4.12b.

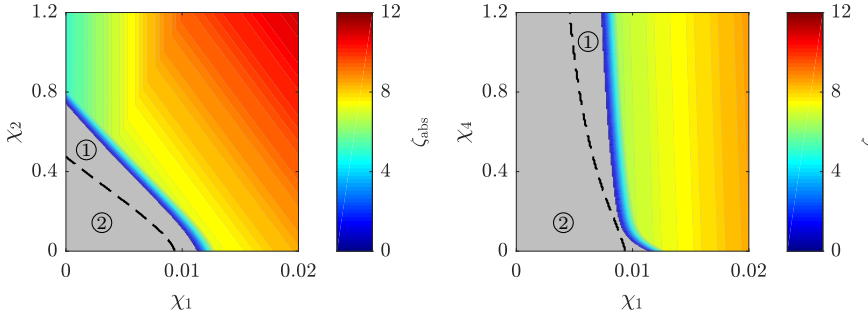

(a) Pads over disc for $\chi_4 = 0$.

(b) Caliper over disc for $\chi_2 = 0$.

Figure 4.12: Effects of damping in disc, pads, and caliper on the degree of stability at 'REF'. ◍ $\zeta_{\mathrm{abs}} < 0$, i.e. flutter instability.

From a quantitative perspective, the degree of stability is most sensitive to disc damping. The larger χ_1 for a given χ_2 or χ_4, respectively, the higher in general ζ_{abs}. The influence of energy dissipation in pads and caliper is smaller by orders of magnitude. The latter is rather insignificant as lines of constant ζ_{abs} in Fig. 4.12b are approximately parallel to the ordinate. However, an increase of loss factors χ_2 and χ_4 does not adversely affect stability. Searching for an advantageous configuration confirms these evaluations. Within the domain which is restricted linearly by Eq. (4.12), optimization suggests disc damping to be the most beneficial contribution. The optimum is determined by the weighting factors $\alpha_1^{\mathrm{opt}} = 3$, $\alpha_2^{\mathrm{opt}} = 0$, and $\alpha_4^{\mathrm{opt}} = 0$. Hence, energy

dissipation in pads and caliper is found to have a minor significance with regard to stability. In opposition to both minimal models, this distribution is robust against natural parameter fluctuations. It is completely independent of the friction coefficient and the angular velocity of the disc. An increase of Ω, for example, moves the stability boundary towards the upper right corner of the respective plane, yet the system continues to exhibit the same favorable damping distribution. In the entire operating regime considered, the optimum is invariably located on the edge of the admissible parameter space.

In Fig. 4.13, contour plots of two damping configurations are compared at constant braking torque and various angular velocities and friction coefficients. The non-optimized state is covered in Fig. 4.13a where all weighting factors are equal to unity. The corresponding degree of stability shows a weak dependence on angular speed and is more sensitive to an altering friction coefficient. For a wide velocity span and moderate μ, the maximum stability reserve is around 65 % of its optimized counterpart, yet it decays rapidly towards the stability boundary. For $\mu > 0.62$, the trivial solution is unstable independent of Ω.

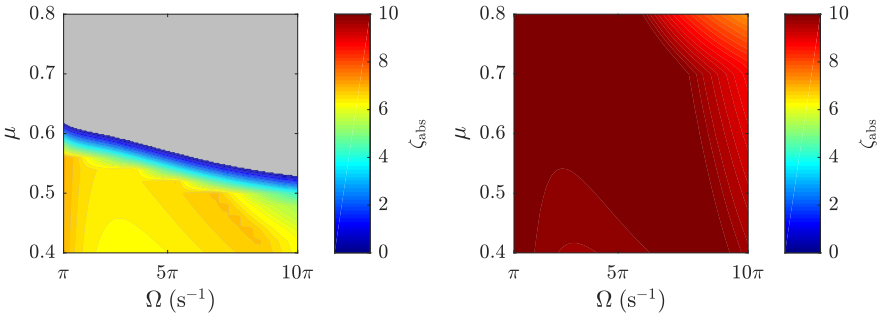

(a) Non-optimized. **(b)** Optimized.

Figure 4.13: Degree of stability for constant braking torque over various angular velocities and friction coefficients. ● $\zeta_{\mathrm{abs}} < 0$, i.e. flutter instability.

The optimized configuration in Fig. 4.13b is characterized by the weighting factors $\alpha_1^{\mathrm{opt}} = 3$, $\alpha_2^{\mathrm{opt}} = 0$, and $\alpha_4^{\mathrm{opt}} = 0$ which are constant over the entire plot range. Similarly, the optimized degree of stability is virtually constant and

insusceptible to perturbations; it only decays slightly in the upper right corner of the Ω-μ-plane. The tailored damping configuration moves the stability boundary towards higher friction coefficients and angular velocities such that ζ_{abs} remains positive. As a result, its maximum value is enhanced by about 50 % when damping is shifted from pads and caliper to the disc.

Model 4.10b

In comparison to the lower dimensional variant, the finite element model used in industry exhibits a qualitatively similar stability behavior. The degree of stability is most sensitive to damping in the disc, while energy dissipation in pads, back plates, and caliper plays a minor, yet non-negligible role. This is confirmed by numerical simulations in a parameter space which is linearly constrained via Eq. (4.12). Independent of Ω and μ, the optimum weighting factors are found to read $\alpha_1^{\mathrm{opt}} = 4$, $\alpha_2^{\mathrm{opt}} = 0$, $\alpha_3^{\mathrm{opt}} = 0$, and $\alpha_4^{\mathrm{opt}} = 0$. However, contrary to the simplified version 4.10a, a higher energy dissipation in the more complex model is not necessarily advantageous since adding damping may contribute to destabilization.

This paradox is visualized in Fig. 4.14, where the optimized weighting factors of back plates and caliper are plotted over various angular velocities and friction coefficients. The parameter domain is restricted by Eq. (4.33) determining the upper and lower bounds of $\boldsymbol{\alpha}$. Each weighting factor can vary between 0.5 and 2. Hence, the initial loss factor of each brake component listed in Tab 4.4 may at most be doubled or reduced by half. Despite an optimum distribution, asymptotic stability is not ensured within these impositions. Parameter combinations which are located on the right of the white dashed line yield an unstable trivial solution. For stabilization, the system's total damping needs to be increased, e.g. via increasing the initial χ_i.

Optimization results reveal the benefit of disc and pad damping. The corresponding weighting factors $\alpha_1^{\mathrm{opt}} = \alpha_2^{\mathrm{opt}} = 2$ lie on their upper bound and are robust against perturbations. While the weighting factors of disc and pads are found to be constant over the entire range of interest, contour plots in Fig. 4.14 depict regions where energy dissipation in back plates and caliper

adversely affects stability. In these regions, α_3^{opt} and α_4^{opt}, which are functions of Ω and μ, lie on their lower limit. The admissible parameter space is not fully exploited. In Fig. 4.14a, the triangular regime of unfavorable back plate damping corresponds to medium to large angular velocities and friction coefficients. The transition between the upper and lower bound is continuous, yet small changes of Ω and μ lead to drastic changes of α_3^{opt}. In the stable domain, the transition runs parallelly to the stability boundary at slightly lower values of μ. These observations apply similarly to Fig. 4.14b. The band of unfavorable caliper damping is larger as it extends over the entire velocity range. Apart from the upper right corner, where the trivial solution is unstable, caliper damping merely contributes to stabilization in the triangular lower left half of the Ω-μ-plane. Prior to reaching the stability boundary, α_4^{opt} drops to the lower bound of the admissible parameter space reflecting the advantage of small caliper damping in this domain.

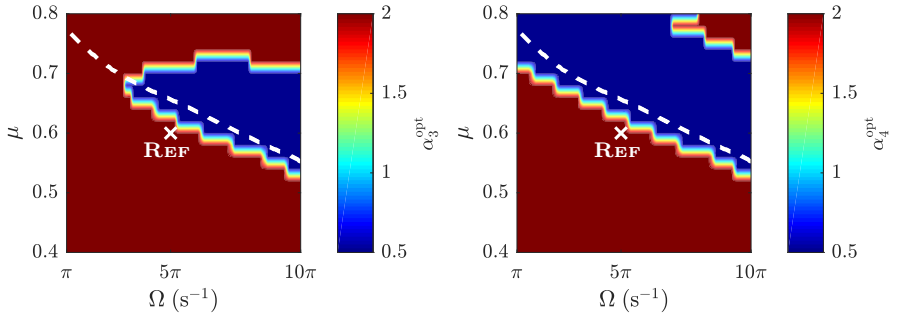

(a) Back plate damping. **(b)** Caliper damping.

Figure 4.14: Favorable damping in back plates and caliper for constant braking torque over various angular velocities and friction coefficients.

In agreement with the discussion in sections 4.1.5 and 4.2.5, damping properties in real systems cannot be chosen individually for a given parameter combination. Instead, materials and corresponding loss factors are optimized to be compatible with a specific operating regime which is subject to natural fluctuations. Contour diagrams shown in Fig. 4.15 emphasize the difference

between the non-optimized case, where all weighting factors are equal to unity, and a configuration which is tuned to the virtual operating point 'Ref'. The degree of stability ζ_{abs} is normalized with respect to its optimized equivalent $\zeta_{\text{abs}}^{\text{opt}}$, which is obtained from determining a set of α_i^{opt} at each point in the Ω-μ-plane. Within linear constraints (4.33), the trivial solution is as stable as possible when $\zeta_{\text{abs}}/\zeta_{\text{abs}}^{\text{opt}} = 1$.

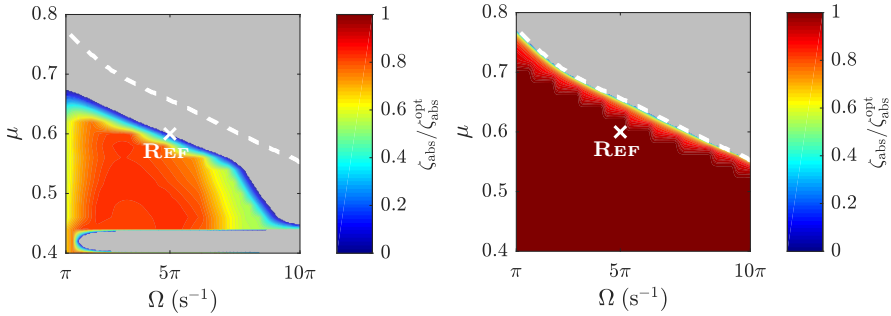

(a) $\zeta_{\text{abs}}(\alpha_1 = 1, \ldots, \alpha_4 = 1)$. **(b)** $\zeta_{\text{abs}}(\alpha_1 = \alpha_{1,\text{ref}}^{\text{opt}}, \ldots, \alpha_4 = \alpha_{4,\text{ref}}^{\text{opt}})$.

Figure 4.15: Normalized degree of stability for constant braking torque over various angular velocities and friction coefficients. ● $\zeta_{\text{abs}} < 0$, i.e. flutter instability.

The non-optimized state is featured in Fig. 4.15a in which two regions of instability occur. For $\mu < 0.44$, the trivial solution is unstable in almost the entire velocity range. For larger friction coefficients, the absolute stability reserve increases abruptly and reaches its maximum at approximately 80 % of its theoretically possible optimum value. There exists no band where the ratio $\zeta_{\text{abs}}/\zeta_{\text{abs}}^{\text{opt}}$ equals identity. In comparison to the optimized case, the stability boundary is shifted towards the lower left corner of the Ω-μ-plane. For a wide interval of Ω, the boundary runs parallelly to the white dashed line, which indicates its optimized counterpart. At high angular velocities, i.e. $\Omega > 7\pi\,\text{s}^{-1}$, the non-optimized configuration exhibits a decrease of ζ_{abs} as the stability boundary is shifted further towards lower friction coefficients.

The configuration tailored to the reference point is illustrated in Fig. 4.15b. In contrast to the non-optimized state, there is only one confined domain of

flutter instability, while the second unstable region at small friction coefficients vanishes. The adapted damping distribution predominantly yields an optimum degree of stability, i.e. the ratio $\zeta_{\mathrm{abs}}/\zeta_{\mathrm{abs}}^{\mathrm{opt}}$ is equal to one, which is similar to the simplified finite element model. The absolute stability reserve decreases to approximately $0.8\,\zeta_{\mathrm{abs}}^{\mathrm{opt}}$ when approaching the unstable regime. However, the stability boundary associated with a configuration tailored to 'REF' is not congruent to the boundary calculated from individual combinations of Ω and μ. The latter can only be reached upon changing the weighting factors since back plate and caliper damping are no longer beneficial. In this region, α_3^{opt} and α_4^{opt} undergo a transition to their lower bound, cf. Fig. 4.14. Hence, the optimum degree of stability is not completely attained for the reference configuration, where all weighting factors lie on their upper bound.

#	f_{crit} (Hz)	type	nodal diameters	color in Fig. 4.16
①	529	bending	1	●
②	938	bending	2	●
③	1160	torsion	–	●
④	1797	bending	3	●
⑤	3000	bending	4	●
⑥	4490	bending	5	●

Table 4.5: Frequencies and mode shapes corresponding to the eigenvalue with largest real part.

Besides the sign of ζ_{abs}, the qualitative stability behavior is closely related to the mode shape and frequency of the eigenvalue with largest real part. This critical frequency is defined mathematically by the discontinuous function

$$f_{\mathrm{crit}}(\lambda) := \frac{\mathrm{Im}\,(\lambda)}{2\pi} \quad \text{for} \quad \mathrm{Re}(\lambda) = -\zeta_{\mathrm{abs}}, \tag{4.34}$$

which is visualized in Fig. 4.16. Depending on the damping distribution, up to six modes can be identified between f_{lb} and f_{ub}, all of which are associated with disc eigenfrequencies. As listed in Tab. 4.5, one of these motions describes

a torsional vibration of the brake disc, while the other five are ascribed to bending modes with one nodal circle. The latter are further characterized in terms of the number of nodal diameters which in this case is affiliated to the critical frequency in ascending order.

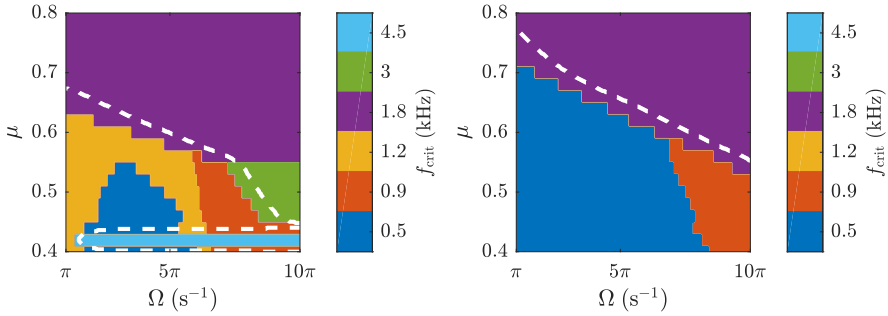

(a) Non-optimized. **(b)** Optimized.

Figure 4.16: Frequency of the eigenvalue with largest real part for constant braking torque over various angular velocities and friction coefficients.

In the non-optimized state depicted in Fig. 4.16a, the critical frequency adopts six discrete values. The two regions of instability are governed by three bending modes with three to five nodal diameters. Modes ④ and ⑤ determine the unstable regime in the upper right corner of the Ω-μ-plane, while the instability for small friction coefficients is exclusively due to mode ⑥. The contour diagram validates that the white dashed line enclosing the upper region of instability has a certain offset to the line connecting points of the same critical frequency. For a given friction coefficient and growing angular velocity, for example, the critical frequency first changes to 1.8 kHz or 3 kHz, respectively, before a further increase of Ω leads to instability.

In the optimized case plotted in Fig. 4.16b, the adapted damping distribution generally transfers the critical modes to lower frequencies. The number of distinct frequency values declines by three. Both the torsional mode as well as the bending motions with four and five nodal diameters are no longer critical. Thus, the region of instability for small friction coefficients is cancelled.

The domain below the stability boundary is split into two sections. For small to medium angular velocities, mode ① is critical, while for larger Ω, mode ② is decisive. The unstable regime is merely determined by the bending motion with three nodal diameters since mode ⑤ does not occur. The disappearance of this critical mode also explains the shift of the stability boundary towards higher friction coefficients for $\Omega > 7\pi\,\mathrm{s}^{-1}$. Similar to the non-optimized state, the stability limit is approximately parallel to the boundary of the purple domain, yet it is located at a certain distance to it.

The results presented above are summarized by an example illustrating the evolution of the weighting factors and the degree of stability for a constant friction coefficient and varying angular velocity. As depicted in Fig. 4.17, the plot range is classified into two sectors via the dashed line at $\Omega_1 \approx 6\pi\,\mathrm{s}^{-1}$. At this angular velocity, the objective eigenvalue changes leading to non-differentiability of the optimized degree of stability. The corresponding critical frequency jumps discontinuously from 0.5 kHz in regime ① to 1.8 kHz in regime ②, cf. Fig. 4.17a. In sector ①, energy dissipation is beneficial in all components of the brake assembly. The respective α_i^{opt} of disc, pads, back plates, and caliper lie on the upper bound of the admissible parameter space. Near Ω_1, the optimized weighting factors of back plates and caliper exhibit a sharp decrease as they drop to their lower limit. Hence, energy dissipation in sector ② is merely advantageous in disc and pads, whereas adding damping in back plates and caliper contributes to destabilization in this vibration mode.

The corresponding optimized degree of stability is visualized in Fig. 4.17b. An initial decay of $\zeta_{\mathrm{abs}}^{\mathrm{opt}}$ (blue) is followed by an increase until Ω_1 is reached. As soon as the eigenvalue with maximum real part corresponds to $f_{\mathrm{crit}} = 1.8\,\mathrm{kHz}$, the degree of stability starts to decrease monotonically. An adjustment of energy dissipation prevents this drop from occurring at $\Omega \approx 3.5\pi\,\mathrm{s}^{-1}$ due to which the non-optimized system (red) becomes unstable for $\Omega > 5\pi\,\mathrm{s}^{-1}$. Tuning the damping distribution among all brake components involved additionally yields an enlarged absolute stability reserve.

If damping is tailored to the operating point ‘Ref’ (yellow), the maximum possible ζ_{abs} is attained at a slightly smaller angular velocity than in the individually optimized scenario. Since in the reference point configuration

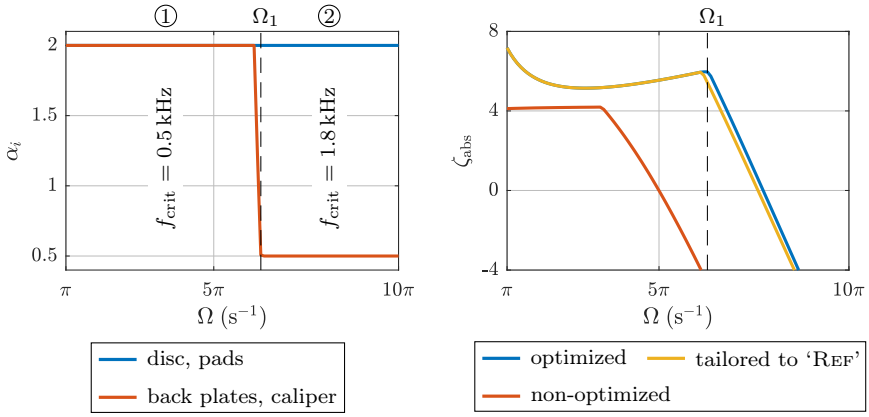

(a) Weighting factors.

(b) Degree of stability.

Figure 4.17: Evolution of objective function and solution of optimization problem (4.32) at $\mu = 0.6$ for varying angular velocity.

all weighting factors are fixed to their upper bound, beneficial reduction of energy dissipation in back plates and caliper is not incorporated. Hence, the degree of stability tailored to 'Ref' runs below the optimized counterpart once its maximum is reached. However, the stability gap between these two configurations is small as it is governed by back plate and caliper damping, yet ζ_{abs} is primarily sensitive to disc damping. As a result of this gap, the system tailored to 'Ref' becomes unstable at smaller angular velocities when compared to the individually optimized case.

4.4 Discussion

The present chapter highlights the determination of beneficial damping configurations in disc brake systems with regard to stability. Four different variants are numerically analyzed: two rather academic minimal models with two and eight degrees of freedom, respectively, as well as two higher dimensional models originating from a finite element environment. The damping matrix is decomposed into several component matrices which, depending on the model,

may have a special structure or physical origin. Variation of the ratio of these component matrices is performed to either stabilize or increase the degree of stability of the equilibrium state subject to sensible constraints. Within the scope of this study, a system is considered to be more stable if its eigenvalue with largest real part is as negative as possible.

Investigations in previous publications have been conducted for one particular operating point [81, 187] or a specific line of varying angular velocities at a constant friction coefficient [82]. Optimization results presented herein encompass the entire Ω-μ-plane which enables an assessment of the calculated optima with respect to natural parameter fluctuations. Especially the friction coefficient depends strongly on the operating conditions of the brake, e.g. temperature, lubrication, and wear [111]. Compensation of these uncertainties motivates the assumption of a constant braking torque, which is required for the reduction of vehicle speed.

To a certain extent, both minimal models exhibit a qualitatively similar stability behavior. When angular velocities and friction coefficients are small, disc damping is advantageous, whereas for large Ω and μ, energy dissipation in the pads becomes more beneficial. This is ascribable to gyroscopic terms, which are proportional to the angular speed of the disc. In consideration of section 3.3, uniformly distributed damping through the disc is unsatisfactory for large Ω. Hence, gyroscopic perturbations need to be compensated rather by means of non-uniform dissipation associated with the pads.

Analogously, both magnitude and location of energy dissipation are decisive for stability of the finite element models. From a quantitative perspective, the degree of stability is most sensitive to damping in the disc, while the impact of pads, back plates, and caliper is smaller by orders of magnitude. However, contrary to the simplified model 4.10a, a higher energy dissipation in the more complex model 4.10b is not necessarily advantageous since adding damping in back plates and caliper may contribute to destabilization. This context is also reflected in the optimization which identifies the disc to be the most beneficial damping component followed by the pads. In comparison to both minimal models, the optimized weighting factors are more robust against perturbations as they arise, for example, from an altering friction coefficient.

While the weighting factors of disc and pads are found to be constant over the entire range of interest, energy dissipation in back plates and caliper may adversely affect stability in the model used in industry. Their contribution to the overall damping is particularly disadvantageous in the vicinity of the boundary between stable and unstable regime.

In all models considered, an adaption of damping properties for each parameter combination enlarges the stable domain since the stability boundary is shifted towards higher angular velocities and friction coefficients. A fixed parameter configuration is able to approach this boundary if the ratio of energy dissipation at the reference point corresponds qualitatively to the ratio at the stability limit. Both configurations, i.e. individually optimized and tailored to a specific operating regime, lead to an increase of the maximum degree of stability as well as its mean value. In opposition to the minimal models, where the optimized degree of stability is susceptible to parameter fluctuations, in the finite element variants it is virtually constant over the entire range of interest. Moreover, an adapted damping distribution generally transfers the mode shapes which correspond to the eigenvalue with largest real part to lower frequencies. This transfer leads to a decline in the number of critical frequencies involved.

The relevance of gyroscopic effects on the stability of circulatory systems is outlined, for instance, in [69] and [72]. Numerical studies of finite element brake models conducted in [49] confirm their impact on both magnitude and sign of the real part of the eigenvalues even for small angular velocities of the disc. These studies in conjunction with the optimization results presented here refute the often prevailing view of gyroscopic effects. According to Marschner [123] and Wallner [183], these effects can be neglected in squeal simulations for small angular velocities of the disc. However, this assumption is not justified herein since a beneficial damping configuration depends decisively on the angular velocity and thus on the gyroscopic terms.

In the finite element model used in industry, the loss factors can vary between half and double of their initial value given in Tab. 4.4. Within these preset bounds, their magnitude agrees with numerical values encountered in literature [136]. Thus, technical implementation of the damping distribution

obtained from optimization is generally assured. An increase of energy dissipation in the disc via a suitable material selection is particularly beneficial since the degree of stability is most sensitive to an altering disc damping. This is confirmed by experiments conducted in [170], where a disc made of steel is compared to a disc made of cast iron. The latter inherently features a higher material damping leading to a reduction of squeal tendency. An adaption of the brake pad and its lining material is also advantageous in the entire range of interest, yet it has a significantly smaller impact on the degree of stability contrasted to the disc.

An alternative countermeasure to remedy noise issues of brake systems is the modification of the back plate material. In the industrial finite element model, adding damping in this component is comparable to the application of shims. These lumped insulators are usually comprised of thin, multi-layered structures of metal and elastomers which are bonded between back plates and caliper [151]. The benefit of shims is not clearly evidenced and is discussed critically in literature. While Flint [38] and Kinkaid et al. [88] claim their global advantage regarding stability, finite element analyses from Festjens et al. [37] show that their positive effect is not determined a priori. The attachment of shims may even trigger instabilities which otherwise would not occur. Although the latter paradox does not appear during optimization, the findings of the present study are generally confirmed since energy dissipation in the back plates does not invariably contribute to stabilization.

In conclusion, two major aspects are highlighted. On the one hand, the academic minimal models are able to describe qualitatively the sensitivities of the degree of stability in relation to all brake components involved. Two degrees of freedom are sufficient to identify the disc as the dominating part. Moreover, the destabilizing effect of back plate damping is reproduced by the extended minimal model with eight degrees of freedom. On the other hand, computed damping configurations differ between both model groups. While beneficial weighting factors of the minimal models strongly depend on angular speed and friction coefficient, they are virtually constant over the entire range of interest in the finite element environment. This applies similarly to the corresponding optimized absolute stability reserve.

5 Optimum damping in systems with taut strings

This chapter deals with the transverse dynamics of two systems with taut strings. An analytical derivation of the equations of motion incorporates internal and external mechanisms of energy dissipation. The design parameters of the corresponding damping elements, i.e. viscosities and locations, are then tuned for a maximum damping ratio aiming to mitigate vibration modes affiliated to the lowest eigenfrequencies.

5.1 Single cable with internal and external damping

5.1.1 Modeling

Serving as an introductory example, Fig. 5.1 depicts a string which is spanned along the x-axis to a length l and clamped at both ends. The one-dimensional, elastic continuum is specified in terms of tension T and mass per unit length μ, both of which are assumed to be constant over length. Per definition, a string does not resist or transmit bending moment [59]. The cable-like structure interacts with two energy dissipating components. First, an external damper with damping coefficient d_{ex} is installed at a distance x_{ex} from the left end and supported to ground. Second, a massless damping element of width b with damping coefficient d_{in} is attached to the string at $x = x_{\mathrm{in}}$. This is a simplified (viscous) representation of internal energy dissipation due to friction between the individual cable layers. Transverse oscillations are restricted to the x-z-plane, while longitudinal motion is neglected. The planar movement of any

point on the string is described by the field variable $w = w(x,t)$, which is a function of position x and time t.

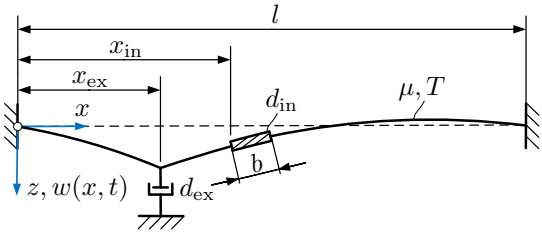

Figure 5.1: Taut string in interaction with internal and external damping elements.

5.1.2 Equations of motion

The transverse dynamics of a continuous system with discrete and distributed damping according to Fig. 5.1 is completely governed by LAGRANGE's equations (2.1). Corresponding functionals of kinetic and potential energy read

$$\mathcal{T} = \frac{1}{2}\mu \int_0^l \dot{w}^2(x,t)\,\mathrm{d}x, \tag{5.1}$$

$$\mathcal{U} = \frac{1}{2}T \int_0^l w'^2(x,t)\,\mathrm{d}x, \tag{5.2}$$

respectively, where the overdot denotes differentiation with respect to t and the apostrophe indicates spatial derivatives with respect to x. RAYLEIGH's dissipation function

$$\mathcal{D} = \frac{1}{2}d_{\mathrm{in}} \int_{x_{\mathrm{in}}}^{x_{\mathrm{in}}+b} \dot{w}'^2(x,t)\,\mathrm{d}x + \frac{1}{2}d_{\mathrm{ex}}\dot{w}^2(x_{\mathrm{ex}},t) \tag{5.3}$$

is stated accordingly and accounts for internal and external energy sinks [57]. Up to this point, energy expressions (5.1)–(5.3) are defined in terms of the unknown function $w(x,t)$. In order to analyze the continuum, a RITZ series expansion is performed seeking solutions of the form

$$w(x,t) = \sum_{i=1}^{n} W_i(x)\, q_i(t). \tag{5.4}$$

This *ansatz* discretizes the string domain with a finite number of degrees of freedom; the approximation is exact when n approaches infinity [59]. The solution is a sum of products of two functions which are exclusively dependent on location and time, respectively. By means of this separation of variables, the system of partial differential equations is transformed into a system of ordinary differential equations. The field variable $w(x,t)$ is projected onto shape functions $W_i(x)$ which need to fulfill all geometric boundary conditions. For the present model, the displacement at both clamped ends equals zero, i.e. $W_i(0) = W_i(l) = 0$. Hence, a set of linearly independent admissible functions is, for instance,

$$W_i(x) = \sin\left(\frac{\pi i x}{l}\right). \tag{5.5}$$

The resulting discretized equations of motion are of type

$$\mathbf{M}\ddot{\mathbf{q}} + \mathbf{D}\dot{\mathbf{q}} + \mathbf{K}\mathbf{q} = \mathbf{0}, \tag{5.6}$$

where $\mathbf{q} = [q_1(t), q_2(t), \ldots, q_n(t)]^{\mathrm{T}}$ is the vector of generalized coordinates. The entries of the respective system matrix are given in closed form for any arbitrary number of degrees of freedom. The mass matrix $\mathbf{M} \equiv \mathbf{I}$ equals identity and the stiffness matrix $\mathbf{K} = \operatorname{diag}\left(\omega_1^2, \omega_2^2, \ldots, \omega_n^2\right)$ is diagonal with the squares of the undamped circular eigenfrequencies

$$\omega_i = \frac{\pi c i}{l}, \qquad i = 1, \ldots, n, \tag{5.7}$$

occupying the diagonal elements. Therein, the constant $c = \sqrt{T/\mu}$ is the speed of transverse waves, which specifies the propagation of a disturbance created at a point on the string. The n^2 elements determining the damping matrix $\mathbf{D}$ are more involved, yet they are still defined explicitly as itemized in appendix A.2. In order to treat their physical origins independently, the damping matrix $\mathbf{D} = \mathbf{D}_{\mathrm{in}} + \mathbf{D}_{\mathrm{ex}}$ is decomposed into two contributions, both of which are positive semi-definite. However, the impact on the system's behavior differs for the summands. While $\mathbf{D}_{\mathrm{in}}$ is pervasive for arbitrary combinations of non-zero parameter triplets x_{in}, b, and d_{in}, the external portion $\mathbf{D}_{\mathrm{ex}}$ does not necessarily act in all vibration modes. When the damper

position x_{ex} is chosen such that the ratio ix_{ex}/l in Eq. (A.4b) is an integer for any value of i, one node is located at x_{ex} whereby the system is not controllable at this position. As a result, certain modes remain undamped as the total mechanical energy of the string does not decrease monotonically in time. A further special case occurs for vanishing external energy dissipation in conjunction with uniformly distributed internal damping over the entire string domain, i.e. $x_{\mathrm{in}} = 0$, $b = l$, $d_{\mathrm{in}} > 0$, and $\mathbf{D}_{\mathrm{ex}} = \mathbf{0}$. In this case, the overall damping matrix is diagonal, which facilitates the decoupling of the equations of motion (5.6) into a collection of single degree of freedom oscillators.

5.1.3 Optimization approach

In view of system (5.6) and the properties of its governing matrices, self-excitation is impossible as long as $\mathbf{M}$ and $\mathbf{K}$ are positive definite and $\mathbf{D}$ is at least positive semi-definite [62]. In spite, the damping matrix can be tuned for maximum stability. A common requirement is, for example, to compensate for perturbations which potentially arise from circulatory forces or other external excitations. An appropriate quantitative measure thereof is the damping ratio (2.22), which describes the system's relative stability reserve. Besides the tailoring of damper viscosities, numerical optimization of the present model additionally involves the determination of suitable damper locations. This is reflected in the vector of design variables $\boldsymbol{\alpha} = (d_{\mathrm{ex}}, d_{\mathrm{in}}, x_{\mathrm{ex}}, x_{\mathrm{in}}, b)^{\mathrm{T}}$.

Using complex eigenvalue analysis, stability can be enhanced by variation of $\boldsymbol{\alpha}$. Stability enhancement implies the damping ratio ζ_{rel} to be as large as possible. According to section 2.4, the above is stated mathematically as

$$\begin{aligned} &\max_{\boldsymbol{\alpha}} \zeta_{\mathrm{rel}} \\ &\text{subject to} \\ &i_{\mathrm{lb}} \leq i \leq i_{\mathrm{ub}} \quad \text{and} \quad \boldsymbol{\alpha}_{\mathrm{lb}} \leq \boldsymbol{\alpha} \leq \boldsymbol{\alpha}_{\mathrm{ub}}. \end{aligned} \tag{5.8}$$

The positive integer $i \in \mathbb{N}$ numbers the modes in ascending order starting with the smallest eigenfrequency of the string. The lower and upper bounds i_{lb} and i_{ub} thus limit the objective function to a desired frequency range. Linear restrictions on the parameter vector are imposed via $\boldsymbol{\alpha}_{\mathrm{lb}}$ and $\boldsymbol{\alpha}_{\mathrm{ub}}$.

Serving as a representative example, parameters are chosen with reference to Tab. 5.1. Inserting preset numerical values for μ, l, and T into Eq. (5.7), the first three eigenfrequencies appear within the interval $f \in [0, 1]\,\mathrm{Hz}$. This is typical for real technical systems, such as overhead transmission lines [55] or stay cables of suspension bridges [164], whose general structure is similar to the model depicted in Fig. 5.1. The given parameter set is therewith justified. Since the objective function ζ_{rel} exhibits points of infinite slope, a generalized pattern search algorithm is applied which is implemented in MATLAB's global optimization toolbox, cf. section 2.4.

symbol	numerical value	unit	parameter description
μ	1.165	kg/m	mass per unit length
l	150	m	cable length
T	7500	N	tension

Table 5.1: Parameter set of the string system shown in Fig. 5.1.

For the presentation of optimization results, it is convenient to introduce the dimensionless damping measure

$$\xi := \frac{d}{d_{\mathrm{crit}}} = \frac{d}{2\sqrt{\mu T}}, \tag{5.9}$$

which expresses the level of actual damping d relative to critical damping d_{crit}. In analogy to a one degree of freedom oscillator, normalization is sought using the square root of mass per unit length and tension [62]. For the study of internal and external energy dissipation, the respective coefficients d_{in} and d_{ex} are considered individually.

The problem of finding the optimum viscosity of an external damper which is located close to one end of a horizontally taut string has first been studied by KOVACS [106]. His semi-empirical method reveals that the highest possible damping ratio is approximately half the relative location of the damper from the support. This result is confirmed numerically by PACHECO et al. [142] who computed a universal curve for damping estimation of stay cables and ex-

tended Kovacs' reasoning to any specified mode. More recently, Krenk [107] obtained an analytical formula for the problem of a vibrating string in interaction with an isolated viscous damper. If the distance of the damper from the anchorage is within several percent of the cable length, the optimum dimensionless damping coefficient is given explicitly by

$$\xi_{\mathrm{opt}} = \frac{1}{2\pi i \frac{x_{\mathrm{ex}}}{l}}. \tag{5.10}$$

This relation directly involves an asymptotic estimate for the maximum possible modal damping ratio

$$\zeta_{\mathrm{rel}}^{\mathrm{opt}} = \frac{x_{\mathrm{ex}}}{2l}, \tag{5.11}$$

which is mode independent. All these investigations are valid for a single target mode, i.e. optimum damper size and location determined with Eq. (5.10) are restricted to one specific mode number i. In practical applications, however, self-excited cable vibrations occur in a broader frequency band since neighboring eigenfrequencies are closely spaced [58]. Designing an external damper therefore requires a robust tuning with respect to multiple objective modes. To this end, the optimum damping coefficient (5.10) is generalized. Summation of the individual ξ_{opt} and subsequent division by the total number of modes of interest leads to

$$\xi_{\mathrm{opt}}^{i_{\mathrm{ub}}} = \frac{\frac{1}{i_{\mathrm{ub}}} \sum_{i=1}^{i_{\mathrm{ub}}} \frac{1}{i}}{2\pi \frac{x_{\mathrm{ex}}}{l}}, \tag{5.12}$$

which naturally includes coefficient (5.10) as a special case for $i_{\mathrm{ub}} = 1$. Generalized expression (5.12) approximates the optimum damping coefficient for mitigation of the first i_{ub} cable modes. By means of this estimation, a compromise tuning of a single external damper can be realized.

5.1.4 Optimization results

Due to their dependence on different design variables, internal and external energy dissipation are featured separately in Fig. 5.2. External damping is particularly advantageous in the vicinity of large cable amplitudes, e.g. in the

middle of the span when merely the first mode is of interest. However, certain design constraints may prescribe an attachment near the anchorage. As depicted in Fig. 5.2a, any length normalized installation point x_{ex}/l corresponds to an optimum damping coefficient ξ_{opt}. The closer the external damper is located at the clamped end, the higher its viscosity ought to be. The effectiveness of an external device depends on its location as the optimized relative stability reserve $\zeta_{\mathrm{rel}}^{\mathrm{opt}}$ increases with distance to the support. This distance dependence cannot be compensated completely by a suitable choice of ξ. When considering an arbitrary single mode, the maximum possible ζ_{rel} is obtained since Eq. (5.11) does not show a mode dependency.

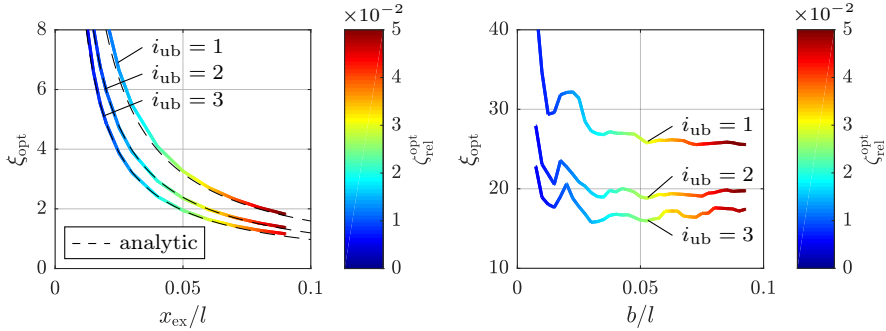

(a) External damping. **(b)** Internal damping with $x_{\mathrm{in}} = x_{\mathrm{in}}^{\mathrm{opt}}$.

Figure 5.2: Optimum parameters of the taut string in interaction with discrete and distributed damping elements, where the lower bound of the considered mode range is set to $i_{\mathrm{lb}} = 1$.

The outlined behavior applies likewise when external damping is tailored not only to one single mode but also to multiple modes ($i_{\mathrm{ub}} > 1$). The more modes considered, the lower is the optimum damping coefficient for a given location. Hence, profiles illustrated in Fig. 5.2a exhibit a similar course, yet they are shifted towards the lower left corner for growing i_{ub}. In addition, the maximum attainable $\zeta_{\mathrm{rel}}^{\mathrm{opt}}$ decreases for a specific installation point. Regarding the first three modes at $x_{\mathrm{ex}} = 0.05l$, for example, the optimized stability reserve is reduced by about 13 % when compared to a first-mode adjustment. Nevertheless, such a compromise tuning is able to provide almost equally high

damping ratios ζ_{rel} in all assigned modes. In contrast, tuning of an individual mode may adversely affect stability of non-objective modes. Numerically computed results show a high agreement with analytical estimation (5.12), which is indicated by the dashed lines; deviations are negligible. This conformity thus validates both the discretization of equations of motion (5.6) and the correct implementation of optimization problem (5.8).

In case of internal energy dissipation, comparative analytical results do not exist. Beneficial locations of the internal damping element are assumed to be solely in the vicinity of large cable curvature. This conjecture is confirmed by numerical simulations. In fact, independent of the relative width b/l, the optimum installation point $x_{\mathrm{in}}^{\mathrm{opt}}$ is within a few percent distance to the clamped end. The general behavior of internal damping displayed in Fig. 5.2b is qualitatively similar to the external case. This similarity is not intuitive since the characteristic parameter is exchanged, i.e. the external damper location x_{ex} is replaced by the internal damper width b. The overall negative trend for lines of constant i_{ub} is captured by internal damping. However, their course is not monotonically decreasing when compared to external damping in Fig. 5.2a. After exhibiting a sharp initial decline, the individual ξ_{opt} show convergence for growing b/l. Moreover, the magnitude of the relative stability reserve does not change significantly going from an external damper location to an internal damper width. In order to reach $\zeta_{\mathrm{rel}}^{\mathrm{opt}}$, however, corresponding internal damping coefficients ξ_{opt} have to experience a notable growth. At $b = 0.05l$, for instance, the optimized internal damping coefficients are approximately eight times larger than their external counterparts at $x_{\mathrm{ex}} = 0.05l$.

5.2 Bundled cables with multiple self-damping spacers

5.2.1 Modeling

High voltage overhead transmission lines are susceptible to wind-induced vibrations. Especially ice or wet snow covered multi-conductor bundles exposed to a steady airstream undergo low-frequency oscillations ($f < 1\,\mathrm{Hz}$), with a

single or a few loops of predominant standing waves per span [86]. A widely used countermeasure to remedy this so-called galloping phenomenon is the employment of spacer dampers. These devices maintain the distance between the individual conductors and possess adaptable inertial, elastic, and damping properties for the absorption of vibration energy [23].

A straightforward model which is able to mimic the outlined situation is visualized in Fig. 5.3. The model is comprised of a bundle of two vertically arranged strings which are spanned along the x-axis to a length l and clamped at both ends. The elastic continua are governed by tensions T_{I} and T_{II} as well as masses per unit length μ_{I} and μ_{II}, respectively. The cables are assumed to exhibit zero bending stiffness. At the positions $x = x_r$ $(r = 1, \ldots, n_d)$, the horizontally taut strings are coupled by n_d spacers whose vertical motion is described by coordinates $q_r(t)$. The spacers are specified in terms of mass m_d, stiffness k_d, and damping coefficients d_r^{ex}. The clamping points are of mass m_c. Over the widths b_r, they additionally feature a distributed damping denoted by the coefficients d_r^{in}. In a simplified manner, this accounts for internal energy dissipation in helical reinforcements, which are often attached to reduce bending strains [86]. Transverse oscillations are assumed to be planar, while longitudinal motion is neglected. Hence, the field variables $w_{\mathrm{I}}(x,t)$ and $w_{\mathrm{II}}(x,t)$ constitute the movement of any point on the strings.

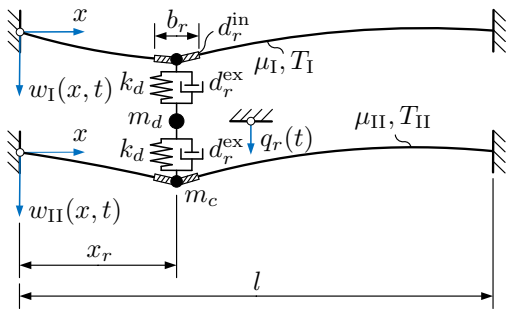

Figure 5.3: Horizontally taut strings coupled by n_d spacers, where clamping regions additionally feature internal damping.

5.2.2 Equations of motion

In analogy to the procedure applied in section 5.1.2, equations of motion are derived via a direct formulation of energy functionals and a subsequent use of LAGRANGE's formalism. The kinetic energy

$$\begin{aligned}\mathcal{T} = &\frac{1}{2}\mu_{\mathrm{I}} \int_0^l \dot{w}_{\mathrm{I}}^2(x,t)\,\mathrm{d}x + \frac{1}{2}\mu_{\mathrm{II}} \int_0^l \dot{w}_{\mathrm{II}}^2(x,t)\,\mathrm{d}x \\ &+ \frac{1}{2} m_c \sum_{r=1}^{n_d} \left[\dot{w}_{\mathrm{I}}^2(x_r,t) + \dot{w}_{\mathrm{II}}^2(x_r,t)\right] + \frac{1}{2} m_d \sum_{r=1}^{n_d} \dot{q}_r^2(t)\end{aligned} \tag{5.13}$$

is composed of the kinetic energy of each string and the kinetic energy ascribed to the inertia of clamps and spacer dampers. Similarly, the potential energy

$$\begin{aligned}\mathcal{U} = &\frac{1}{2}T_{\mathrm{I}} \int_0^l w_{\mathrm{I}}'^2(x,t)\,\mathrm{d}x + \frac{1}{2}T_{\mathrm{II}} \int_0^l w_{\mathrm{II}}'^2(x,t)\,\mathrm{d}x \\ &+ \frac{1}{2} k_d \sum_{r=1}^{n_d} \left[q_r(t) - w_{\mathrm{I}}(x_r,t)\right]^2 + \left[w_{\mathrm{II}}(x_r,t) - q_r(t)\right]^2\end{aligned} \tag{5.14}$$

contains portions originating from both the strings and the stiffness of the spacers. RAYLEIGH's dissipation function

$$\begin{aligned}\mathcal{D} = &\frac{1}{2} \sum_{r=1}^{n_d} d_r^{\mathrm{ex}} \left\{\left[\dot{q}_r(t) - \dot{w}_{\mathrm{I}}(x_r,t)\right]^2 + \left[\dot{w}_{\mathrm{II}}(x_r,t) - \dot{q}_r(t)\right]^2\right\} \\ &+ \frac{1}{2} \sum_{r=1}^{n_d} d_r^{\mathrm{in}} \int_{x_r - b_r/2}^{x_r + b_r/2} \left\{\dot{w}_{\mathrm{I}}'^2(x,t) + \dot{w}_{\mathrm{II}}'^2(x,t)\right\} \mathrm{d}x\end{aligned} \tag{5.15}$$

is defined accordingly. The terms in square brackets describe the relative velocities between the attaching points on the respective string and the mass particle m_d representing the inertia of the spacer. The first summand of $\mathcal{D}$ is due to viscous damping in the spacers, while the second summand accounts for distributed energy dissipation in the clamping regions.

An approximation of energy expressions (5.13)–(5.15) by means of RITZ' series expansion (5.4) along with admissible shape functions (5.5) and usage of LAGRANGE's formalism (2.1) yields a system of ordinary differential equations. The resulting discretized equations of motion are found to be of

type (5.6), i.e. the dynamics is completely governed by matrices $\mathbf{M}$, $\mathbf{D}$, and $\mathbf{K}$. In opposition to the single cable examined previously, these matrices now exhibit a block form. As itemized in appendix A.3, elements of each block are specified explicitly in closed form for any arbitrary number of degrees of freedom $n = n_{\mathrm{I}} + n_{\mathrm{II}} + n_d$. The mass matrix, for instance, is diagonal with the submatrices of strings and spacers, i.e. $\mathbf{M}^{\mathrm{I}}$, $\mathbf{M}^{\mathrm{II}}$, and $\mathbf{M}^{\Delta}$, occupying the diagonal elements. In contrast, the damping and the stiffness matrix are densely populated as they contain additional coupling terms on their off-diagonals.

5.2.3 General observations

Discretization of the examined infinite dimensional, continuous system is based on a transformation projecting the field variables $w_{\mathrm{I}}(x,t)$ and $w_{\mathrm{II}}(x,t)$ onto a domain of lower dimension. The quality of this approximation depends on the number of shape functions spanning the corresponding subspace. For a study of the subspace size and its qualitative influence on the damping ratio, one single spacer is used ($n_d = 1$). Cable and spacer parameters are chosen in accordance with Tab. 5.1 and Tab. 5.2, where internal and external dimensionless damping coefficients are exemplarily set to $\xi_{\mathrm{in}} = \xi_{\mathrm{ex}} = 0.1$.

Fig. 5.4a shows the evolution of ζ_{rel} over the number of shape functions n within the interval $f \in [0,1]\,\mathrm{Hz}$. The damping ratio is normalized with respect to its converged equivalent $\zeta_{\mathrm{rel}}^{\mathrm{conv}}$, which is obtained when n approaches infinity. For all three spacer locations considered, the relative deviation from the effective value decreases with n. The respective damping ratios converge from above, i.e. the approximations of ζ_{rel} are overestimated in the entire plot range. The further away the spacer is located from the clamped end, the fewer shape functions are generally required to reach convergence. Even at installation points close to the cable support, e.g. $x_1/l = 0.01$, the computed error for $n > 80$ is less than one percent in comparison to $\zeta_{\mathrm{rel}}^{\mathrm{conv}}$. This rapid convergence is due to the chosen frequency interval of interest since the considered eigenvalues are affiliated to low cable eigenfrequencies.

Similar to the disc brake models, governing parameters of systems with taut strings are subject to natural fluctuations originating from environmen-

tal influences. The horizontal tension T, for instance, is a function of the actual cable length and sag, both of which vary with ambient temperature. Besides, tension is not necessarily equal in both cables leading to different eigenfrequencies. A simplified measure thereof is the wave speed ratio

$$\eta = \frac{c_{\mathrm{II}}}{c_{\mathrm{I}}}, \tag{5.16}$$

which quantifies the speed difference of transverse waves between string I and string II. This dimensionless measure directly affects the relative velocity between the attaching points, which according to Eq. (5.15) determines the dissipated energy in the spacer. Indeed, the damping ratio ζ_{rel} varies with η for a given spacer configuration and position. For all three installation points depicted in Fig. 5.4b, the damping ratio initially grows until a maximum value is reached. A further increase of η leads to a decline of ζ_{rel}. Merely when the spacer is located close to the anchorage, e.g. $x_1/l = 0.01$, the wave speed ratio has no significant influence as ζ_{rel} remains virtually constant over the plot range. Yet, at any installation point, there exists a specific η for which the damping ratio becomes as large as possible. In the frequency interval considered here, the maximum is shifted towards the upper right corner with distance of the spacer to the cable support.

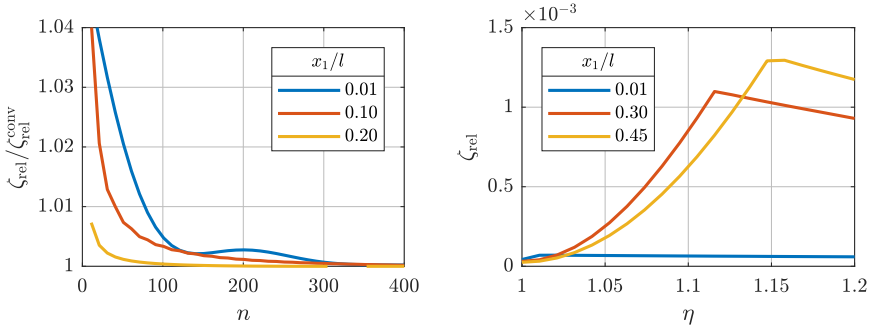

(a) Convergence behavior. **(b)** Influence of wave speed ratio.

Figure 5.4: General properties of taut cables coupled by one self-damping spacer.

5.2.4 Optimization approach

Various scenarios for stability enhancement in terms of a preferably large damping ratio ζ_{rel} are possible in the bundled cables model. A rather general approach, for example, is the individual adaption of mass, stiffness, and damping properties at each spacer position. Within the scope of this study, however, the emphasis is on parameters directly related to energy dissipation, such as internal and external damper viscosities. Besides, numerical optimization involves the determination of beneficial spacer locations, where the clamping regions are assumed to have a constant width of $b_r = 0.01l$. This is reflected in the vector of design variables $\boldsymbol{\alpha} = \left(d_r^{\mathrm{ex}}, d_r^{\mathrm{in}}, x_r\right)^{\mathrm{T}}$ whose dimension $(r = 1, \ldots, n_d)$ is determined by the number of spacers considered.

Since energy dissipation in the clamping regions is assumed to be smaller by orders of magnitude in comparison to energy dissipation in the spacer, an upper limit is assigned to the internal damping coefficients d_r^{in} [58]. Remaining design variables, i.e. external damping coefficients d_r^{ex} and spacer locations x_r, are allowed to vary freely within the respective domain. Thus, the admissible parameter space is linearly restricted by the lower and upper bounds $\boldsymbol{\alpha}_{\mathrm{lb}} = \mathbf{0}$ and $\boldsymbol{\alpha}_{\mathrm{ub}} = (\infty, 0.06\, d_{\mathrm{crit}}, l)^{\mathrm{T}}$, respectively. In analogy to section 5.1.3, the objective of finding favorable parameter configurations for mitigation of the first few cable modes is mathematically expressed in Eq. (5.8). Corresponding numerical values governing mass and stiffness of cables and spacers are chosen with reference to Tab. 5.1 and Tab. 5.2. Numerical optimization is performed using MATLAB's global optimization toolbox, cf. section 2.4.

symbol	numerical value	unit	parameter description
b_r	$0.01l$	m	width of clamping region
m_c	0.45	kg	mass of clamp
m_d	3.50	kg	mass of damper
k_d	250	N/m	stiffness of damper

Table 5.2: Parameter set governing the spacer dampers.

5.2.5 Optimization results

Conducted numerical simulations indicate that internal damping is generally preferred in comparison to external damping. Independent of the number of spacers considered, results show a close location of the installation points to the clamped end of the cables. However, spacers are not only applied to absorb vibration energy, they further maintain the distance between the individual conductors. The most favorable location for a single damper is exactly at half the length of the span, cf. Fig. 5.5a. For a total number of three spacers, Gross [53] suggests advantageous locations to be at $\frac{1}{6}l$, $\frac{1}{2}l$, and $\frac{5}{6}l$. His investigations reveal the impact on the first five mode shapes to be greatest here. A further increase of the number of spacers to $n_d = 5$ leads to a preferably equidistant distribution of one sixth of the cable length.

The corresponding maximum attainable damping ratio depicted in Fig. 5.5b increases with the number of spacers deployed. This growth is nonlinear as a normalization of $\zeta_{\mathrm{rel}}^{\mathrm{opt}}$ with respect to n_d is not constant. The individual contribution of one damper to the overall $\zeta_{\mathrm{rel}}^{\mathrm{opt}}$ is higher for $n_d = 3$ and $n_d = 5$ when compared to $n_d = 1$. This behavior is ascribed to two aspects which are visualized in Fig. 5.5c. First, the optimum viscosity for every single external damper grows with n_d, i.e. the height of the bar segments enlarges with the number of spacers used. Second, the more spacers installed, the higher is the number of locations where energy is dissipated. Since the total amount of damping in the system increases, the maximum attainable stability reserve $\zeta_{\mathrm{rel}}^{\mathrm{opt}}$ grows accordingly.

Although in theory ξ_{ex} is able to grow infinitely large, the admissible parameter space is not fully exploited during optimization. Optimum values of individual external damper viscosities are found in the range of $\xi_{\mathrm{ex}}^{\mathrm{opt}} = 0.7$ for $n_d = 1$ and $\xi_{\mathrm{ex}}^{\mathrm{opt}} = 0.8$ for three and five spacers. While these values lie within the admissible parameter regime, optimum internal coefficients $\xi_{\mathrm{in}}^{\mathrm{opt}}$ are located on their upper bound independent of n_d, cf. Fig. 5.5d. For different limits of $\boldsymbol{\alpha}_{\mathrm{ub}}$, optimization predicts a finite $\xi_{\mathrm{in}}^{\mathrm{opt}} \approx 80$. However, this specific value is several orders of magnitude above the technically relevant scope. Within a certain cable spacer configuration, i.e. $n_d = \text{const.}$, indi-

vidual damping coefficients are equal which applies likewise for the internal and external case. Hence, independent of the number of spacers deployed, energy dissipation is distributed preferably symmetrically over the entire cable domain. Considering the absence of the skew-symmetric matrices **G** and **N** in the present **MDK**-system, a uniform (symmetric) damping distribution is expected. According to section 3.3, only the presence of gyroscopic and circulatory terms, for example, demands a non-uniformly distributed energy dissipation in order to compensate for these perturbations.

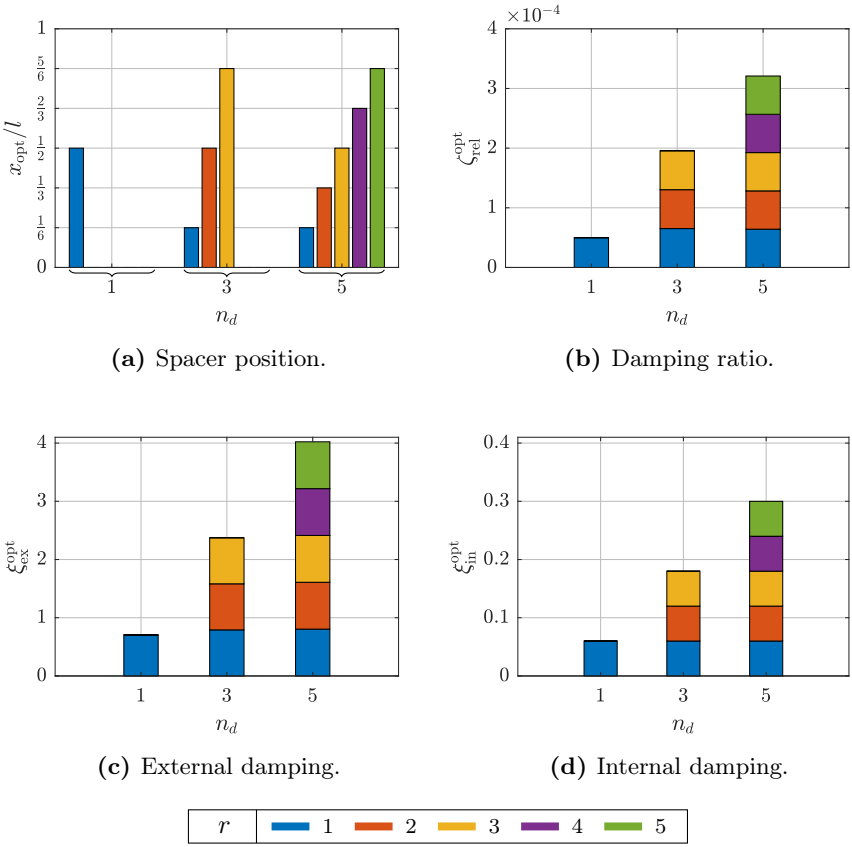

(a) Spacer position. **(b)** Damping ratio.

(c) External damping. **(d)** Internal damping.

Figure 5.5: Optimum design variables of the bundled cables model with multiple spacers in the frequency interval $f \in [0, 1]$ Hz and at a wave speed ratio of $\eta = 1.01$.

Up to this point, optimization results apply for a specific η. In real applications, however, the wave speed ratio depends on fluctuations, such as an altering ambient temperature, cf. section 5.2.3. Moreover, installation points of spacer packages are subject to uncertainties. In order to ensure an adequate damping ratio, the robustness of a damping distribution tailored to the virtual operating point 'Ref' is investigated in Fig. 5.6. Contour plots emphasize the difference between a configuration with one single spacer and $n_d = 3$ when both the position of the central spacer and the wave speed ratio are varied. The attachment of the considered spacer exactly in the middle of the span, i.e. at $x_{\text{opt}}^{\text{ref}} = 0.5l$, results in a mirror symmetry of ζ_{rel}. Thus, when the damping device is moved away from this initial position, the system response does not depend on the direction of the displacement.

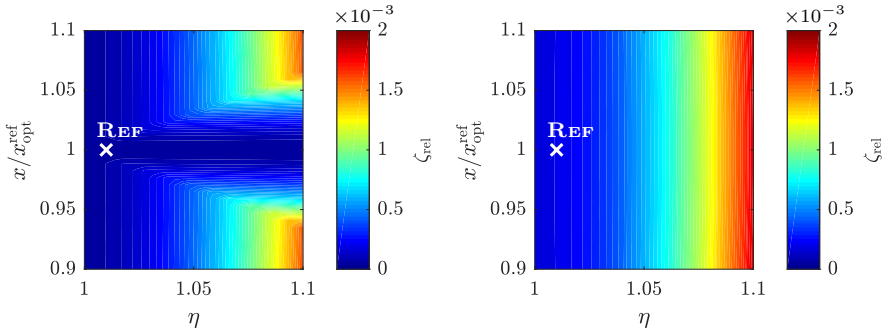

(a) $n_d = 1$. **(b)** $n_d = 3$.

Figure 5.6: Robustness of a damping configuration tailored to 'Ref' with respect to altering wave speed ratios and installation points of the central spacer in the frequency interval $f \in [0, 1]$ Hz, where $\zeta_{\text{rel}} = \zeta_{\text{rel}}(\xi_{\text{in}} = \xi_{\text{in}}^{\text{ref}}, \xi_{\text{ex}} = \xi_{\text{ex}}^{\text{ref}})$.

Either configuration, i.e. $n_d = 1$ und $n_d = 3$, is robust against perturbations. In the entire plot range, a displacement of the central damper position does not disadvantageously affect stability. Yet, a deviation of the wave speed ratio from the reference point causes a change of the relative stability reserve. As depicted in Fig. 5.4b, this relation is a fundamental property observed in the coupled string system. A growing wave speed ratio leads to an enhanced stability and vice versa. Moreover, a configuration comprising three spacers

is preferable when compared to a single spacer configuration. A multi damper system is able to compensate deviations from the central installation point for $\eta > 1.07$. This enhanced robustness is visualized in Fig. 5.6b by a color coded increase of ζ_{rel} along the η-axis. The respective single damper configuration shown in Fig. 5.6a is not able to capture this pronounced color gradient.

5.3 Discussion

The present chapter highlights effects of internal and external energy dissipation on the stability of systems with taut strings. Besides the tailoring of damper viscosities, optimization additionally involves the determination of suitable damper locations aiming to enhance stability within a predefined frequency range. Similar to chapter 4, a system is considered to be more stable if the damping ratio (relative stability reserve) is as large as possible. Analyses encompass two different models: first, a single string with an attached internal damping element and an external damper supported to ground and second, a system with two strings coupled by self-damping spacers. Equations of motion of both models are derived analytically using Lagrange's formalism. After discretization by means of a Ritz series expansion, corresponding system matrices are given in closed form and can be specified explicitly for an arbitrary number of degrees of freedom.

For the problem of a vibrating string in interaction with an external damper, Krenk [107] obtained an analytical formula to estimate the optimum damper viscosity when a single mode is objective. In the present study, his findings are generalized for the application to multiple target modes. A comparison to numerically computed results shows high agreement and thus validates the proposed optimization technique. The more modes considered, the lower are the optimum damping coefficient and the maximum attainable stability reserve for a given installation point. Such a compromise tuning is able to provide almost equal damping ratios in all assigned modes, whereas an individual mode adjustment may adversely affect stability of non-objective modes. The above behavior is qualitatively similar for internal energy dissipation. However, the governing parameter exchanges, i.e. the external damper location is

replaced by the internal damper width. Moreover, optimum internal damping coefficients are notably larger when compared to the external case.

Numerical simulations of a system with bundled cables indicate that the damping ratio is generally more sensitive to internal damping due to its pervasive character. Coherent to the single string model, beneficial installation points are within a few percent distance to the clamped end of the cables. This finding applies independent of the number of spacers used as long as stability enhancement is exclusively paramount. As suggested by Gross [53], the maintenance of the distance between the individual conductors requires a uniform spacer distribution over the entire span. For a total number of five spacers, for instance, advantageous locations are found to be at multiples of one sixth of the cable length. The corresponding maximum attainable stability reserve increases with the number of spacers deployed, yet it is small compared to a single damper supported to ground. Even with an optimum configuration of five spacers, the damping ratio is below one per mill. With regard to real applications, where damping ratios of several per mill are desired, this confirms observations from field trials conducted by Edwards & Ko [35] and Havard [65]. In their work, they challenge the thorough ability of self-damping spacers to completely suppress galloping vibrations. Despite these surveys, the susceptibility of the conductors to large amplitude motions is also reported to be reduced by an installation of interphase spacers [23].

Optimization results in this study predict finite values of external damping coefficients as the admissible parameter space is not fully exploited. Depending on the number of spacers, beneficial damper viscosities are found in the range of $70-80\,\%$ of critical damping. In contrast, optimum internal damping coefficients are invariably located on a prescribed upper bound since energy dissipation in the clamping regions is assumed to be much smaller than inside the spacer. Independent of the number of spacers deployed, damping is distributed preferably symmetric over the entire cable domain which applies likewise for the internal and external case. This uniform distribution in the present **MDK**-system confirms the finding from section 3.3. Whereby, only the presence of gyroscopic or circulatory perturbations, for example, demands a compensation via a non-uniformly distributed energy dissipation.

6 Conclusion

Undesirable manifestations of self-excitation are encountered in a wide range of engineering applications, e.g. squealing of automotive brakes or galloping of overhead transmission lines. Such oscillations are often accompanied by negative consequences which are associated with high expenses for warranty, maintenance, and repair. The onset of self-excitation mostly originates from an instability which is either related to negative damping or to non-conservative (circulatory) coupling of motion coordinates. A peculiar characteristic of circulatory systems is their stability behavior under the impact of dissipative forces. In a linearized description, the equilibrium state is particularly sensitive to the structure of the damping matrix. Considering the distinct physical origins and locations of energy dissipation, some of the resulting damping matrices contribute to stabilization, while others may induce the contrary.

In this context, the present thesis attains two major objectives: First, a deeper understanding is fostered regarding the impact of different types of damping on the stability of circulatory systems. Second, favorable damping configurations are determined in order to mitigate the tendency of self-excitation. These scientific questions are addressed in chapter three to five, where respective conclusions are framed in the following.

Chapter 3 elucidates the role of velocity proportional terms in linear mechanical systems of type **MDGKN**. A general system with two degrees of freedom facilitates an analytical assessment delivering detailed insights into the required structure of the damping matrix either for stabilization or the avoidance of destabilization. The application of a necessary and sufficient stability criterion yields an explicit boundary between stable and unstable regime. The phenomenon of stabilization with arbitrarily small damping is found to be essentially governed by two factors. While asymmetric stiffness properties, which induce the separation of neighboring eigenfrequencies, en-

large the potential parameter range for its occurrence, gyroscopic terms evoke the opposite. However, gyroscopic effects are identified as crucial when the damping matrix is merely positive semi-definite or even indefinite. Conducted analyses reveal how these effects ensure the pervasiveness of energy dissipation or extend the stable regime, respectively. Following from these observations, elements located on the off-diagonal of the damping matrix adversely affect stability as they partly cancel the advantageous impact of diagonal elements. Moreover, the benefit of a uniform damping distribution is shown not to be a priori certain. Gyroscopic perturbations are found to require a compensation via rather non-uniform dissipation which implies unequal modal damping levels. Hence, negligence of gyroscopic effects is not justified since the optimum structure of the damping matrix depends decisively on a specific parameter combination comprising gyroscopic and off-diagonal damping terms.

On the basis of these theoretical findings, a technique for stability optimization is formulated. By decomposing the damping matrix into several component matrices, the individual contributions may exhibit a special structure or be ascribed to a distinct physical origin. A suitable variation of the ratio of these submatrices results in either stabilizing or increasing the degree of stability of the equilibrium position. To tailor the optimization problem, coefficients of the component matrices underly predefined constraints. Optimum damping configurations are assessed in terms of dependence on natural parameter fluctuations and technical feasibility. Industrial relevance is assured as the outlined approach is applicable to systems of arbitrary dimension. To further support and elaborate the knowledge gained from chapter 3, two technically relevant systems featuring self-excitation are intensely studied.

In chapter 4, disc brake systems are investigated with regard to the determination of beneficial damping configurations. Performed analyses encompass four variants differing in setup and complexity. For the study of basic features, two minimal models prove to be sufficient with two and eight degrees of freedom, respectively. These models are of fundamental value to gain general insights, yet they lack technical relevance due to their reduced level of complexity. Thus, as an extension, two higher dimensional models are examined which originate from a finite element environment. In all models considered,

both magnitude and location of energy dissipation are identified as key factors for stability. The rather academic minimal models are able to describe qualitatively the sensitivities of the degree of stability with regard to all brake components involved. Two degrees of freedom are shown to be effectual for the identification of the disc as the dominating brake component, as suggested by the more complex models. The detected impact of pads, back plates, and caliper is smaller by orders of magnitude. Moreover, the destabilizing effect of back plate damping, which is comparable to the action of shims, is reproduced. While the different model groups exhibit similar stability properties, optimum damping configurations indicate divergence. Beneficial weighting factors in the minimal models display strong dependence on angular speed and friction coefficient. In contrast, optimum weighting factors are far more robust to parameter changes in the finite element environment. This applies similarly to the optimized absolute stability reserve. An overall conclusion for all models is the enhanced maximum degree of stability as well as its mean value when tailoring the damping distribution. Technical implementation of the optimum configurations is generally assured, e.g. via a suitable material selection for disc and pads.

In chapter 5, effects of internal and external energy dissipation on the stability of systems with taut strings are addressed. Besides the tailoring of damper viscosities, suitable damper locations along the strings are calculated. Conducted analyses incorporate two models with a different setup. First, a single string is considered with an attached internal damping element and an external damper supported to ground. In order to estimate the optimum external damper viscosity for multiple objective modes, existing analytical results are transferred to a more general level. High agreement is obtained when compared to a numerical approach and thus the optimization technique presented herein is validated. The behavior of internal and external damping is demonstrated to be similar, yet a difference is reported in the governing parameter. While for external damping the damper location is decisive, for internal damping the width of the damping element is determined to be more relevant. Second, a system comprised of two strings coupled by self-damping spacers is studied. In this model, the damping ratio is shown to be more

sensitive to internal energy dissipation due to its pervasive character. Beneficial installation points are identified in close proximity to the clamped end of the cables as long as stability enhancement is exclusively paramount. However, the maintenance of the distance between the cables requires a symmetric spacer distribution over the span. Optimum internal damping coefficients are invariably located on a prescribed upper bound, whereas beneficial external damper viscosities are found in the range of $70-80$ % of critical damping. In conclusion, energy dissipation is recognized to be preferably advantageous when uniformly distributed over the cable domain.

The optimization technique established in this thesis is universally applicable to a broad variety of mechanical systems independent of the number of degrees of freedom. For future research, due to its generality, the approach can be transferred straightforwardly to study other self-excited phenomena, such as ground resonance of helicopters or oil-whirl instabilities of high-speed rotors with fluid bearings. An extension to account for time-periodic system matrices is directly attainable from this work via replacing complex eigenvalue analysis by Floquet theory. In addition, the assessment of optimum damping configurations in terms of economic aspects or their robustness against environmental influences are possible subsequent steps.

Bibliography

[1] Adhikari, S.: Damping Modelling Using Generalized Proportional Damping, *Journal of Sound and Vibration*, 293(1-2):156–170, 2006.

[2] Adhikari, S.: *Structural Dynamic Analysis with Generalized Damping Models: Analysis*, Mechanical Engineering and Solid Mechanics, Wiley-ISTE, London, 2014.

[3] Akay, A.: Acoustics of Friction, *The Journal of the Acoustical Society of America*, 111(4):1525–1548, 2002.

[4] Anderson, K.; Hagedorn, P.: On the Energy Dissipation in Spacer Dampers in Bundled Conductors of Overhead Transmission Lines, *Journal of Sound and Vibration*, 180(4):539–556, 1995.

[5] Ast, M.; Kirchgäßner, B.: Brake Squeal Analysis with PERMAS, *PERMAS Users' Conference*, Stuttgart, 2008.

[6] Bajer, A.; Belsky, V.; Kung, S.W.: The Influence of Friction-Induced Damping and Nonlinear Effects on Brake Squeal Analysis, SAE International (Editor), *Proceedings of 22nd Annual Brake Colloquium & Exhibition*, SAE Technical Paper Series, Warrendale, 2004.

[7] Beards, C.F.: Damping in Structural Joints, *The Shock and Vibration Digest*, 11(9):35–41, 1979.

[8] Beards, C.F.: *Structural Vibration: Analysis and Damping*, Arnold, London, 1996.

[9] Becker, E.; Föppl, O.: Dauerversuche zur Bestimmung der Festigkeitseigenschaften: Beziehungen zwischen Baustoffdämpfung und Verformungsgeschwindigkeit, Forschungsarbeit auf dem Gebiete des Ingenieurwesens 304, Berlin, 1928.

[10] Benner, P.; Tomljanović, Z.; Truhar, N.: Dimension Reduction for Damping Optimization in Linear Vibrating Systems, *Zeitschrift für Angewandte Mathematik und Mechanik*, 91(3):179–191, 2011.

[11] Besselink, B.; Tabak, U.; Lutowska, A.; van de Wouw, N.; Nijmeijer, H.; Rixen, D.J.; Hochstenbach, M.E.; Schilders, W.: A Comparison of Model Reduction Techniques from Structural Dynamics, Numerical Mathematics and Systems and Control, *Journal of Sound and Vibration*, 332(19):4403–4422, 2013.

[12] Blevins, R.D.: *Flow-Induced Vibration*, van Nostrand Reinhold, New York, 1990, 2nd edition.

[13] Blevins, R.D.; Iwan, W.D.: The Galloping Response of a Two-Degree-of-Freedom System, *Journal of Applied Mechanics*, 41(4):1113, 1974.

[14] Bock, G.: Schwingungsdämpfung unter Ausnutzung der Werkstoffdämpfung, *Zeitschrift für Angewandte Mathematik und Mechanik*, 12(5):261–274, 1932.

[15] Bograd, S.; Reuss, P.; Schmidt, A.; Gaul, L.; Mayer, M.: Modeling the Dynamics of Mechanical Joints, *Mechanical Systems and Signal Processing*, 25(8):2801–2826, 2011.

[16] Bolotin, V.V.: *Nonconservative Problems of the Theory of Elastic Stability*, Pergamon Press, Oxford, 1963.

[17] Brabender, K.: *Optimale Dämpfung von linearen Schwingungssystemen*, PhD Thesis, FernUniversität Hagen, Hagen, 1998.

[18] Burg, K.; Haf, H.; Wille, F.; Meister, A.: *Höhere Mathematik für Ingenieure: Band I: Analysis*, Springer-Lehrbuch, Springer Vieweg, Wiesbaden, 2013, 10th edition.

[19] Cantone, F.; Massi, F.: A Numerical Investigation into the Squeal Instability: Effect of Damping, *Mechanical Systems and Signal Processing*, 25(5):1727–1737, 2011.

[20] Caughey, T.K.: Classical Normal Modes in Damped Linear Dynamic Systems, *Journal of Applied Mechanics*, 27(2):269–271, 1960.

[21] Caughey, T.K.; O'Kelly, M.E.J.: Classical Normal Modes in Damped Linear Dynamic Systems, *Journal of Applied Mechanics*, 32(3):583–588, 1965.

[22] Chopra, A.K.: *Dynamics of Structures: Theory and Applications to Earthquake Engineering*, Prentice-Hall International Series in Civil Engineering and Engineering Mechanics, Prentice Hall, Englewood Cliffs, 1995.

[23] Conseil International des Grands Réseaux Électriques (Editor): *State of the Art of Conductor Galloping*, volume 322 of *Technical Brochure*, Paris, 2005.

[24] Corriga, G.; Sanna, S.; Usai, G.: Parametric Optimization of Wind-Excited Vibration Dampers for Overhead Transmission Lines, *Applied Mathematical Modelling*, 18(10):577–581, 1994.

[25] Cox, S.J.: Designing for Optimal Energy Absorption, III: Numerical Minimization of the Spectral Abscissa, *Structural Optimization*, 13(1):17–22, 1997.

[26] Cox, S.J.: Designing for Optimal Energy Absorption, I: Lumped Parameter Systems, *Journal of Vibration and Acoustics*, 120(2):339–345, 1998.

[27] Crandall, S.H.: The Role of Damping in Vibration Theory, *Journal of Sound and Vibration*, 11(1):3–18, 1970.

[28] Crespo da Silva, M.R.M.: Attitude Stability of a Gravity-Stabilized Gyrostat Satellite, *Celestial Mechanics*, 2(2):147–165, 1970.

[29] Damm, T.; Homeyer, J.: On Indefinite Damping and Gyroscopic Stabilization, *IFAC Proceedings Volumes*, 44(1):7589–7593, 2011.

[30] de Coulomb, C.A.: *Théorie des Machines Simples*, Bachelier, Paris, 1821.

[31] Den Hartog, J.P.: Transmission Line Vibration due to Sleet, *Transactions of the American Institute of Electrical Engineers*, 51(4):1074–1076, 1932.

[32] Desai, Y.M.; Yu, P.; Popplewell, N.; Shah, A.H.: Finite Element Modelling of Transmission Line Galloping, *Computers & Structures*, 57(3):407–420, 1995.

[33] Diana, G.; Cheli, F.; Manenti, A.; Nicolini, P.; Tavano, F.: Oscillation of Bundle Conductors in Overhead Lines due to Turbulent Wind, *IEEE Transactions on Power Delivery*, 5(4):1910–1922, 1990.

[34] Done, G.T.S.: Damping Configurations that have a Stabilizing Influence on Nonconservative Systems, *International Journal of Solids and Structures*, 9(2):203–215, 1973.

[35] Edwards, A.T.; Ko, R.G.: Interphase Spacers for Controlling Galloping of Overhead Conductors, *IEEE Symposium on Mechanical Oscillations of Overhead Transmission Lines*, Vancouver, 1979.

[36] Ehrich, F.F.: Self-Excited Vibration, C.M. Harris; A.G. Piersol (Editors), *Harris' Shock and Vibration Handbook*, McGraw-Hill Handbooks, pp. 5.1–5.25, McGraw-Hill, New York, 2002.

[37] Festjens, H.; Gaël, C.; Franck, R.; Jean-Luc, D.; Remy, L.: Effectiveness of Multilayer Viscoelastic Insulators to Prevent Occurrences of Brake Squeal: A Numerical Study, *Applied Acoustics*, 73(11):1121–1128, 2012.

[38] Flint, J.: A Review of Theories on Constrained Layer Damping and Some Verification Measurements on Shim Material, SAE International (Editor), *Proceedings of 21st Annual Brake Colloquium & Exhibition*, SAE Technical Paper Series, Warrendale, 2003.

[39] Freitas, P.; Lancaster, P.: On the Optimal Value of the Spectral Abscissa for a System of Linear Oscillators, *SIAM Journal on Matrix Analysis and Applications*, 21(1):195–208, 1999.

[40] Frik, M.: Zur Stabilität nichtkonservativer linearer Systeme, *Zeitschrift für Angewandte Mathematik und Mechanik*, 52(11):T47–T49, 1972.

[41] Fritz, G.; Sinou, J.J.; Duffal, J.M.; Jézéquel, L.: Effects of Damping on Brake Squeal Coalescence Patterns: Application on a Finite Element Model, *Mechanics Research Communications*, 34(2):181–190, 2007.

[42] Fritz, G.; Sinou, J.J.; Duffal, J.M.; Jézéquel, L.: Investigation of the Relationship Between Damping and Mode-Coupling Patterns in Case of Brake Squeal, *Journal of Sound and Vibration*, 307(3-5):591–609, 2007.

[43] Gasch, R.; Knothe, K.; Liebich, R.: *Strukturdynamik: Diskrete Systeme und Kontinua*, Springer, Berlin, 2012, 2nd edition.

[44] Gasch, R.; Nordmann, R.; Pfützner, H.: *Rotordynamik*, Springer, Berlin, 2006, 2nd edition.

[45] Gaul, L.; Nitsche, R.: The Role of Friction in Mechanical Joints, *Applied Mechanics Reviews*, 54(2):93–106, 2001.

[46] Genta, G.; Amati, N.: On the Equivalent Viscous Damping for Systems with Hysteresis, *Accademia delle Scienze di Torino*, 32:21–45, 2008.

[47] Giannini, O.; Akay, A.; Massi, F.: Experimental Analysis of Brake Squeal Noise on a Laboratory Brake Setup, *Journal of Sound and Vibration*, 292(1-2):1–20, 2006.

[48] Goldstein, H.; Poole, C.P.; Safko, J.L.: *Classical Mechanics*, Addison-Wesley, Boston, 2002, 3rd edition.

[49] Gräbner, N.: *Analyse und Verbesserung der Simulationsmethode des Bremsenquietschens*, PhD Thesis, Technische Universität Berlin, Berlin, 2016.

[50] Gräbner, N.; Gödecker, H.; von Wagner, U.: On the Influence of Damping on Brake Vibrations, *Proceedings of the International Conference on Engineering Vibration*, Ljubljana, 2015.

[51] Gräbner, N.; Mehrmann, V.; Quraishi, S.; Schröder, C.; von Wagner, U.: Numerical Methods for Parametric Model Reduction in the Simulation of Disk Brake Squeal, *Zeitschrift für Angewandte Mathematik und Mechanik*, 96(12):1388–1405, 2016.

[52] Grandhi, R.: Structural Optimization with Frequency Constraints: A Review, *AIAA Journal*, 31(12):2296–2303, 1993.

[53] Groß, V.: *Numerische Simulation des Seiltanzens von Hochspannungs-Freileitungen*, volume 285 of *Fortschrittberichte VDI*, VDI, Düsseldorf, 2000.

[54] Gutzer, U.: *Dynamische Identifikation statischer Hysterese am Beispiel eines Leiterseils*, Normed, Bad Homburg, 1998.

[55] Hagedorn, P.: Schwingungsprobleme an Hochspannungsleitungen, *VDI-Berichte*, 419:77–82, 1981.

[56] Hagedorn, P.: *Non-Linear Oscillations*, volume 10 of *The Oxford Engineering Science Series*, Clarendon Press, Oxford, 1988, 2nd edition.

[57] Hagedorn, P.: *Technische Schwingungslehre: Lineare Schwingungen kontinuierlicher mechanischer Systeme*, Springer, Berlin, 1989.

[58] Hagedorn, P.: *Leiterseilschwingungen in Theorie und Praxis: Ein Überblick*, volume 26 of *etz-Report*, vde, Berlin, 1990.

[59] Hagedorn, P.; DasGupta, A.: *Vibrations and Waves in Continuous Mechanical Systems*, Wiley, Chichester, 2007.

[60] Hagedorn, P.; Eckstein, M.; Heffel, E.; Wagner, A.: Self-Excited Vibrations and Damping in Circulatory Systems, *Journal of Applied Mechanics*, 81(10):101009–1–9, 2014.

[61] Hagedorn, P.; Heffel, E.; Lancaster, P.; Müller, P.C.; Kapuria, S.: Some Recent Results on MDGKN-systems, *Zeitschrift für Angewandte Mathematik und Mechanik*, 95(7):695–702, 2015.

[62] Hagedorn, P.; Hochlenert, D.: *Technische Schwingungslehre: Schwingungen linearer diskreter mechanischer Systeme*, Edition Harri Deutsch, Europa-Lehrmittel, Haan-Gruiten, 2015, 2nd edition.

[63] Hagedorn, P.; Kraus, M.: On the Performance of Spacer Dampers in Bundled Conductors, *European Transactions on Electrical Power*, 3(4):305–311, 1993.

[64] Hartman, P.: A Lemma in the Theory of Structural Stability of Differential Equations, *Proceedings of the American Mathematical Society*, 11(4):610–620, 1960.

[65] Havard, D.G.: Fifteen Years Field Trials of Galloping Controls for Overhead Power Lines, *Proceedings of 7th International Workshop on Atmospheric Icing of Structures*, Chicoutimi, 1996.

[66] Herrmann, G.: Dynamics and Stability of Mechanical Systems with Follower Forces, Contractor Report 1782, National Aeronautics and Space Administration, Washington, 1971.

[67] Herrmann, G.; Bungay, R.W.: On the Stability of Elastic Systems Subjected to Nonconservative Forces, *Journal of Applied Mechanics*, 31(3):435–440, 1964.

[68] Herrmann, G.; Jong, I.C.: On the Destabilizing Effect of Damping in Nonconservative Elastic Systems, *Journal of Applied Mechanics*, 32(3):592–597, 1965.

[69] Hetzler, H.: *Zur Stabilität von Systemen bewegter Kontinua mit Reibkontakten am Beispiel des Bremsenquietschens*, volume 8 of *Schriftenreihe des Instituts für Technische Mechanik*, Univ.-Verl. Karlsruhe, Karlsruhe, 2008.

[70] Hetzler, H.: On the Effect of Nonsmooth Coulomb Friction on Hopf Bifurcations in a 1-DoF Oscillator with Self-Excitation due to Negative Damping, *Nonlinear Dynamics*, 69(1-2):601–614, 2012.

[71] Hetzler, H.: On the Effect of Non-Smooth Coulomb Damping on Flutter-Type Self-Excitation in a Non-Gyroscopic Circulatory 2-DoF-System, *Nonlinear Dynamics*, 73(3):1829–1847, 2013.

[72] Hochlenert, D.: *Selbsterregte Schwingungen in Scheibenbremsen: Mathematische Modellbildung und aktive Unterdrückung von Bremsenquietschen*, Berichte aus dem Maschinenbau, Shaker, Aachen, 2006.

[73] Hochlenert, D.; Spelsberg-Korspeter, G.; Hagedorn, P.: Friction Induced Vibrations in Moving Continua and Their Application to Brake Squeal, *Journal of Applied Mechanics*, 74(3):542–549, 2007.

[74] Hoffmann, N.; Fischer, M.; Allgaier, R.; Gaul, L.: A Minimal Model for Studying Properties of the Mode-Coupling Type Instability in Friction Induced Oscillations, *Mechanics Research Communications*, 29(4):197–205, 2002.

[75] Hooke, R.; Jeeves, T.A.: Direct Search Solution of Numerical and Statistical Problems, *Journal of the Association for Computing Machinery*, 8(2):212–229, 1961.

[76] Hou, J.; Guo, X.; Sun, G.; Zhang, J.: Suppression of Brake Squeal Noise Applying Viscoelastic Damping Insulator, L. Yu (Editor), *Proceedings of the International Joint Conference on Computational Sciences and Optimization*, pp. 167–171, IEEE, Piscataway, 2009.

[77] Hurwitz, A.: Ueber die Bedingungen, unter welchen eine Gleichung nur Wurzeln mit negativen reellen Theilen besitzt, *Mathematische Annalen*, 46(2):273–284, 1895.

[78] INTES (Editor): *PERMAS: Examples Manual*, volume 550 of *INTES Publication*, Stuttgart, 2014.

[79] INTES (Editor): *PERMAS: User's Reference Manual*, volume 450 of *INTES Publication*, Stuttgart, 2014.

[80] Jearsiripongkul, T.: *Squeal in Floating Caliper Disk Brakes: A Mathematical Model*, Forschen und Wissen - Mechanik, GCA, Waabs, 2005.

[81] Jekel, D.; Clerkin, E.; Hagedorn, P.: Robust Damping in Self-Excited Mechanical Systems, *Proceedings in Applied Mathematics and Mechanics*, 16(1):695–696, 2016.

[82] Jekel, D.; Hagedorn, P.: Optimization of Damping for Squeal Avoidance in Disc Brakes, *Proceedings in Applied Mathematics and Mechanics*, 17(1):373–374, 2017.

[83] Jekel, D.; Hagedorn, P.: Stability of Weakly Damped MDGKN-Systems: The Role of Velocity Proportional Terms, *Zeitschrift für Angewandte Mathematik und Mechanik*, 97(9):1128–1135, 2017.

[84] Jenkins, A.: Self-Oscillation, *Physics Reports*, 525(2):167–222, 2013.

[85] Kang, J.: Finite Element Modelling for the Investigation of In-Plane Modes and Damping Shims in Disc Brake Squeal, *Journal of Sound and Vibration*, 331(9):2190–2202, 2012.

[86] Kießling, F.; Nefzger, P.; Kaintzyk, U.: *Freileitungen: Planung, Berechnung, Ausführung*, Springer, Berlin, 2001, 5th edition.

[87] Kimball, A.L.; Lovell, D.E.: Internal Friction in Solids, *Physical Review*, 30(6):948–959, 1927.

[88] Kinkaid, N.M.; O'Reilly, O.M.; Papadopoulos, P.: Automotive Disc Brake Squeal, *Journal of Sound and Vibration*, 267(1):105–166, 2003.

[89] Kirchgäßner, B.: Dynamik II: Erweiterungen und spezielle Anwendungen, *PERMAS-Workshop*, Stuttgart, 2015.

[90] Kirchgäßner, B.: Finite Elements in Rotordynamics, *Procedia Engineering*, 144:736–750, 2016.

[91] Kirillov, O.N.: Destabilization Paradox, *Doklady Physics*, 49(4):239–245, 2004.

[92] Kirillov, O.N.: A Theory of the Destabilization Paradox in Non-Conservative Systems, *Acta Mechanica*, 174(3-4):145–166, 2005.

[93] Kirillov, O.N.: Gyroscopic Stabilization in the Presence of Nonconservative Forces, *Doklady Mathematics*, 76(2):780–785, 2007.

[94] Kirillov, O.N.: *Nonconservative Stability Problems of Modern Physics*, volume 14 of *De Gruyter Studies in Mathematical Physics*, De Gruyter, Berlin, 2013.

[95] Kirillov, O.N.; Seyranian, A.P.: Stabilization and Destabilization of a Circulatory System by Small Velocity-Dependent Forces, *Journal of Sound and Vibration*, 283(3-5):781–800, 2005.

[96] Kirillov, O.N.; Seyranian, A.P.: The Effect of Small Internal and External Damping on the Stability of Distributed Non-Conservative Systems, *Journal of Applied Mathematics and Mechanics*, 69(4):529–552, 2005.

[97] Kirillov, O.N.; Verhulst, F.: Paradoxes of Dissipation-Induced Destabilization or Who Opened Whitney's Umbrella?, *Zeitschrift für Angewandte Mathematik und Mechanik*, 90(6):462–488, 2010.

[98] Kirillov, O.N.; Verhulst, F.: Dissipation-Induced Instabilities and Symmetry, *Acta Mechanica Sinica*, 27(1):2–6, 2011.

[99] Klamt, K.: *Zur optimalen Schwingungsdämpfung durch trockene Reibung in lokalen und ausgedehnten Fügestellen*, volume 134 of *Fortschrittberichte VDI*, VDI, Düsseldorf, 1990.

[100] Kliem, W.; Müller, P.C.: Gyroscopic Stabilization of Indefinite Damped Systems, *Zeitschrift für Angewandte Mathematik und Mechanik*, 77(S1):S163–S164, 1997.

[101] Kliem, W.; Pommer, C.: Stability and Response Bounds of Non-Conservative Linear Systems, *Archive of Applied Mechanics*, 73(9-10):627–637, 2004.

[102] Kliem, W.; Pommer, C.: Indefinite Damping in Mechanical Systems and Gyroscopic Stabilization, *Zeitschrift für Angewandte Mathematik und Physik*, 60(4):785–795, 2009.

[103] Kliem, W.; Pommer, C.: A Note on Circulatory Systems: Old and New Results, *Zeitschrift für Angewandte Mathematik und Mechanik*, 97(1):92–97, 2017.

[104] Knothe, K.; Wessels, H.: *Finite Elemente: Eine Einführung für Ingenieure*, Lehrbuch, Springer Vieweg, Berlin, 2017, 5th edition.

[105] Kollmann, F.G.; Schösser, T.F.; Angert, R.: *Praktische Maschinenakustik*, VDI, Springer, Berlin, 2006.

[106] Kovacs, I.: Zur Frage der Seilschwingungen und der Seildämpfung, *Bautechnik*, 59(10):325–332, 1982.

[107] Krenk, S.: Vibrations of a Taut Cable With an External Damper, *Journal of Applied Mechanics*, 67(4):772–776, 2000.

[108] Kruse, S.; Tiedemann, M.; Zeumer, B.; Reuss, P.; Hetzler, H.; Hoffmann, N.: The Influence of Joints on Friction Induced Vibration in Brake Squeal, *Journal of Sound and Vibration*, 340:239–252, 2015.

[109] Kuchling, H.: *Taschenbuch der Physik*, Hanser, München, 2014, 21st edition.

[110] Kuzmanović, I.; Tomljanović, Z.; Truhar, N.: Optimization of Material with Modal Damping, *Applied Mathematics and Computation*, 218(13):7326–7338, 2012.

[111] Lange, J.; Degenstein, T.; Dohle, A.; Elvenkemper, A.: Der μ-Wert: Reibwertbestimmung in Bremssystemen, B. Breuer (Editor), *Proceedings of XXVI International μ-Symposium*, Verkehrstechnik/Fahrzeugtechnik, VDI, Düsseldorf, 2006.

[112] Lazan, B.J.: *Damping of Materials and Members in Structural Mechanics*, Pergamon Press, Oxford, 1968.

[113] Lewis, R.M.; Torczon, V.: Pattern Search Algorithms for Bound Constrained Minimization, *SIAM Journal on Optimization*, 9(4):1082–1099, 1999.

[114] Lewis, R.M.; Torczon, V.; Trosset, M.W.: Why Pattern Search Works, Technical Report, National Aeronautics and Space Administration, Hampton, 1998.

[115] Lewis, R.M.; Torczon, V.; Trosset, M.W.: Direct Search Methods: Then and Now, *Journal of Computational and Applied Mathematics*, 124(1-2):191–207, 2000.

[116] Liénard, A.; Chipart, M.H.: Sur le Signe de la Partie Réelle des Racines d'une Équation Algébrique, *Journal de Mathématiques Pures et Appliquées*, 10(6):291–346, 1914.

[117] Liu, P.; Zheng, H.; Cai, C.S.; Wang, Y.Y.; Lu, C.; Ang, K.H.; Liu, G.R.: Analysis of Disc Brake Squeal Using the Complex Eigenvalue Method, *Applied Acoustics*, 68(6):603–615, 2007.

[118] Lyapunov, A.M.: The General Problem of the Stability of Motion, *International Journal of Control*, 55(3):531–773, 1992.

[119] Magnus, K.: Der Einfluß verschiedener Kräftearten auf die Stabilität linearer Systeme, *Zeitschrift für Angewandte Mathematik und Physik*, 21(4):523–534, 1970.

[120] Magnus, K.: *Kreisel: Theorie und Anwendungen*, Springer, Berlin, 1971.

[121] Magnus, K.; Popp, K.; Sextro, W.: *Schwingungen: Grundlagen, Modelle, Beispiele*, Springer-Lehrbuch, Springer Vieweg, Wiesbaden, 2016, 10th edition.

[122] Markert, R.: *Strukturdynamik*, Mechanik, Shaker, Aachen, 2013.

[123] Marschner, H.: Mit Sicherheit leise: Neue Wege zur geräuscharmen Bremse, B. Breuer (Editor), *Proceedings of XXX International μ-Symposium*, Verkehrstechnik/Fahrzeugtechnik, pp. 52–66, VDI, Düsseldorf, 2011.

[124] Masing, G.: Zur Heyn'schen Theorie der Verfestigung der Metalle durch verborgen elastische Spannungen, C.D. Harris (Editor), *Wissenschaftliche Veröffentlichungen aus dem Siemens-Konzern*, pp. 231–239, Springer, Berlin, 1923.

[125] MathWorks (Editor): *MATLAB: Global Optimization Toolbox Users's Guide: R2017b*, Natick, 2017.

[126] MotionGenesis (Editor): *MotionGenesis Kane 5.9: Symbolic Solutions for Forces and Motion*, Stanford, 2017.

[127] Müller, P.C.: Asymptotische Stabilität von linearen mechanischen Systemen mit positiv semidefiniter Dämpfungsmatrix, *Zeitschrift für Angewandte Mathematik und Mechanik*, 51(S1):T197–T198, 1971.

[128] Müller, P.C.: *Stabilität und Matrizen: Matrizenverfahren in der Stabilitätstheorie linearer dynamischer Systeme*, Ingenieurwissenschaftliche Bibliothek, Springer, Berlin, 1977.

[129] Müller, P.C.: Stabilization of Circulatory Systems, *14th German-Polish Workshop on Dynamical Problems in Mechanical Systems*, Wandlitz, 2015.

[130] Müller, P.C.; Schiehlen, W.O.: *Lineare Schwingungen: Theoretische Behandlung von mehrfachen Schwingern*, Akademische Verlagsgesellschaft, Wiesbaden, 1976.

[131] Nakić, I.: *Optimal Damping of Vibrational Systems*, PhD Thesis, Fern-Universität Hagen, Hagen, 2003.

[132] Nakić, I.: Minimization of the Trace of the Solution of Lyapunov Equation Connected with Damped Vibrational Systems, *Mathematical Communications*, 18:219–229, 2013.

[133] Nelder, J.A.; Mead, R.: A Simplex Method for Function Minimization, *The Computer Journal*, 7(4):308–313, 1965.

[134] Neubauer, M.; Oleskiewicz, R.: Brake Squeal Control with Shunted Piezoceramics: Efficient modelling and experiments, *Proceedings of the Institution of Mechanical Engineers, Part D: Journal of Automobile Engineering*, 222(7):1141–1151, 2008.

[135] Neumark, S.: Concept of Complex Stiffness Applied to Problems of Oscillations with Viscous and Hysteretic Damping, Reports and Memoranda 3269, Aeronautical Research Council, London, 1962.

[136] Niehues, K.K.: *Identifikation linearer Dämpfungsmodelle für Werkzeugmaschinenstrukturen*, volume 318 of *Forschungsberichte IWB*, Utz Herbert, München, 2016.

[137] Nigol, O.; Buchan, P.: Conductor Galloping – Part II: Torsional Mechanism, *IEEE Transactions on Power Apparatus and Systems*, PAS-100(2):708–720, 1981.

[138] Noiseux, D.U.: Similarity Laws of the Internal Damping of Stranded Cables in Transverse Vibrations, *IEEE Transactions on Power Delivery*, 7(3):1574–1581, 1992.

[139] Orlando, L.: Sul Problema di Hurwitz Relativo alle Parti Reali delle Radici di un' Equazione Algebrica, *Mathematische Annalen*, 71(2):233–245, 1911.

[140] Ouyang, H.: Prediction and Assignment of Latent Roots of Damped Asymmetric Systems by Structural Modifications, *Mechanical Systems and Signal Processing*, 23(6):1920–1930, 2009.

[141] Ouyang, H.; Nack, W.V.; Yuan, Y.; Chen, F.: Numerical Analysis of Automotive Disc Brake Squeal: A Review, *International Journal of Vehicle Noise and Vibration*, 1(3/4):207–231, 2005.

[142] Pacheco, B.M.; Fujino, Y.; Sulekh, A.: Estimation Curve for Modal Damping in Stay Cables with Viscous Damper, *Journal of Structural Engineering*, 119(6):1961–1979, 1993.

[143] Pars, L.A.: *A Treatise on Analytical Mechanics*, Heinemann, London, 1968.

[144] Popp, K.: Stabilität mechanischer Systeme mit nicht durchdringender Dämpfung, *Zeitschrift für Angewandte Mathematik und Physik*, 23(4):587–603, 1972.

[145] Popp, K.; Panning, L.; Sextro, W.: Vibration Damping by Friction Forces: Theory and Applications, *Journal of Vibration and Control*, 9(3-4):419–448, 2003.

[146] Qi, G.; Zhang, G.; Pu, X.: The Effect of the Composition and Microstructure of Gray Cast Iron Brake Rotor on Squeal Noise, SAE International (Editor), *Proceedings of 31st Annual Brake Colloquium & Exhibition*, SAE Technical Paper Series, Warrendale, 2013.

[147] Rios, L.M.; Sahinidis, N.V.: Derivative-Free Optimization: A Review of Algorithms and Comparison of Software Implementations, *Journal of Global Optimization*, 56(3):1247–1293, 2013.

[148] Robinson, C.S.: *Modeling and Analysis of Helicopter Ground Resonance Utilizing Symbolic Processing and Dynamic Simulation Software*, Engineer's Thesis, Naval Postgraduate School, Monterey, 1997.

[149] Scanlan, R.H.: Linear Damping Models and Causality in Vibrations, *Journal of Sound and Vibration*, 13(4):499–503, 1970.

[150] Schlippe, B.: Die innere Dämpfung, *Ingenieur-Archiv*, 6(2):127–133, 1935.

[151] Schmid, D.; Gräbner, N.; von Wagner, U.: Experimental Investigations of Brake Pad Shim Properties, *Proceedings in Applied Mathematics and Mechanics*, 17(1):41–44, 2017.

[152] Schmidt, A.; Bograd, S.: Experimentelle Ermittlung von Kennwerten zur Werkstoff- und Fügestellendämpfung sowie deren Berücksichtigung in Finite-Elemente-Berechnungen, Technical Report 859, Forschungsvereinigung Verbrennungskraftmaschinen, Frankfurt am Main, 2008.

[153] Schweizer, B.: Total Instability of Turbocharger Rotors: Physical Explanation of the Dynamic Failure of Rotors with Full-Floating Ring Bearings, *Journal of Sound and Vibration*, 328(1-2):156–190, 2009.

[154] Schweizer, B.: Dynamics and Stability of Turbocharger Rotors, *Archive of Applied Mechanics*, 80(9):1017–1043, 2010.

[155] Sestieri, A.; Ibrahim, S.R.: Analysis of Errors and Approximations in the Use of Modal Coordinates, *Journal of Sound and Vibration*, 177(2):145–157, 1994.

[156] Seyranian, A.P.; Mailybaev, A.A.: *Multiparameter Stability Theory with Mechanical Applications*, volume 13 of *Series on Stability, Vibration, and Control of Systems. Series A*, World Scientific, Singapore, 2003.

[157] Shin, K.; Brennan, M.J.; Oh, J.E.; Harris, C.J.: Analysis of Disc Brake Noise Using a Two-Degree-of-Freedom Model, *Journal of Sound and Vibration*, 254(5):837–848, 2002.

[158] Sinou, J.J.; Jézéquel, L.: Mode Coupling Instability in Friction-Induced Vibrations and its Dependency on System Parameters Including Damping, *European Journal of Mechanics - A/Solids*, 26(1):106–122, 2007.

[159] Sinou, J.J.; Jézéquel, L.: The Influence of Damping on the Limit Cycles for a Self-Exciting Mechanism, *Journal of Sound and Vibration*, 304(3-5):875–893, 2007.

[160] Sinou, J.J.; Jézéquel, L.: On the Stabilizing and Destabilizing Effects of Damping in a Non-Conservative Pin-Disc System, *Acta Mechanica*, 199(1-4):43–52, 2008.

[161] Spelsberg-Korspeter, G.: Breaking of Symmetries for Stabilization of Rotating Continua in Frictional Contact, *Journal of Sound and Vibration*, 322(4-5):798–807, 2009.

[162] Spelsberg-Korspeter, G.: Structural Optimization for the Avoidance of Self-Excited Vibrations Based on Analytical Models, *Journal of Sound and Vibration*, 329(23):4829–4840, 2010.

[163] Spelsberg-Korspeter, G.: *Robust Structural Design Against Self-Excited Vibrations*, SpringerBriefs in Applied Sciences and Technology, Springer, Heidelberg, 2013.

[164] Starossek, U.: *Brückendynamik: Winderregte Schwingungen von Seilbrücken: Zum dynamischen Verhalten von Seilbrücken unter Windeinwirkung*, Vieweg, Braunschweig, 1992.

[165] Stickland, M.T.; Scanlon, T.J.; Craighead, I.A.; Fernandez, J.: An Investigation into the Mechanical Damping Characteristics of Catenary Contact Wires and their Effect on Aerodynamic Galloping Instability, *Proceedings of the Institution of Mechanical Engineers, Part F: Journal of Rail and Rapid Transit*, 217(2):63–71, 2003.

[166] Strutt, Baron Rayleigh, J.W.: *The Theory of Sound: Volume I*, Macmillan and Co., London, 1877.

[167] Thomas, M.: *Extension of a Minimal Model of Disc Brake and Subsequent Stability Analysis*, Master Thesis, Technische Universität Darmstadt, Darmstadt, 2017.

[168] Thomson, W.; Tait, P.G.: *Treatise on Natural Philosophy: Part I: New Edition*, Cambridge University Press, Cambridge, 1888.

[169] Tiedemann, M.: *The Dynamics of Assembled Structures Excited by Friction*, Berichte aus der Mechanik, Shaker, Aachen, 2015.

[170] Tiedemann, M.; Kruse, S.; Hoffmann, N.: Dominant Damping Effects in Friction Brake Noise, Vibration and Harshness: The Relevance of Joints, *Proceedings of the Institution of Mechanical Engineers, Part D: Journal of Automobile Engineering*, 229(6):728–734, 2015.

[171] Torczon, V.: On the Convergence of Pattern Search Algorithms, *SIAM Journal on Optimization*, 7(1):1–25, 1997.

[172] Truhar, N.; Tomljanović, Z.; Veselić, K.: Damping Optimization in Mechanical Systems with External Force, *Applied Mathematics and Computation*, 250:270–279, 2015.

[173] Ulbrich, M.; Ulbrich, S.: *Nichtlineare Optimierung*, Mathematik Kompakt, Birkhäuser, Basel, 2012.

[174] Verein Deutscher Ingenieure (Editor): *Werkstoff- und Bauteildämpfung*, volume 3830 of *VDI-Richtlinien*, Beuth, Berlin, 2004.

[175] Veselić, K.: On Linear Vibrational Systems with One Dimensional Damping II, *Integral Equations and Operator Theory*, 13(6):883–897, 1990.

[176] Vomstein, T.: *Strukturmodifikation moderner Bremsscheiben: Mathematische Modellierung und passive Unterdrückung von Bremsenquietschen*, Berichte aus dem Maschinenbau, Shaker, Aachen, 2008.

[177] von Wagner, U.; Hochlenert, D.; Hagedorn, P.: Minimal Models for Disk Brake Squeal, *Journal of Sound and Vibration*, 302(3):527–539, 2007.

[178] von Wagner, U.; Hochlenert, D.; Jearsiripongkul, T.; Hagedorn, P.: Active Control of Brake Squeal Via "Smart Pads", SAE International (Editor), *Proceedings of 22nd Annual Brake Colloquium & Exhibition*, SAE Technical Paper Series, pp. 43–49, Warrendale, 2004.

[179] Wagner, A.: *Avoidance of Brake Squeal by a Separation of the Brake Disc's Eigenfrequencies: A Structural Optimization Problem*, volume 31 of *Forschungsbericht*, Studienbereich Mechanik, Darmstadt, 2013.

[180] Walker, J.A.: A Note on Stabilizing Damping Configurations for Linear Nonconservative Systems, *International Journal of Solids and Structures*, 9(12):1543–1545, 1973.

[181] Walker, J.A.: On the Application of Liapunov's Direct Method to Linear Lumped-Parameter Elastic Systems, *Journal of Applied Mechanics*, 41(1):278–284, 1974.

[182] Wallaschek, J.: Zur Dämpfung winderregter Schwingungen in den Bündelleitern elektrischer Freileitungen, *Zeitschrift für Angewandte Mathematik und Mechanik*, 71(7-8):300–303, 1991.

[183] Wallner, D.: *Experimental and Numerical Investigations on Brake Squeal: Development of a Smart Friction Force Measuring Sensor*, volume 3 of *Monographic Series TU Graz FTG, Reihe Fahrzeugtechnik*, Verl. der Techn. Univ. Graz, Graz, 2013.

[184] Wang, J.: Overhead Transmission Line Vibration and Galloping, *Proceedings of the International Conference on High Voltage Engineering and Application*, pp. 120–123, IEEE, Chongqing, 2008.

[185] Wang, J.; Lilien, J.L.: A New Theory for Torsional Stiffness of Multi-Span Bundle Overhead Transmission Lines, *IEEE Transactions on Power Delivery*, 13(4):1405–1411, 1998.

[186] Wang, J.; Lilien, J.L.: Overhead Electrical Transmission Line Galloping: A Full Multi-Span 3-DOF Model, Some Applications and Design Recommendations, *IEEE Transactions on Power Delivery*, 13(3):909–915, 1998.

[187] Wehner, J.H.; Jekel, D.; Sampaio, R.; Hagedorn, P.: *Damping Optimization in Simplified and Realistic Disc Brakes*, SpringerBriefs in Applied Sciences and Technology, Springer, Cham, 2018.

[188] Wiendl, S.: *Modellierung von Schwingungsphänomenen in Papierkalandern*, PhD Thesis, Technische Universität Darmstadt, Darmstadt, 2001.

[189] Woernle, C.: *Mehrkörpersysteme: Eine Einführung in die Kinematik und Dynamik von Systemen starrer Körper*, Springer Vieweg, Berlin, 2016, 2nd edition.

[190] Yang, S.; Gibson, R.F.; Li, D.; Hecht, R.L.: Damping and Microstructures of Brake Rotor Materials, *International Journal of Materials and Product Technology*, 13(3-6):155–166, 1998.

[191] Zainudin, M.A.; Abu Bakar, A.R.: Preventing Disc Brake Squeal Using a Thin Plate Shim, *International Journal of Vehicle Structures and Systems*, 4(1):23–27, 2012.

[192] Ziegler, H.: Die Stabilitätskriterien der Elastomechanik, *Ingenieur-Archiv*, 20(1):49–56, 1952.

[193] Ziegler, H.: Linear Elastic Stability: A Critical Analysis of Methods, *Zeitschrift für Angewandte Mathematik und Physik*, 4(2):89–121, 1953.

Appendix

A.1 Damping matrix of brake model with eight degrees of freedom

$$\tilde{\mathbf{D}} = \tilde{\mathbf{D}}_c + \tilde{\mathbf{D}}_t + \tilde{\mathbf{D}}_p + \tilde{\mathbf{D}}_b^n + \tilde{\mathbf{D}}_b^t \tag{A.1}$$

with

$$\tilde{\mathbf{D}}_c = \mu \begin{pmatrix} \frac{\kappa^2}{2\tilde{\Omega}} & -\frac{\kappa\tilde{d}_p}{2} & -\frac{\tilde{d}_p}{2} & \frac{\tilde{d}_p}{2} & 0 & 0 & 0 & 0 \\ & 0 & 0 & 0 & \frac{\kappa\tilde{d}_p}{4} & \frac{\kappa\tilde{d}_p}{4} & 0 & 0 \\ & & 0 & 0 & \frac{\tilde{d}_p}{2} & 0 & 0 & 0 \\ & & & 0 & 0 & -\frac{\tilde{d}_p}{2} & 0 & 0 \\ & \text{sym.} & & & 0 & 0 & 0 & 0 \\ & & & & & 0 & 0 & 0 \\ & & & & & & 0 & 0 \\ & & & & & & & 0 \end{pmatrix} \tag{A.2a}$$

$$\tilde{\mathbf{D}}_t = \tilde{d}_t \begin{pmatrix} 1 & 0 & 0 & 0 & 0 & 0 & 0 & 0 \\ & 1 & 0 & 0 & 0 & 0 & 0 & 0 \\ & & 0 & 0 & 0 & 0 & 0 & 0 \\ & & & 0 & 0 & 0 & 0 & 0 \\ & \text{sym.} & & & 0 & 0 & 0 & 0 \\ & & & & & 0 & 0 & 0 \\ & & & & & & 0 & 0 \\ & & & & & & & 0 \end{pmatrix} \tag{A.2b}$$

$$\tilde{\mathbf{D}}_p = \tilde{d}_p \begin{pmatrix} 2 & 0 & 0 & 0 & -1 & -1 & 0 & 0 \\ & 0 & 0 & 0 & 0 & 0 & 0 & 0 \\ & & 0 & 0 & 0 & 0 & 0 & 0 \\ & & & 0 & 0 & 0 & 0 & 0 \\ & \text{sym.} & & & 1 & 0 & 0 & 0 \\ & & & & & 1 & 0 & 0 \\ & & & & & & 0 & 0 \\ & & & & & & & 0 \end{pmatrix} \tag{A.2c}$$

$$\tilde{\mathbf{D}}_b^n = \tilde{d}_b^n \begin{pmatrix} 0 & 0 & 0 & 0 & 0 & 0 & 0 & 0 \\ & 0 & 0 & 0 & 0 & 0 & 0 & 0 \\ & & 0 & 0 & 0 & 0 & 0 & 0 \\ & & & 0 & 0 & 0 & 0 & 0 \\ & \text{sym.} & & & 1 & 0 & -1 & 0 \\ & & & & & 1 & 0 & -1 \\ & & & & & & 1 & 0 \\ & & & & & & & 1 \end{pmatrix} \tag{A.2d}$$

$$\tilde{\mathbf{D}}_b^t = \tilde{d}_b^t \begin{pmatrix} 0 & 0 & 0 & 0 & 0 & 0 & 0 & 0 \\ & 0 & 0 & 0 & 0 & 0 & 0 & 0 \\ & & 1 & 0 & 0 & 0 & 0 & 0 \\ & & & 1 & 0 & 0 & 0 & 0 \\ & \text{sym.} & & & 0 & 0 & 0 & 0 \\ & & & & & 0 & 0 & 0 \\ & & & & & & 0 & 0 \\ & & & & & & & 0 \end{pmatrix} \tag{A.2e}$$

A.2 Damping matrix of single cable with internal and external energy sinks

$$\mathbf{D} = \mathbf{D}^{\mathrm{in}} + \mathbf{D}^{\mathrm{ex}} = \begin{pmatrix} D_{11} & D_{12} & \cdots & D_{1j} \\ D_{21} & D_{22} & & \vdots \\ \vdots & & \ddots & \vdots \\ D_{i1} & \cdots & \cdots & D_{ij} \end{pmatrix}, \qquad i,j = 1,\ldots,n \tag{A.3}$$

with

$$D_{ij}^{\mathrm{in}} = \frac{\pi d_{\mathrm{in}}}{\mu l^2} \begin{cases} \frac{\pi b i^2}{l} + \frac{i}{2}\left[\sin\left(\frac{2\pi i(x_{\mathrm{in}}+b)}{l}\right) - \sin\left(\frac{2\pi i x_{\mathrm{in}}}{l}\right)\right] & \text{if } i = j \\ \frac{ij}{i+j}\left[\sin\left(\frac{\pi(i+j)(x_{\mathrm{in}}+b)}{l}\right) - \sin\left(\frac{\pi(i+j)x_{\mathrm{in}}}{l}\right)\right] & \\ + \frac{ij}{|i-j|}\left[\sin\left(\frac{\pi|i-j|(x_{\mathrm{in}}+b)}{l}\right) - \sin\left(\frac{\pi|i-j|x_{\mathrm{in}}}{l}\right)\right] & \text{if } i \neq j \end{cases} \tag{A.4a}$$

$$D_{ij}^{\mathrm{ex}} = \frac{2d_{\mathrm{ex}}}{\mu l} \sin\left(\frac{\pi i x_{\mathrm{ex}}}{l}\right) \sin\left(\frac{\pi j x_{\mathrm{ex}}}{l}\right) \tag{A.4b}$$

A.3 System matrices of bundled cables with multiple spacer dampers

A.3.1 Mass matrix

$$\mathbf{M} = \begin{pmatrix} \mathbf{M}^{\mathrm{I}} & \mathbf{0} & \mathbf{0} \\ \mathbf{0} & \mathbf{M}^{\mathrm{II}} & \mathbf{0} \\ \mathbf{0} & \mathbf{0} & \mathbf{M}^{\Delta} \end{pmatrix} \tag{A.5}$$

with

$$M_{ij}^{\mathrm{I}} = \frac{\mu_{\mathrm{I}} l}{2}\delta_{ij} + m_c \sum_{r=1}^{n_d} \sin\left(\frac{\pi i x_r}{l}\right) \sin\left(\frac{\pi j x_r}{l}\right), \qquad i,j = 1,\ldots,n_{\mathrm{I}} \tag{A.6a}$$

$$M_{ij}^{\mathrm{II}} = \frac{\mu_{\mathrm{II}} l}{2}\delta_{ij} + m_c \sum_{r=1}^{n_d} \sin\left(\frac{\pi i x_r}{l}\right) \sin\left(\frac{\pi j x_r}{l}\right), \qquad i,j = 1,\ldots,n_{\mathrm{II}} \tag{A.6b}$$

$$M_{ij}^{\Delta} = m_d \delta_{ij}, \qquad i,j = 1,\ldots,n_d \tag{A.6c}$$

A.3.2 Stiffness matrix

$$\mathbf{K} = \begin{pmatrix} \mathbf{K}^{\mathrm{I}} & \mathbf{0} & \mathbf{\Psi}^{\mathrm{I}^{\mathrm{T}}} \\ \mathbf{0} & \mathbf{K}^{\mathrm{II}} & \mathbf{\Psi}^{\mathrm{II}^{\mathrm{T}}} \\ \mathbf{\Psi}^{\mathrm{I}} & \mathbf{\Psi}^{\mathrm{II}} & \mathbf{K}^{\Delta} \end{pmatrix} \tag{A.7}$$

with

$$K_{ij}^{\mathrm{I}} = \frac{\pi^2 i j T_{\mathrm{I}}}{2l}\delta_{ij} + k_d \sum_{r=1}^{n_d} \sin\left(\frac{\pi i x_r}{l}\right) \sin\left(\frac{\pi j x_r}{l}\right), \qquad i,j = 1,\ldots,n_{\mathrm{I}} \tag{A.8a}$$

$$K_{ij}^{\mathrm{II}} = \frac{\pi^2 i j T_{\mathrm{II}}}{2l}\delta_{ij} + k_d \sum_{r=1}^{n_d} \sin\left(\frac{\pi i x_r}{l}\right) \sin\left(\frac{\pi j x_r}{l}\right), \qquad i,j = 1,\ldots,n_{\mathrm{II}} \tag{A.8b}$$

$$K_{ij}^{\Delta} = 2k_d \delta_{ij}, \qquad i,j = 1,\ldots,n_d \tag{A.8c}$$

$$\Psi_{rj}^{\mathrm{I}} = -k_d \sin\left(\frac{\pi j x_r}{l}\right), \qquad \begin{matrix} r = 1,\ldots,n_d \\ j = 1,\ldots,n_{\mathrm{I}} \end{matrix} \tag{A.8d}$$

$$\Psi_{rj}^{\mathrm{II}} = -k_d \sin\left(\frac{\pi j x_r}{l}\right), \qquad \begin{matrix} r = 1,\ldots,n_d \\ j = 1,\ldots,n_{\mathrm{II}} \end{matrix} \tag{A.8e}$$

A.3.3 Damping matrix

$$\mathbf{D} = \begin{pmatrix} \mathbf{D}^{\mathrm{I}} & \mathbf{0} & \mathbf{\Phi}^{\mathrm{I}\,\mathrm{T}} \\ \mathbf{0} & \mathbf{D}^{\mathrm{II}} & \mathbf{\Phi}^{\mathrm{II}\,\mathrm{T}} \\ \mathbf{\Phi}^{\mathrm{I}} & \mathbf{\Phi}^{\mathrm{II}} & \mathbf{D}^{\Delta} \end{pmatrix} \tag{A.9}$$

with

$$D_{ij}^{\mathrm{I}} = \sum_{r=1}^{n_d} d_r^{\mathrm{ex}} \sin\left(\frac{\pi i x_r}{l}\right) \sin\left(\frac{\pi j x_r}{l}\right) + \sum_{r=1}^{n_d} \frac{\pi d_r^{\mathrm{in}}}{2l} \begin{cases} \frac{\pi b_r i^2}{l} + \frac{i}{2}\left[\sin\left(i\Lambda_r^+\right) - \sin\left(i\Lambda_r^-\right)\right] & \text{if } i = j \\ \frac{ij}{i+j}\left[\sin\left(\frac{(i+j)\Lambda_r^+}{2}\right) - \sin\left(\frac{(i+j)\Lambda_r^-}{2}\right)\right] & \\ + \frac{ij}{|i-j|}\left[\sin\left(\frac{|i-j|\Lambda_r^+}{2}\right) - \sin\left(\frac{|i-j|\Lambda_r^-}{2}\right)\right] & \text{if } i \neq j \end{cases} \tag{A.10a}$$

$$\Lambda_r^{\pm} = \frac{(2x_r \pm b_r)\pi}{l}, \qquad r = 1, \ldots, n_d \tag{A.10b}$$

$$D_{ij}^{\mathrm{II}} = D_{ij}^{\mathrm{I}}, \qquad i, j = 1, \ldots, n_{\mathrm{II}} \tag{A.10c}$$

$$D_{ij}^{\Delta} = 2 d_r^{\mathrm{ex}} \delta_{rj}, \qquad r, j = 1, \ldots, n_d \tag{A.10d}$$

$$\Phi_{rj}^{\mathrm{I}} = -d_r^{\mathrm{ex}} \sin\left(\frac{\pi j x_r}{l}\right), \qquad \begin{matrix} j = 1, \ldots, n_{\mathrm{I}} \\ r = 1, \ldots, n_d \end{matrix} \tag{A.10e}$$

$$\Phi_{rj}^{\mathrm{II}} = -d_r^{\mathrm{ex}} \sin\left(\frac{\pi j x_r}{l}\right), \qquad \begin{matrix} j = 1, \ldots, n_{\mathrm{II}} \\ r = 1, \ldots, n_d \end{matrix} \tag{A.10f}$$